https://doi.org/10.5194/egusphere-2025-3579 Preprint. Discussion started: 19 August 2025

Understanding drivers and biases of simulated CO emissions by the INFERNO fire model over South America

Maria P. VeláquezVelásquez-García[1,2], Richard J. Pope[1,2], Steven T. Turnock[3,4], Chetan Deva[1], David P. Moore[5,6],
Guilherme Mataveli[7,8], Steve R. Arnold[1], Ruth M. Doherty[9], and Martyn P. ChiperffieldChipperfield[1,2]

[1]School of Earth and Environment, University of Leeds, Leeds, UK
[2]National Centre for Earth Observation, University of Leeds, Leeds, UK
[3]Met Office Hadley Centre, Exeter, UK
[4]Met Office@Leeds, University of Leeds, UK
[5]Department of Physics and Astronomy, University of Leicester, Leicester, UK
[6]National Centre for Earth Observation, University of Leicester, Leicester, UK
[7]Earth Observation and Geoinformatics Division, National Institute for Space Research, São José dos Campos, Brazil
[8]Tyndall Centre for Climate Change Research, School of Environmental Sciences, University of East Anglia, Norwich, UK [9]School of GeoSciences, University of Edinburgh, Edinburgh, UK Correspondence: Maria P. Veláquez García (eempvg@leeds.ac.uk)

Correspondence: Maria P. Velásquez-García (eempvg@leeds.ac.uk)

Abstract.

Integrating fire simulation representation into climate models enhancesimproves our understanding of ecosystem-fire-climate interactions, clarifying the role of fire in by including connections between the carbon cycle and other processes.atmospheric composition. The Interactive Fires and Emissions algorithm for Natural Environments (INFERNO) is one of thea new modules incomponent of the upgraded UK Earth System Model (UKESM). Here, we use a version of INFERNO coupled only withto the Joint UK Land Environment Simulator (JULES), land surface model) in an offline configuration to evaluate itsthe performance and biases over South America (SA); a region that accounts for ~15% of global fire carbon emissions. For this, we comparedof the simulated carbon monoxide (CO) estimatesemissions from INFERNO (2004-2021) with five satellite-based biomass-burning inventories, conductedfires in South America. In addition, we use sensitivity experiments and developed a machine learning (ML) model targetingapproach to identify the key biases. INFERNO was able to represent and processes driving simulated CO emissions in most of the fire-active zone in SA, particularly the southern Amazon 'Arc of Deforestation', but overestimates emissions (~100%) outside them (e.g. within the Amazon forest). The ML model (R^2 = 64%) indicates that tree categories of Plant Functional Types (PFTs) and soil moisture — through its role in flammability and gross primary productivity (GPP) —

https://doi.org/10.5194/egusphere-2025-3579 Preprint. Discussion started: 19 August 2025

significantly influence spatiotemporal biases. In northern SA, CO emissions were overestimated by approximately 300% due to seasonal cycle inaccuracies, while INFERNO showed lower biases in southern SA emissions despite lacking seasonal representation. Both flammability and GPP underpinned the limited simulation of the seasonal cycle. Although INFERNO misrepresented emissions trends in. In South America, INFERNO accurately represents the Arc of Deforestation, in the southern Amazon as a primary source region of CO emissions, but it successfully captured the increase in emissions in the eastern Andean Mountains from 2014tends to 2021, albeit underestimating their magnitude. Sensitivity experiments revealed that the underlying overestimate these emissions by about 72%. The simulated emission patterns in this region are largely determined by Plant Functional Type (PFT affected spatiotemporal variability (115%) and trends (167%) in CO emissions, while flammability influenced the seasonal cycle (116%) and trends (158%). These findings highlight the need for enhanced PFT accuracy and a deeper understanding of the roles of precipitation/soil moisture in GPP and flammability, as well as the consideration of landscape fragmentation to represent land management and forest fire vulnerability.), particularly tree fractions, with meteorological conditions significantly affecting emission seasonality. In particular, emissions were highly sensitive to drought conditions, with simulations showing a 100% increase of CO emissions in response to the use of drier meteorological conditions from reanalysis data (i.e. one of the sensitivity experiments). The machine learning model identified soil moisture as a major contributor to these biases, suggesting the need for better representation of fuel moisture. INFERNO shows a sensitivity to carbon load as it typically underestimates CO emissions in areas dominated by pastures and grasses, possibly due to the tree fraction being too low. This sensitivity to carbon load further contributes to misinterpreting the seasonal emission cycle, particularly in southern South America. Other potential factors, such as crop fraction and the Human Development Index, were identified as having important constraints on anthropogenic ignition, and with further improvement could reduce simulation biases.

1 Introduction

Wildfires (both naturalFires and anthropogenic)their emissions can significantly impact our climate and ecosystems through complex land surface-fire-climate inter-actions. Annually, fires burn approximately 770 megahectares Chen et al. (2023) and emit around 7.3 petagrams of CO^2 into the atmosphere van der Werf et al. (2017), among other important greenhouse gases and air pollutants. As widely reported, the occurrence, propagation, and emissions of fires are strongly controlled by meteorological conditions and the type of vegetation present, even when fires are predominantly caused by human activity (Kelley et al., 2019; Forkel et al., 2019). becomingIn fact, fires are increasingly frequent and intense in key ecosystems around the world, largely due to driven by

https://doi.org/10.5194/egusphere-2025-3579 Preprint. Discussion started: 19 August 2025

climate change and land use practices (Cunninghamin our warming world (Liu et al., 2022b; Burton et al., 2024; Zheng et al., 2021). The recent increase in wild). However, these

climate-induced fires in tropicalintroduce feedback through perturbations to the land surface and boreal forests has led to a rise in carbon corresponding atmospheric emissions from fires, despite the ongoing decline in global burned area (Zheng et al., 2023, 2021). Due to the lack of resilience of these ecosystems to fires, the success of(i.e. aerosols and greenhouse gases). Frequent fire activity influences ecosystem competition, favouring fire-prone ecosystems is enhanced over the burned area. As a result, these fires cause forests to shift to a negative carbon balance, i.e. becoming a net source of carbon (Yue et al., 2016). Annually, fires emit 7.3 Pg of CO_2 to the atmosphere (van der Werf et al., 2017), along with large quantities of other greenhouse gasesmore sensitive ones, such as methane (CH_4) and nitrous oxide (N_2O) (Heilmanforested regions (Beckett et al., 2014). The effects of fire emissions, however, become complex with the additional release of large amounts of aerosols, including black carbon and organic aerosols, which have different interactions with clouds, radiation, precipitation and atmospheric circulation (Magahey and Kooperman, 2023; Thornhill et al., 2018; Wu et al., 2011). Other air pollutants, which can be precursors to ozone (O_3) formation, such as nitrogen dioxide (NO_2), are also emitted from fires. With this, fire emissions can adversely impact ecosystems through O_3 stress, which affects plant growth (Pacifico et al., 2015). Additionally, fire2022). Furthermore, wildfire emissions can alter the biogeochemical cycles of certain key plant-growth elements for plant growth, such as carbon, phosphorus, nitrogen, and iron (Bauters et al., 2018; Hamilton et al., 2022). Humans significantly influence 2022), leading to nutrient losses in burnt areas and are influenced by ecosystem-fire-climate interactions. These interactions can affect ecosystem functions, crop yields, and overall human health. The increase in air pollutants from wildfires has led to higher hospitalisation rates, increased nutrients in areas of deposition. Additionally, fire emissions (particularly among children (Arrizaga et al., 2023), as well as human lung cell damage (de Oliveira Alvesaerosols) have strong direct and indirect impacts on climate through atmospheric scattering and cloud properties. Aerosols can suppress precipitation, driven by more cloud condensation nuclei (Wu et al., 2011; Thornhill et al., 2018), smaller drops and more evaporation and less convection provoked by a warmer cloud layer (Magahey and Kooperman, 2023; Thornhill et al., 2018; Wu et al., 2017), and cases of low birth weight (Candido da Silva et al., 2014).2011). On a large scale, the most highly abnormal wildfire emissions influence global circulation by altering the balance between tropospheric and stratospheric radiation budgets (Zhou et al., 2020; Senf et al., 2023; Liu et al., The limited representation of this complex climate-fire-ecosystem interaction in 35 2005). The effect on the radiation balance can, in turn, influence ecosystems. In the Amazon, diffuse radiation enhanced by aerosols from fires increases plant growth. Consequently, fires, ecosystems and climate are all strongly coupled, shaping the future evolution of all components involved.

https://doi.org/10.5194/egusphere-2025-3579 Preprint. Discussion started: 19 August 2025

Despite the clear importance of fire in the Earth's system, many Earth System Models (ESMs) has led, which model climate interactions, rely on prescribed data to represent fires and their emissions, leading to large uncertainties in future climate projections (Canadell et al., 2021In-tergovernmental Panel on Climate Change (IPCC), 2023; Kloster and Lasslop, 2017; Hanan et al., 2022). This issue is further exacerbated by ESMs often lacking an interactive fire model component to represent the coupling of fire, land, atmosphere and climate interactions (Lasslop et al., 2019). There is particularly high uncertainty of the impact of fire on biogeochemical cycles and, in turn, the contribution to ecosystem change and climate (Lasslop2022). When prescribed, although the effects of fires are parametrised, the fire feedbacks on the land surface are not represented. Multiple et al., 2019). Multiple coupled models have attempted to understandrepresent the complex climate-fire-ecosystem interactions in the lastpast few decades (Hantson et al., 2016). Still, includingHowever, developing fully coupled fire models within global climate models is a growing and challenging development. In fact, the number of fire-related variables submitted by ESMs in the sixthan active area of research with complex challenges still to overcome (Lasslop et al., 2019).

For the seventh Coupled Model Intercomparison Project (CMIP6) has doubled compared to its predecessor, CMIP5 (Hantson et al., 2016; Li et al., 2024). Additionally, efforts to enhance our understanding of fire processes and their representation in global models are being enhanced through collaborations, such as the Fire Modelling Intercomparison Project (FireMIP) (Li et al., 2019; Hantson et al., 2020).

To improve the representation of climate-fire-ecosystem dynamics within CMIP7 experiments, the United Kingdom Earth System Model (UKESM) will couple the Interactive Fires and Emissions algorithm for Natural Environments (INFERNO) (Mangeon et al., 2016) to its land surface model (the Joint UK Land Environment Simulator - JULES) and atmospheric chemistry model (UK Chemistry and Aerosols Model - UKCA). INFERNO, coupled to JULES, has already participated in the Fire Modelling Intercomparison

(Mangeon et al., 2016) to its vegetation model (the Joint UK Land Environment Simulator - JULES) and atmospheric model (including coupling with the UK Chemistry and Aerosols Model - UKCA). INFERNO coupled to JULES has already partici-

pated in Project (FireMIP,), where INFERNO provided an accurate representation of global burnedburnt area and carbon emissions (Hantson et al., 2020; Teixeira et al., 2021) and). In FireMIP, INFERNO outperformed most of the studied coupled models in simulating the spatial patterns of fire carbon emissions (Hantson et al., 2020). However, the model has also faced challenges in different parts of representing regional fire regimes across the world, such asincluding South America (SA), where INFERNO. Here, INFERNO's representation of fire properties has been limited by the complexity of socioeconomic and political influences on land management withinin the region (Burton et al., 2022). In general, FireMIP showed differences between models and a frequent

In general, FireMIP showed differences between models and a frequent overestimation of emissions in this regionSouth America, where anthropogenic influences on fires (e.g., deforestation) are the main challenge (Li et al., 2019; Hantson et al., 2020). Enhancing global model performance in SA is crucial, as the region accounts for 15% of annual fire carbon emissions. Furthermore, changes in the carbon balance and land cover in the Amazon can provoke significant regional and global effects (Snyder, 2010; Zhou et al., 2021; Wang et al., 2023). Moreover, parts of the Amazon have already become a carbon source due to deforestation and climate change (Gatti et al., 2021).South

The current research on simulated fire emissions from INFERNO over SA lacks a thorough evaluation of the sensitivity and biases of the model. This study decisively addresses this gap by rigorously assessing the performance of the model, as well as examining the sensitivity of simulated fire emissions and the biases associated with various model processes and parameters. For this, we compare the carbon monoxide (CO) emissions from fires simulated by JULES-INFERNO with various biomass burning inventories and satellite-retrieved total column CO (TCCO). We focus on CO due to its significant emission rate from

fires and the availability of complementary satellite missions that retrieve atmospheric TCCO. In SA, TCCO has been suggested as a valuable addition to fire activity monitoring since fire is the main source of CO in the region (Naus et al., 2022; Jury and Pabón, 2021). Additionally, inventories generally align well with CO emissions in SA (Liu et al., 2020; America contributes around 15% of annual global fire carbon emissions and 40% of deforestation-related emissions (van der Werf et al., 2010), mainly due to deforestation in the Amazon. Changes in carbon balance and land cover in the Amazon can introduce significant regional and global impacts (Snyder, 2010; Zhou et al., 2020; Wang et al., 2023a). Moreover, parts of the Amazon have already become a substantial carbon source due to deforestation and climate change (Gatti et al., 2021).

INFERNO has already been used to investigate a range of scenarios and events in South America (Burton et al., 2019, 2020), supported by global and specific performance evaluations (Burton et al., 2020; Hantson et al., 2020; Teixeira et al., 2021). However, previous studies have primarily focused on carbon emissions from fires, whereas this study aims to evaluate the simulation of fire-derived emissions in atmospheric models. We seek to identify areas for development and improvement by analysing the biases associated with these emissions. In Section 3, we present our results focusing on the evaluation of

INFERNO against fire emission inventories, use sensitivity experiments to investigate key drivers influencing CO emissions and finally quantify the model processes contributing to the calculated model-inventory biases. Discussion of the results and our conclusions are presented in Section 4.

2 Data and methods

Hua et al., 2024). To describe the sensitivity of the estimated CO emissions and their biases, we used sensitivity experiments and a machine learning (ML) approach.

https://doi.org/10.5194/egusphere-2025-3579 Preprint. Discussion started: 19 August 2025

2 Data and methods

This study utilised five biomass burning inventories to evaluate INFERNO CO emissions simulations in terms of spatiotemporal distribution, seasonal cycle, and regional trend in SA from 2004 to 2021. To support the assessment, we also used TCCO retrievals. The inventories and TCCO products are introduced in Section 2.2 and 2.3, respectively. In Section 2.4, we provide a brief overview of the JULES-ES setup of the third simulation round of the Inter Sectoral Impact Model Intercomparison Project (ISIMIP3). This section also presents the JULES-INFERNO coupling and the key equations that it uses. Throughout the study, the JULES-ES model using the ERA5 reanalysis served as the control model for most of the comparisons with inventories. However, we conducted multiple sensitivity experiments, presented in Section 2.5, that modify the representation of different processes within JULES-INFERNO. These experiments were compared to the inventories and the control run. We also developed a machine learning (ML) model to explain CO emissions biases in SA in order to analyse the processes driving the INFERNO biases.

2.1 Study area

This study focuses on continental SA and uses a regional classification that divides SA into three areas: northern SA (NorthSA), central SA (Mid-SA) and southern SA (South-SA). North-SA consider the territory from latitude 0.5 ◦ N to the continental boundary between Colombia and Panama, Mid-SA ranges from 17.5 ◦ S to 0 ◦ , and South-SA ranges from 55 ◦ S to 17 ◦ S (see Fig. S1). This classification aligns with the method used by Li et al. (2024), which identifies the "Arc of Deforestation" zone, here referred to as Mid-SA, separating it from the remaining southern hemisphere SA. The region commonly defined as the "Southern Hemisphere South America - SHSA" (van der Werf et al., 2017) encompasses both Mid-SA and South-SA. To facilitate a comparative analysis, we will refer to it as Mid-SA/South-SA when convenient.

Multiple factors are responsible for wildfires in SA, both of natural and anthropogenic origin. Yet, most are directly related to anthropogenic activities in highly fire-prone ecosystems, such as Cerrado and Llanos, and sensitive ecosystems, such as the Amazon rainforest (Chen et al., 2013; Menezes70 This study assesses the spatial distribution, seasonality and temporal evolution of CO fire emissions in continental South America (a key global region for fire activity and emissions). We focus on three regions: Northern South America (North-SA), Central South America (Mid-SA), and Southern South America (South-SA), as shown in Fig. 1. These regions are designed to capture emissions from the main fire-active regions of South America, while also accounting for unique fire patterns. These regions are consistent with previous work that evaluated the ability of CMIP models' to simulate fire emissions, including

assessing trends and biases, across South America (Li et al., 2024; van Marle et al., 2017). The North-SA region experiences a unique fire season because its cycle is opposite to that of the southern region, due to the migration of the Intertropical Convergence Zone. The Mid-SA region encompasses fire emissions from the important Arc of Deforestation front (Pereira et al., 2022; van der Werf et al., 2010). In SA, frequent fire occurrences are mainly concentrated in the transition forest region, recognised as the "Arc of Deforestation." This), an area is not only highlighted threatened by the continued land-use conversion but also for being and recognised as the world's largest savanna-forest transition

(Marques et al., 2020). The Importantly, defining Mid-SA as a broad but bounded region provides a practical scale for evaluating

fire models like INFERNO, which are not designed for fine-scale simulations in highly variable zones such as the Arc of Deforestation in this study is located in . South-SA includes an important source of fire emissions from the Chaco biome. Although the division between Mid-SA, and South-SA intersects the Cerrado fire-prone ecoregion, Mid-SA includes the deforestation front in the northern part of the Cerrado, where fires occur more frequently (Kim et al., 2025). of Bolivia, Brazil

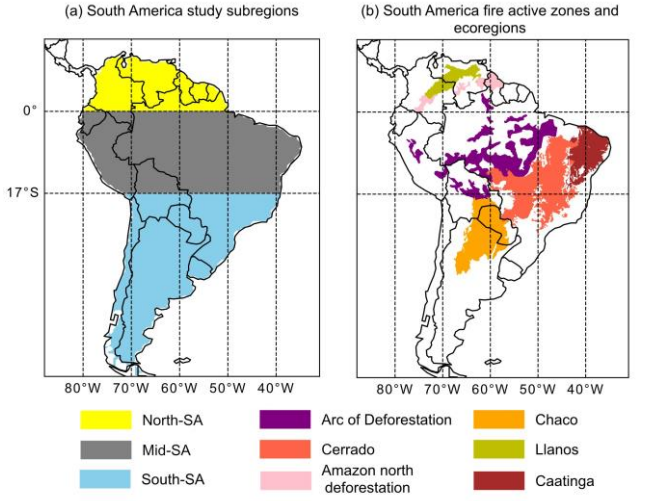

Figure 1. Studied (a) subregions and Perú. This study assessed (b) fire active zones and ecoregions in South America.

This study also assessed CO emissions onfrom deforestation fronts and particularspecific ecoregions of SASouth America using the shapefilesshape-files provided inby Pacheco et al. (2021) and Dinerstein et al. (2017), respectively. These zones are displayed byin Fig. S1b.1 (b). For the Arc of Deforestation, we used the deforestation fronts from Bolivia, Brazil, and Perú.

2.2 Biomass burning emission inventories

To evaluate the simulated CO emissions from fire, we utilised fivefour biomass burning inventories, including . One of the key sources was the Global Fire Emissions Database (GFED), which is frequentlycommonly used for model output comparisons due to modelling studies given its extensive historical data record. and reliability. We specifically employed both the GFED Beta version 5 (GFEDvn5beta (GFED5) and version 4.1s (GFEDvn4sGFED4s) (van der Werf et al., 2017; Chen et al., 2023), alongside) to assess the consistencies/differences between them. Additionally, we incorporated the Global Fire Assimilation System version 1.2 (GFASvn1.2GFAS) (Kaiser et al., 2012) and the Fire INventory from NCAR version 2.5 (FINNvn2.5) (Wiedinmyer et al., 2023). Additionally, a regional inventory, the Brazilian Biomass Burning Emission Model (3BEM-FRP)(3BEMFRP) (Pereira et al., 2022), was utilised.).

These inventories are based on three distincttwo different fire products:. GFED uses the burnt area (BA) as the baseits primary satellite product, FINNvn2.5 uses active fire hotspots (from which the BA is calculated), andwhile GFASvn1.295 GFAS and 3BEM-FRP are basedrely on fire radiative power (FRP). GFASvn1.2, FINNvn2.5GFED4s was the first version of GFED to account for small fires by utilising the 500m MODIS bands (van der Werf et al., 2017). For GFED5, efforts to include small fires continued, incorporating corrections based on observations from Landsat and Sentinel-2 (Chen et al., 2023). GFAS exploits real-time emissions estimates using the MODIS near-real-time FRP product (Kaiser et al., 2012). Similarly, 3BEM-FRP utilises FRP data from MODIS, although it is not a near-real-time product. 3BEM-FRP uses an adjustment factor to account for fires that exceed the spatial and temporal resolution of MODIS FRP based on hotspots from VIIRS and the geostationary satellites GOES and SEVIRI (Pereira et al., 2022).

The estimates of CO emissions from these inventories vary significantly because each one calculates the amount of burnt dry matter differently (Hua et al., 2024). However, they consistently convert this burnt matter into emissions using emission factors (EF) [gkg^{-1}] that vary by land use and land cover. The EFs are commonly taken from Akagi et al. (2011) and Andreae and Merlet (2001). This consistency in the factor is particularly evident for CO, where EFs are consistent across different inventories (Liu et al., 2020; Hua et al., 2024). GFASvn1.2 and 3BEM-FRP also use a combustion factor to determine the

https://doi.org/10.5194/egusphere-2025-3579 Preprint. Discussion started: 19 August 2025

amount of biomass burnt at different FRP energy levels. For this, they rely on external products, GFEDv3.1 for GFAS and the Fire Energetics and Emissions Research v1 (FEERv1) for 3BEM-FRP (Kaiser et al., 2012; Pereira et al., 2022).

hadGFAS and 3BEM-FRP were downloaded daily data with a spatial resolution of 0.1 ° × 0.1 °. While GFEDvn5GFED5 and GFEDvn4sGFED4s were downloaded with a monthly resolution and a spatial resolution of 0.25 ° × 0.25 °. All the inventories were resampled to a monthly temporal resolution and a spatial resolution of 0.5 ° × 0.5 ° to match the model outputs dimensions in the JULES-INFERNOJULESINFERNO configuration (Section 2.43).

GFEDvn4s was the first GFED version to consider a correction for small fires using 500m MODIS bands (van der Werf

115For the machine learning analysis of INFERNO biases (Section 2.6) and for visualising differences in selected figures, we calculated an ensemble average (mean) dataset based on the four inventories: GFED4s, GFED5, GFAS, and 3BEM-FRP. Each inventory was equally weighted in the average. GFED4s and GFAS are well-established inventories in the literature. While they have outperformed other inventories in their emissions estimate in South America (Hua et al., 2024; Reddington et al., 2019), their biases have also been noted (Naus et al., 2022; Liu et al., 2020). In contrast, 3BEM-FRP and GFED5 (the beta version) are considered next-generation inventories. They have been adjusted to better represent small fires and include updated and more accurate land cover data (Mataveli et al., 2023). However, these newer inventories lack the extensive long-term validation that GFED4s and GFAS have undergone. Overall, using an average of these inventories represents a balance between incorporating innovative methodologies and relying on well-established datasets for this study.

et al., 2017). With GFEDvn5, the efforts for including small fires were reiterated by including a correction based on Landsat or Sentinel-2 observations (Chen et al., 2023). FINNvn2.5 has a special adjustment to calculate BA in forest areas, where hotspots of fire activity are clustered together to overcome low visibility caused by tree canopy interference (Wiedinmyer et al., 2023). GFASvn1.2 uses the MODIS near-real-time FRP product to estimate real-time emissions (Kaiser et al., 2012). 3BEM-FRP also uses FRP from MODIS observation, applying an adjustment factor to account for fires beyond the spatial and temporal

120 resolution of the product. This adjustment is based on comparisons with VIIRS and the geostationary satellites GOES and SEVIRI (Pereira et al., 2022).

The estimation of CO emissions by these inventories varies significantly due to differences in how each one calculates the amount of burned dry matter (Hua et al., 2024). However, to convert this burned matter into

emissions, all inventories rely on emission factors (EF) [gkg^{-1}] that vary by land use and land cover. The EFs are consistently derived or partially derived from the studies conducted by Akagi et al. (2011) and Andreae and Merlet (2001). Particularly, the EF for CO shows less variation across different inventories compared to other compounds (Liu et al., 2020; Hua et al., 2024). GFASvn1.2 and 3BEM-FRP use a combustion factor to determine the amount of biomass burnt by different levels of energy. They rely on external products, GFEDvn3.1 for GFASvn1.2 and the Fire Energetics and Emissions Research vn1 (FEERvn1) for 3BEM-FRP (Kaiser et al., 2012; Pereira et al., 2022).

Annual Land cover is another important input for the inventories. Here, the MODIS MDC12Q1 collection 5.1 or 6 is used. Specific for Brazil and the Amazon, 3BEM-FRP includes the MapBiomas collection 6, which better captures the deforestation process in the Amazon and forest formation in northern Cerrado (Mataveli et al., 2023).

2.3 TCCO retrievals JULES-ES setup

We used the TCCO from the Infrared Atmospheric Sounding Interferometer (IASI) by the University of Leicester IASI Re-

trieval Scheme (ULIRS) (Illingworth et al., 2011), and the version 9 level 2 product from the Measurements Of Pollution In The Troposphere (MOPITT) developed by NASA/LARC/SD/ASDC (2022) (Deeter et al., 2022). The IASI TCCO record used in this study is between 2014 and 2021 since ULIRS was applied to the instrument on Metop-B (satellite launched in September 2012). IASI has a circular footprint at nadir with a diameter of 12 km, extending to an ellipse of ~ 39 km × 20 Km at the edge of the swath. Due to its wide swath, the global coverage is achieved in 12 hours. To estimate the TCCO, ULIRS used the IASI

band centred on 4.7μm, with absorption ranging from 2040 to 2190 cm^{-1}, but because there are other stronger absorbers in this domain (e.g., H_2O, CO_2, O_3), then only the range 2143 cm^{-1} to 2181 cm^{-1} is utilized. From this, ULIRS uses an optimal estimation method to determine the CO profile from the measured radiance (Illingworth et al., 2011).

MOPITT is on-board Terra and has a horizontal resolution of 22 km ×22 km, a swath of 640 km and a global coverage every 3-4 days. Three retrieved products are available: TIR only, NIR only, and TIR/NIR. For this study, we used the TIR/NIR

product, which has the highest sensitivity in the lower troposphere. MOPITT uses the radiative transfer model recognised as the MOPITT operational fast forward model (MOPFAS) and an optimal estimation based algorithm to retrieve TCCO (Deeter et al., 2017).

https://doi.org/10.5194/egusphere-2025-3579 Preprint. Discussion started: 19 August 2025

The TCCO products were gridded at 0.5 ◦ × 0.5 ◦ and at a monthly average resolution co-locating the model and inventories.

Only retrievals with a degree of freedom signal (DOFS) ≥1, cloud fraction ≤ 20% and solar zenith angle <90 ◦ were included

in our analysis. This last criterion was established to focus solely on daytime products, ensuring fair comparisons between the retrieval products.

2.4 JULES-ES: ISIMIP3a setup

The We used the JULES-ES configuration for ISIMIP3a was utilised in this study. This configuration is described in from the historical run of the third simulation round of the Inter-Sectoral Impact Model Intercomparison Project (ISIMIP3a) (Mathison et al. (2023) and functions as an offline land/vegetation model, requiring prescribed atmospheric inputs while having a., 2023), as it features a recent setup similarcomparable to that of theJULES in UKESM (Sellar et al., 2019). For this study, we ran the model from 2001 to align with the study period (2004-2021). This .

The JULES-ES configuration has a spatial resolution of setup uses a 0.5 ◦ × 0.5 ◦ latitude–longitude grid. While JULES can be run for several centuries for climate applications, in this study, we ran JULES-ES from 2001 (study period of 2004-2021) to match the satellite era over the past few decades.

ISIMIP3a includes a core of experiments based on climate-related forcings and direct human forcings (Frieler et al., 2024). For climate-related forcings, the models used four standard observation-based meteorological datasets: GSWP3-W5E5, 20CRv3-W5E5, 20CRv3-ERA5, and 20CRv3 (Frieler et al., 2024). Some datasets are composites of two separate reanalysis

datasets: historical andFor climate-related forcings and for the more recent. Aligned with our study period, we utilised only (from around 1980), the most recent part of the dataset. As a result, we only considered the climate forcingproject includes three optional observation-based meteorological datasets: W5E5, ERA5, and 20CRv3. Both GSWP3-W5E5 and 20CRv3-W5E5 relied onThe W5E5 data from 1979 toends in 2019 (Frieler et al., 2024). The, 20CRv3 dataset ends in 2015, while theand ERA5 dataset ends in 2021. (Frieler et al., 2024). In thisour study, ERA5 iswe used ERA5 for the control analysis as this coverssince it encompasses the entire study period (2004 - 2021). The other two datasets (i.e. 20CRv3 and W5E5) were utilised for the flammability sensitivity experiments described in Section 2.5.

2.4. The human-forcing datasets in ISIMIP3a prescribe land- use (agricultural and pasture fractionfractions), population density (PD), and nitrogen deposition. For this study, the human development index (HDI) was prescribed to represent socioeconomic factors as suggested by Teixeira et al. (2021), but only for the experimental work (Section 2.5). Since the original version of INFERNO in ISIMIP3a does not prescribe this, HDI=0 was used in the control run.

https://doi.org/10.5194/egusphere-2025-3579 Preprint. Discussion started: 19 August 2025

In For this setup, the land component, JULES, contains ES includes 13 plant functional types (PFTs) (listed in Table 1), which include four managed and nine natural and four managed PFTs (Mathison et al., 2023). The four natural PFTs are Broadleaf Deciduous Trees, Tropical Broadleaf Evergreen Trees, Temperate Broadleaf Evergreen Trees, Needleleaf Evergreen Trees, Needleleaf Deciduous Trees, Evergreen shrubs, Deciduous shrubs and C3 and C4 Grasses. The managed PFTs are C3 and C4 crops (C3Cr Crops and C4Cr) Pastures. C3 and pastures (C3Pa C4 refer to photosynthetic pathways.

C4 plants are adapted to high temperatures and C4Pa). light intensities, reducing water loss and improving CO_2 fixation under these conditions compared to C3 plants. JULES-ES also contains four non-vegetation land covers (bare soil, lake, ice, urban). The PFTs can be are simulated globally distributed by simulation within JULES-ES using the dynamic global vegetation model (DGVM) called TRIFFID (Top-down Representation of Interactive Foliage and Flora Including Dynamics), which models the PFTs represents PFT competition and their biomass (Burton et al., 2019).

2.43.1 INFERNO

The INFERNO

The INFERNO fire model was developed by Mangeon et al. (2016) uses PFTs as vegetation categories for the estimation of burned and simulates the burnt area (BA), emitted carbon (EC) and emitted species (E_x). To calculate the BA, INFERNO uses total ignition (I_T,) and flammability (F_{PFT}) and an average burned area (BA_{PFT})), as described in by Equation 1. As F_{PFT}, BA is directly scaled based on PFT. This is done by using the factor called average burnt area (BA_{PFT}), which describe the minimum scar of burnt area per PFT.

$$BA_{PFT} = I_T F_{PFT} BA_{PFT} \quad (1)$$

Table 1 lists the BA_{PFT} used for each PFT in this study. I_T and F_{PFT} behave as probabilistic variables ranging from 0 to 1.

In INFERNO, I_T is split into natural ignition (I_N) is composed of natural and anthropogenic ignition (I_A).

Three ignition methods can be used in the model. The first ignitions (I_N and simplest is "constant ignition", where I_N and I_A are constant. Here, I_N assumes a multi-year annual mean I_A), which are calculated using the lightning rate of 2.7 flashes/km^2/yr, where 75% are cloud-to-ground, all of which and population density (PD), respectively. As Equation 2 shows, I_T is further scaled by a factor representing fires not suppressed by humans (f_{NS}). The I_N is equal to 75% of cloud-to-ground lighting per Km^2 in a month. The seasonal lighting cycle is prescribed

https://doi.org/10.5194/egusphere-2025-3579 Preprint. Discussion started: 19 August 2025

into the model. Both I_A and f_{NS} are used in Equations 3 and 4. The Human Development Index (HDI) is also used in the two equations, as a further development of INFERNO added by Teixeira et al. (2021). For this study, we are using HDI=0 in most of the analyses; however, we include HDI in a sensitivity experiment (Section 2.4).

$$I_T = (I_N + I_A)\frac{f_{NS}}{8.64 \times 10^{10}} \quad (2)$$

Table 1: JULES-ES's Plant Functional Type (PFT) and their respective Average Burnt Area (BA_{PFT}) and Emission Factor (EF_{PFT}) for INFERNO modelling

PFT		Short name	$\overline{BA_{PFT}}$ [$km^2 fire^{-1}$]	EF_{CO} [gkg^{-1}]
Broadleaf deciduous trees	BDT	0.6		93
Tropical broadleaf evergreen trees	BET-Tr	0.6		93
Temperate broadleaf evergreen trees	BET-Te	0.6		89
Needleleaf deciduous trees	NDT	0.6		127
Needleleaf evergreen trees	NET	0.6		89
C3 grass	C3G	1.4	$I_A = k_{(PD)}\,PD\alpha\times(1-HDI)$	89 (3)
C3 crop	C3Cr	0.2	$f_{NS} = 7.7(0.05+0.9\times e^{-0.05PD})\times(1-HDI)$	0 (4)
C3 pasture	C3Pa	1.4		98
C4 grass	C4G	1.4		63
C4 crop	C4Cr	0.2		0
C4 pasture	C4Pa	1.4		63
Deciduous Shrub	DSh	1.2		89
Evergreen Shrub	ESh	1.2		127

provoke I_N. The I_A is 1.5 ignitions/km²/month globally, based on GFED estimations (Mangeon et al., 2016). The second ignition method is "varying natural ignition", which uses constant I_A as the first ignition method but varying I_N (i.e., lightning). The annual seasonality of cloud-to-ground lightning is prescribed. The third method, "varying natural and human ignitions", uses the same varying I_N as the second method and a varying I_A, which depends on prescribed PD and optional HDI (Teixeira et al., 2021, 2023). The I_A, described in Equation 2, uses a distinct anthropogenic influence on

Deleted Cells
Deleted Cells

https://doi.org/10.5194/egusphere-2025-3579 Preprint. Discussion started: 19 August 2025

ignitions in rural versus urban areas represented by $k_{(PD)} = 6.8 \times PD^{-0.6}$. In this equation, α is the number of potential ignitions per person per month per 190 km^2 with a constant magnitude of 0.03.

$$I_A = k_{(PD)} PD\alpha \times (1 - HDI) \quad (2)$$

This third ignition method attempts to include anthropogenic fire suppression, so the fraction of fires not suppressed by humans (f_{NS}) is included for the calculation of I_T in Equation 4. Since HDI is not included in the control model, then HDI=0.

$$f_{NS} = 7.7(0.05 + 0.9 \times e^{-0.05PD}) \times (1 - HDI) \quad (3)$$

$$I_T = (I_N + I_A)\frac{f_{NS}}{8.64 \times 10^{10}} \quad (4)$$

For INFERNO, the term F_{PFT} (described in Equation 5) depends on the relative humidity (RH) in %, precipitation rate (R) in mm day^{-1} and temperature in K from the prescribed input meteorological dataset. The land surface model, JULES, provides the inputs of soil moisture content (θ) as a fraction of saturation, and fuel load (leaf carbon and decomposable plant material) [kg m^{-2}]. These are used to calculate the fuel load index (FL) and the Goff-Gratch saturation vapour pressure (α), further explained in Mangeon et al. (2016).

$$F_{PFT} = \begin{cases} 1 & \text{for } RH < RH_{low} \\ \alpha \frac{RH_{high} - RH}{RH_{high} - RH_{low}} e^{-2R} FL_{PFT}(1-\theta) & \text{for } RH_{low} \le RH \le RH_{high} \\ 0 & \text{for } RH > RH_{high} \end{cases} \quad (5)$$

For Equation 5, RH_{low} = 10 % and RH_{high} = 90 %. Those are used to scale the influence of RH from 0 to 1. Consequently, notice that F_{PFT} ranges from 0 to 1. After calculating BA, the

The emitted carbon (EC_{PFT}) is calculated based on BA, the available carbon (C_i) and the combustion completeness (CC) for wood and leaves. This last term describes the minimum and maximum carbon fraction burnt in the fire events and may/may not depend on PFT. For the ISIMIP3a this study, $CC_{min,leaf} = 0.8$, $CC_{max,leaf} = 1$, $CC_{min,wood} = 0$ and $CC_{max,wood} = 0.4$ regardless of PFT. Equation 6 defines the EC_{PFT}.

$$EC_{PFT} = BA_{PFT} \times \sum_{leaf,wood}^{i} (CC_{min,i} + (CC_{max,i} - CC_{min,i})(1-\theta))C_i \quad (6)$$

$$EC_{PFT} = BA_{PFT} \times \sum_{leaf,wood} (CC_{min,i} + (CC_{max,i} - CC_{min,i})(1-\theta))C_i \quad (6)$$

The emission of a compoun X (in this case CO) is described by Equation 7, which includes the EC_{PFT} and the EF for compound X. (EF_X) variesCO for differenteach PFT and is listed in Table 1.

$E_X(EF_{CO,PFT})$.

$$E_{CO,PFT} = EC_{PFT}\, EF_X EF_{CO,PFT}/[C] \quad (7)$$

175In this equation, [C] describes the dry carbon fraction, which is assumed to be 50% (Mangeon et al., 2016).

2.5 Sensitivity experiments on JULES-INFERNO

215 JULES-INFERNO refers to the coupled interaction of INFERNO fire simulation in JULES, but throughout the manuscript, we refer to this only as INFERNO.

Table S1 presents the BA_{PFT} and EF for each PFT modelled. The EF_{CO} from C3-Crop and C4-Crop were not included in this model setup of JULES, which did not account for the crop PFTs. However, we conducted an experiment to assess the impact of fire CO emissions from crops. The experiment showed that excluding crops from simulations produced a negligible change in CO emissions across South America, increasing simulated CO emissions by only 1.4% for South-SA when included

180 (see Fig. S1). However, it is important to note that INFERNO does not model crops differently from other PFTs; meaning that harvesting periods and crop seasonality are not included or represented. In this study, we are, however, evaluating the contributions of the crops' PFT fractions to the model biases (see Section 2.6).

2.4 Sensitivity experiments on INFERNO

We conducted multiple experiments to assess the sensitivity of various processes and parameters controlling simulated fire emissions. We have divided the experiments into seven sub-groups (Table 2): ignitions, flammability, burnt area, combustion completeness, emission factor, feedback and PFTs. The label of the experiments described the subgroup to which they belonged. The experiment names, groups and details are summarised in Table 2. For ignitions, IT_N and IT_A

emissions, and their roles in the INFERNO response. We did this using a one-at-a-time technique, varying individual parameters and variable inputs from the control simulation described in Section 2.3.1. The experiments are briefly summarised in Table 1. We evaluated the role of anthropogenic and natural ignition in different scenarios. First, we simulated total ignition with a constant global anthropogenic ignition rate of 1.5 ignitions/km^2/month, based on GFED estimates (Mangeon et al., 2016).

For this, only I_N varies in Equation 2, which we label IT-NAT. The role of both I_A and I_N was further evaluated by using a scenario with constant magnitudes for both ignitions. 1.5 ignitions/km^2/month for I_A and 2.7 flashes/km^2/yr for I_N. This experiment is called IT-CST. We also analyse socioeconomic scaling in ignition using the HDI as suggested by Teixeira et al. (2021). This experiment directly influences anthropogenic ignitions and fire suppression. The HDI was incorporated into the model using the dataset provided by Kummu et al. (2018). The experiment is labelled IT-HDI.

To analyse the role of the meteorological conditions and the uncertainty it can introduce into the simulations, we use different meteorological datasets from the ISIMIP3a climate-forcing dataset. In this, we compared the ERA5-based control with the simulations using W5E5 and 20CRv3. These experiments are named as F-W5E5 and F-20CR, respectively. Notice that, in addition to flammability in Equation 5, the meteorological conditions also affect EC_{PFT} in Equation 6 through the carbon soil moisture and the available carbon.

Table 1. ~~220 used the different types of I_T provided by INFERNO and used prescribed HDI with a national and subnational dataset (IT-HDI and IT-HDIS), since the control run uses varying natural and human ignitions and HDI=0. Regarding flammability, the control~~

~~Table 2.~~ Description of the experiments run with INFERNO

Short name	~~Impacted~~Direct impacted process	Description
Control		~~Varing I_A~~Vary ignitions and ~~I_N ignition~~ERA5 meteorology
IT-CST	Ignition	~~Constant~~Use constant both I_A and I_N ignition
IT-NAT		~~Constant I_A~~
~~IT-HDI~~		~~Including HDI dataset national resolution~~Use constant I_A and vary I_N ignition
IT-~~HDIs~~HDI		~~Including HDI dataset subnational resolution~~Include HDI at country level
F-W5E5	Flammability and emitted carbon	~~Uses~~Prescribed W5E5 ~~climate forcing dataset~~
~~F-20CR~~ F-20CR		~~Uses 20CRv3 climate forcing dataset~~meteorology Prescribe 20CRv3 meteorology
BA-~~AVG~~	~~Average~~CST ~~Burnt area~~	Burnt area Use constant BA regardless of PFT

https://doi.org/10.5194/egusphere-2025-3579 Preprint. Discussion started: 19 August 2025

BA-RND		Randomly switched BA_{PFT} through PFT
CC-VAR	Emitted carbon	Vary CC across PFTs
CC-VAR CC-EXTDEL	CC	VaryingRemove the constraint brought by CC based on van Leeuwen et al. (2014) Extended CC from 0 to 1burnt carbon
EF-AVG EF-RNDCST	Emission factorEmitted CO	AverageUse constant EF regardless of PFT Randomly switched EF_{PFT} through PFT
NO-FDBK	Feedback	Turn off outputs from INFERNO to JULES
EC-PFT-OBS	PFTsTransversal influence	Turn off outputs from INFERNO to JULESPrescribe observational-based PFTs

We also investigate the impact of factors such as BA_{PFT}, $EF_{CO,PFT}$ and CC on simulated CO. For this, we used two experiments used the ERA5 climate forcing dataset, while F-W5E5 and F-20CR, one with constant BA and the other with constant EF_{CO}. These experiments also provide information on the effect of PFTs on the factors. The experiments are labelled as BA-CST and EF-CST, and for these we respectively used the W5E5 and 20CRv3 datasets. For the burnt area, emitted carbon, and 0.8 km^2 fire^{-1} for BA and 78 gkg^{-1} dry matter for EF_{CO}. Regarding the combustion completeness, the parameters BA_{PFT}, CC, and EF were modified accordingly. factors, for $CC_{min,leaf}$ and $CC_{max,wood}$, we used literature-based values that vary across PFTs (van Leeuwen et al., 2014) (see Table S1), since they are

In addition, a no-feedback experiment was also conducted (NO-FDBK), which disables the outputs from INFERNO being passed to JULES and TRIFFID (i.e., INFERNO does not contribute to carbon losses and does not influence fire disturbance to the PFTs). Aconstant for the control fun. However, we still set $CC_{max,leaf}$ and $CC_{min,wood}$ as 1 and 0, respectively, regardless of PFT, as for the control. We named this experiment CC-VAR. We also use a scenario with CC_{min} and CC_{max} as 0 and 1 for both leaf and wood. In this way, CC is removed from Equation 6 and the EC_{PFT} will then depend on soil moisture to calculate how much carbon from leaf and wood is simulated to be burnt. This experiment is named CC-DEL, as the emission calculations are now effectively independent of CC in INFERNO.

Additionally, for the sensitivity analysis, we included a prescribed PFT experiment was conducted (EF-PFT), using, PFT-OBS, as a way to evaluate the performance and sensitivity of the model to a different and more accurate PFTs. For this, we used an annual- resolution PFTsPFT dataset generated by JULES in the ISIMIP3a team (Mathison et al., 2023) based on the work of Harper et al. (2023)), and prescribed land use from the Land-Use Harmonisation dataset provided for ISIMIP3 (Volkholz and Ostberg, 2022). This dataset covers the study period only until 2019. The dominant prescribed PFTs through SA according to the dataset are

illustrated in Fig. 1a compared with the output from TRIFFID (1b),through 2019, so 2020 and 2021 used the same PFT fractions as 2019. Finally, we wanted to evaluate the scale of INFERNO feedback in its own simulation using a no-feedback scenario, labelled NO-FDBK. In this experiment, the outputs from INFERNO are not passed to JULES or TRIFFID. Therefore, in NO-FDBK, INFERNO does not contribute to carbon losses and PFT perturbation and competition. These processes are parametrised instead (Burton et al., 2019).

Figure 1a illustrates the dominant PFT for the prescribed dataset, while Fig. 1 b shows the modelled PFT by TRIFFID. The distribution of PFT presents slight changes in North SA, where the dominant PFT, according to both, is BET Tr (~50%). For Mid-SA, BET Tr is also dominant; however, the modelled PFT distribution also presents a high fraction of BDT (13%), C4G (18%), and soil (15%). BET Tr for the prescribed dataset is around 50%, while TRIFFID modelled around 27% throughout the study period. Contrary to the other two regions, in South SA, the soil cover dominates (~25%), followed by the PFT C3Pa (~15%) according to both the simulated PFT and the observation-based dataset.

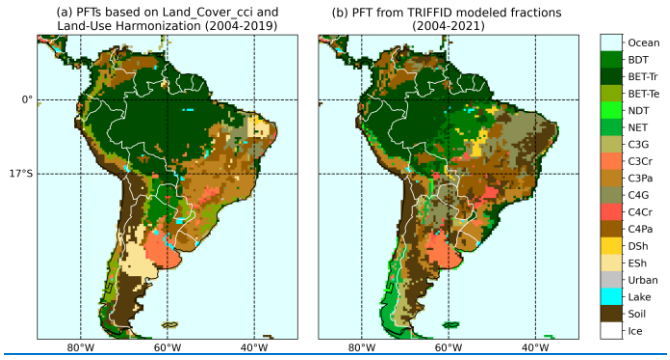

Figure 1. Average dominant Plant Functional Types over South America from 2004 to 2021 (a) generated by JULES ISIMIP3a team (Mathison et al., 2023) based on ESA Land Cover Climate Change Initiative (Land_Cover_cci) and the Land-Use Harmonisation datasets and (b) modelled by TRIFFID for this study.

2.65 CO emissions variability and comparison

https://doi.org/10.5194/egusphere-2025-3579 Preprint. Discussion started: 19 August 2025

2.5.1 Mean relative range

We use the Average Relative mean relative range (Range (ARR) of %) to quantify the average variation in estimated fireannual CO emissions across different inventories to quantify the level of variation among them. for a specified region or zone. To calculate the ARR,Range%, we first computecomputed the annual range of total CO emission estimates (y) for the area for each year i in the study period, defined as the difference between the maximum and minimum values across inventories. These ranges are then normalizednormalised by dividing itthem by the average emission magnitude ofacross the respectiveinventories for each year. The resulting values are averaged over the entire study period and multiplied by 100 to express the ARRRange% as a percentage, as Equation 8 describes.

$$ARR = \frac{1}{N}\sum_{i}^{N}\frac{max(y_i) - min(y_i)}{\overline{y_i}} \times 100 \qquad Range\% = \frac{100}{N}\sum_{i}^{N}\frac{max(y_i) - min(y_i)}{\overline{y_i}} \quad (8)$$

To assess the significance of comparisons between pairs of CO emissions estimated by different inventories or between an inventory and INFERNO, we employ the non-parametric Mann-Whitney U rank test.

The emissions trend was determined using the Man-Kendall test based on annual CO emissions. We calculate the trend for two periods: the complete study period (2004 to 2021), which is the long-term trend, and the period from 2014 to 2021, which is the short-term trend. The short-term period was chosen based on the availability of the IASI-TCCO dataset, which was retrieved from 2014 for the instrument on board Metop-B. We calculate gridded trends, but general assessments are made using regional-scale data.

Range% is designed to inform about the spread of estimated CO emissions magnitudes, considering the wide range of results from satellite-based estimations. The INFERNO simulations do not contribute to this metric.

2.5.2 Trend CO emissions calculation

We use CO emissions trends to assess the temporal evolution of CO emissions from inventories and INFERNO. To calculate the trends, we use the ordinary least squares linear regression (Perktold et al., 2024). This returns absolute trend values ($Ggyr^{-2}$), which we express as a percentage relative to the intercept (i.e., representing CO emissions at the start of the assessment period). We quantified the statistical significance of the CO emissions trend derived from both the inventories and INFERNO using the Mann-Kendall test at the 95% confidence level (Hussain and Mahmud, 2019). The trend and its significance were separately calculated for the individual grid point data and the regional cumulative emissions based on annual CO emissions.

https://doi.org/10.5194/egusphere-2025-3579 Preprint. Discussion started: 19 August 2025

2.5.3 Percentage mean bias

We utilised the percentage mean bias (MBBias%) to assess the model's CO emissions biases related to spatiotemporal variations, seasonal cycles, and trends. As Equation 9 describes, this metric calculates the average difference between a set of gridded values based onfrom the model (denoted as x) and a corresponding set of gridded observational values (denoted as y). The observational values are used to scale these differences as the equation shows.

$$MB\% = \frac{1}{N}\sum_{i}^{N}\frac{x_i - y_i}{y_i} \times 100 \qquad Bias\% = \frac{Mean(\mathbf{x}-\mathbf{y})}{Mean(\mathbf{y})} \times 100 \tag{9}$$

In Equation 9, x and y refer to different variables depending on the MBBias% to be calculated. For the spatiotemporal MBBias%, x and y denote the annual CO emissions, while i refers to each year within the 18-year study period. In contrast and are defined on time-latitude–longitude coordinates. Conversely, for the seasonal cycle MBBias%, x and y indicate the gridded seasonal cycle amplitude for each year, . The amplitude is determined by subtracting the mean of three consecutive months centred on the month of y maximum monthly CO emissions during the peak period from the maximum emissions during average magnitude of the non-fire season (based on observations), withremaining months.

i again representing each year.245 Finally, for the trend MBBias%, x and y correspond to the trend over a specified range of years, and i outlines the sets of years spanning gridded trend of CO emissions from (2014, 2021), (2013, 2021), down to (2014-n, 2021), ultimately reaching (2004, 2021). It is important to note that2004 to 2021, which are calculated as explained in Section 2.5.2. For the seasonal cycle and trend Bias%, x and y are defined on latitude–longitude coordinates.

As this metric was also implemented for the trend MB%, N equals 11 (total set of years included).

Additionallysensitivity analysis, x magnitudes were replaced with the corresponding information from every model run, including control and thesensitivity experiment proposed in Section 2.5. Similarly,run 2.4. While y magnitudes were replaced by the five inventories in this study. So every 265 model control run was compared against every inventorydata.

2.6.1Machine learning for understanding INFERNO CO emission biasbiases explainability

250 Similar to other studies (Hess et al., 2023; Liu et al., 20222022a), we employedutilised machine learning (ML) to assess model biases.to identify the key factors causing annual biases in CO emissions and their potential contributions to mitigate these biases. Specifically, we calculated the annual biases of INFERNO by taking the difference between the total annual emissions simulated by INFERNO andsubtracting the average annual emissions estimated by the inventories. from the total annual emissions simulated by INFERNO. Our target variable consisted of annual pixel-scale

270 biases. The primary objective of our analysis was to identify the key factors contributing to these biases and to determine whether the inputs of INFERNO inputs (both prescribed and

modelled variables) were sufficient to explain the entire biasthem at this scale. For this analysis, we utilised a gradient-boosting framework implemented using the Python library XGBoost. (Chen et al., 2025).

We selectedchose 20 inputs from INFERNO to use as features for the MLmachine learning model, comprising. These comprised prescribed data and JULES outputs used by INFERNO to calculate emissions. These are: population density, lightning flash rates, precipitation rate, relative humidity, temperature, soil moisture, HDI, Wood carbon, leaf carbon and 11 PFTs. All PFTs were considered;

HDI, Wood carbon, leaf carbon and 11 PFTs. From Table 1 all PFTs were considered;however, NDTNeedleleaf Deciduous Trees and Needleleaf Evergreen Trees were merged to a single Needleleaf Trees PFT, and NET

Evergreen Shrubs and Deciduous Shrubs were merged to a single needle leaf (NT) type, and DSh and ESh were merged to a single shrub (Sh) type. From these, soilShrub PFT. Soil moisture, wood carbon, leaf carbon, and PFTs were directly taken from JULES simulations. The other variables were obtained from the original datasets prescribed as inputs to INFERNO. The inputs to the MLmachine learning model are the gridded datasets resampled to an annual resolution for the study period (2004 to 2021). We enable correlated features in the machine learning model, as in a gradient boosting model,

The 20 features were compared to remove those that cause redundancy in our predictors and ensure independence between features. To evaluate multicollinearity, we calculated the correlation between pairs of factors and the variance inflation factor (VIF), which describes how much of the variability of a particular feature can be explained by the other features. A VIF lower than 10 is recommended.

The data were any redundant information is automatically disregarded. This happens because the decision trees are built by splitting features in a series of dependent trees, so they can not make identical splits using correlated features (Power et al., 2024).

The dataset was randomly splitpartitioned into training (80%) and testing (20%) datasets insubsets within a five-fold cross-validation exercise toframework. This strategy helps ensure

the independent that model performance of the specific training/test sets. The model was is evaluated using the coefficient of determination (R^2) metric, the Root Mean Square Error (RMSE) and Mean Absolute Error (MAE).

independently of any single training–testing split, reducing the risk of overfitting and improving generalizability. We ran a hyperparameter tuning to select the parametershyperparameters

that lead to the best model performance. This was conducted using a random search method on each training set in a five-fold cross-validation. We used Sklearn's RandomizedSearchCV with 500 iterations (i.e., n_iter). The considered parameters were: max_depth, gamma, reg_lambda, colsample_bytree, min_child_weight, learning_rate, subsample, n_estimators. For information about these parameters, see Chen et al. (function with 500 iterations (i.e., n_iter=500) (Pedregosa et al., 2011). The model's performance was evaluated using the coefficient of determination (R^2), which indicates how much of the

variability in the target CO emission biases is captured by the XGBoost model. Additionally, the Root Mean Square Error and Mean Absolute Error measure the average difference between the predicted and actual values, with Root Mean Square Error being more sensitive to outliers.

Since the objective was to identify the key factors contributing to the biases in CO emissions from INFERNO, special attention was given to the feature contribution methodology. We employed the Shapley additive explanations (SHAP) method using the Python package from Lundberg et al. (2020). SHAP is based on cooperative game theory and measures each feature's contribution to each prediction by calculating SHAP values. These values are calculated using a weighted average of the differences in predictions when the feature is added to all possible subsets of the remaining features (Lundberg et al., 2020). We have used SHAP values to explain the dominant drivers in fire emissions in a consistent way with other recent studies, which also exploit machine learning methods for wildfire result applications (Wang et al., 2023b, 2022; Liu et al., 2024). SHAP values are computed for every prediction in the test set for every iteration of the five-fold cross-validation process.

~~subsets of the selected features in which the specific feature can contribute (Lundberg and Lee, 2017). A SHAP value is calculated for every predictor in the testing dataset. We calculate the SHAP values using a five-fold cross-validation approach. For this, we randomly split the dataset into five groups. In each of the five iterations, four of the groups are used as the training dataset, while the remaining group serves as the testing dataset. This allows us to calculate a complete set of SHAP values for the whole dataset and calculate a map of contribution. We finished with 18 groups of SHAP values for every pixel that correspond to the number of annual CO emission biases included in the analysis.~~

We utilise two additional features to assess the SHAP values: the first feature categorises the pixels into North-SA, Mid-SA, and South-SA, while the second feature identifies the pixel's location on a map. With this, we can describe SHAP values based on their geographical location. These extra features were only used after calculating the SHAP values, so they were not used to train the model. To calculate the dominant feature by pixel, we identify the feature with the largest positive (negative) SHAP value on pixels with an average positive (negative) CO emission biasesbias. Once we established the most important feature for each pixel across the years, we calculated the mode to identify which feature consistently contributes the most.

3 Results and discussion

3.1 Estimated and modelled CO fire CO emissions in SA

Most of SA's CO fire emissions are concentrated in the The Arc of Deforestation region in Mid-SA, as shown by both accounts for around 40% of the in

310 ventories and INFERNO (Fig. 2). Here, FINNvn2.5 estimates the highest annual fire CO emissions (70.8 $Tgyr^{-1}$), followed by GFEDvn5 (37.0 Tgy^{-1}). GFEDvn4s, GFASvn1.2, 3BEM-FRP and INFERNO are approximately one-third of FINNvn2.5 emissions in the Arc of Deforestation with 21.1 $Tgyr^{-1}$, 19.0 $Tgyr^{-1}$, 21.2 $Tgyr^{-1}$ and 26.3 $Tgyr^{-1}$, respectively. The estimations of in South America. Figure 2 demonstrates the extent to which the inventories on the Arc of Deforestation have an ARR of 157% and are able to represent around 30-80% of the total annual substantial CO emissions source from fires in Mid-SA, listed in Table 3. However, this is lower for INFERNO (23%), despite estimating

315 similar CO emissions as the inventories for both the the deforestation front and Mid-SA. This is in part because INFERNO cannot accurately reproduce the specific details of the deforestation zone, even though it broadly identifies the area. Many fires in this region occur on a smaller scale than the INFERNO resolution, even overlooked by MODIS products (1 km resolution) (Liu et al., 2020). The inventories display finer detail due to their five times higher resolution and adjustments for smaller fires, such as those included in GFEDvn4s and GFEDvn5. However, GFEDvn4s demonstrates limitations in identifying emissions on the. Here,

320 eastern side INFERNO generally captures the broad-scale features of emissions from this source, including its latitude-longitude range.

295 This level of performance in relation to inventories is typical in global fire models like INFERNO. This is due to the inherent challenges in simulating a stochastic process, such as ignition, at a detailed scale using only vegetation data, meteorological information, and population density (Rovithakis et al., 2025). Therefore, simulating fine-scale features in a variable region, such as the Arc of Deforestation, are outside the scope of INFERNO. On this deforestation front, the PFTs appear to drive the spatial distribution of CO emissions in the INFERNO simulations, using the relative abundance of Broadleaf Deciduous

300 Trees and Tropical Broadleaf Evergreen Trees. However, the large area of emissions results in a general overestimation of the Arc of Deforestation in comparison to the updated version, GFEDvn5. According to Teixeira et al. (2021), the INFERNO model CO emissions in areas dominated by both Tree PFTs. INFERNO overestimates CO emissions in this area by up to 300% compared to GFEDvn4s. However, GFEDvn4s likely underestimates Mid-SA with a spatiotemporal Bias% of around 72% (see Table 2).

The Arc of Deforestation, however, demonstrate challenges not only for INFERNO, but also for the inventories, whose annual estimates have a Range% of 84% in the deforestation front. Liu et al. (2020) highlights small fires and surface obscuration

https://doi.org/10.5194/egusphere-2025-3579 Preprint. Discussion started: 19 August 2025

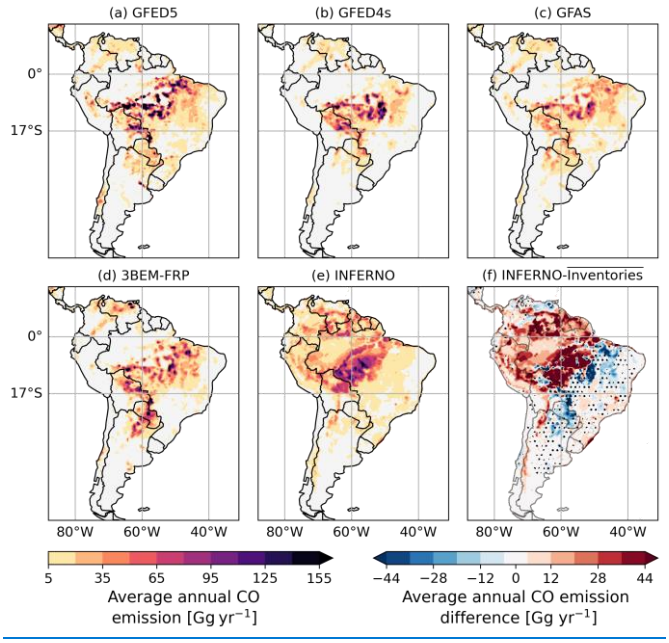

Figure 2. Annual mean fire CO emissions ~~in this~~for 2004-2021 estimated by (a) GFED5, (b) GFED4s, (c) GFAS, (d) 3BEM-FRP, and simulated by (e) INFERNO. (f) shows the absolute differences between the INFERNO simulated and the average estimate of fire CO emissions. The areas hatched with dots in (f) describe when the simulated and estimated emissions are statistically similar according to the Mann-Whitney test.

due to cloud or haze as important sources of uncertainty in the estimations for this region. Here, GFED5 estimates the highest annual total fire CO emissions (37.0 *Tg yr*$^{-1}$). In contrast, GFED4s, GFAS, 3BEM-FRP estimate emissions of 21.1 *Tg yr*$^{-1}$, 19.0 *Tg yr*$^{-1}$ and 21.2 *Tg yr*$^{-1}$ respectively, which are approximately 40% of GFED5 estimations.

The Mid-SA region~~, as highlighted.~~

The Mid-SA region also containsincludes the deforestation front in the Cerrado ecoregion, a fire-prone ecosystem with a mixturemix of grasslands, shrublands, and forests, where fire frequency ranges from 3 to 6 years (Júnior et al., 2014). This accounts for around 10% to 20% of CO

325 emissions in Mid-SA. GFEDvn5, FINNvn2.5 and INFERNO estimate the lower contribution of these zones to the total emissions.. The inventories, however, agree on estimating CO emissions of around 9.3 $Tgyr^{-1}$ (ARR:39%). INFERNO estimation of 7.5 $Tgyr^{-1}$ is in the interquartile range of the annual estimations from most of the inventories (except FINNvn7.5).Range%:42%).

It is clear that GFEDvn5 and FINNvn2.5, as well as INFERNO, present particularly high magnitudes of CO emissions in forest areas (see Figure 1 and 2). This might be related to the higher BA calculated by these inventories. For FINNvn2.5,

330 only for the forest biome, multiple fire detections in adjacent pixels are assumed to correspond to a large fire (Wiedinmyer et al., 2023). However, using this approach plus VIIRS observations led to overestimating CO emissions in the southern part of the Amazon forest (Wiedinmyer et al., 2023). The version of FINNvn2.5 used in this study (i.e., based only on MODIS fire hotspots) estimates significantly lower CO emissions than the version that includes VIIRS hotspots for SA. On the other hand,

GFEDvn5 contains an adjusted BA based on Landsat observations, although this is still a beta version. GFEDvn5 estimations

335 surpass the BA and carbon emissions estimated by GFEDvn4s (Chen et al., 2023; Qi et al., 2024; Blackford et al., 2024), and consistently surpass the CO emissions estimated by GFEDvn4s in this study (p-value <0.05).

For this study, GFASvn1.2 has the lowest average annual CO emission in 310 In this context, the INFERNO estimation of 7.5 $Tg\ yr^{-1}$ falls within the interquartile range of estimates from most inventories. In contrast to the Arc of Deforestation, INFERNO incorporates more of the relevant elements to simulate the fire-prone nature of the Cerrado, which can be highly dependent on both vegetation and meteorological conditions, even when it is also influenced by anthropogenic actions.

Mid-SA, yet with a similar annual regional distribution to 3BEM-FRP and GFEDvn4s (p-value≥0.05), see Table 3. However, Naus et al. (2022) suggest an underestimation of CO emissions from GFASvn1.2 after prescribing the emissions into an atmospheric model and comparing the calculated 340 TCCO against the TCCO retrieved by MOPITT and IASI (Naus et al., 2022).

With ~25% of CO annual CO emissions in SASouth America, North-SA and South-SA also contain hotspots of particularly high CO fire emissions. In particular interest.

315 In North-SA, the fire-prone Llanos ecregionecoregion, a mosaic of grasslands and savannas between Colombia and Venezuela, contains around 35% CO of the region's annual fire CO emissions in the subregion according to most of the inventories,

except for 3BEM-FRP, which estimates 58% of the annual emissions for North-SA contributed by the Llanos ecoregion (4.6 $Tgyr^{-1}$). The ARR magnitude. The CO emissions estimates have a Range% of 33%. In the Llanos ecoregion, INFERNO simulates emissions to be within the inventory's range (2.1 $Tg\ yr^{-1}$); however, for the model, this is only 10% of total North-SA emissions. This is because in North-SA, INFERNO inaccurately simulates higher emissions from areas dominated by Tree PFTs (see Fig. S2). for the Llanos ecoregion, including (not including) 3BEM-FRP is 129% (46%). INFERNO estimates a smaller contribution of 10% (2.1 $Tgyr^{-1}$) for the Llanos ecoregion, but within the inventories range, since the annual estimate of CO emissions for North-SA is significantly higher than for the inventories (p-value <0.05). As in Consequently, the CO emissions simulated by INFERNO in North-SA are 2 to 4 times higher than those shown in the inventories (see Table 2).

Mid-SA, FINNvn2.5 estimated particularly high emissions on the deforestation front in the north of the Amazon (2.7 $Tgyr^{-1}$), four times higher than other inventories, and two times higher than INFERNO. The ARR of inventories in the Amazon northern deforestation front is 212% (37%) including

(excluding) FINNvn2.5. In South-SA, the Dry and Humid Chaco ecoregion contributes around 37% of CO fire CO emissions to the region according to most of the inventories, except for 3BEM-FRP, which estimates a contribution of around 54% (9.4 $Tgyr^{-1}$). The high CO emissions from

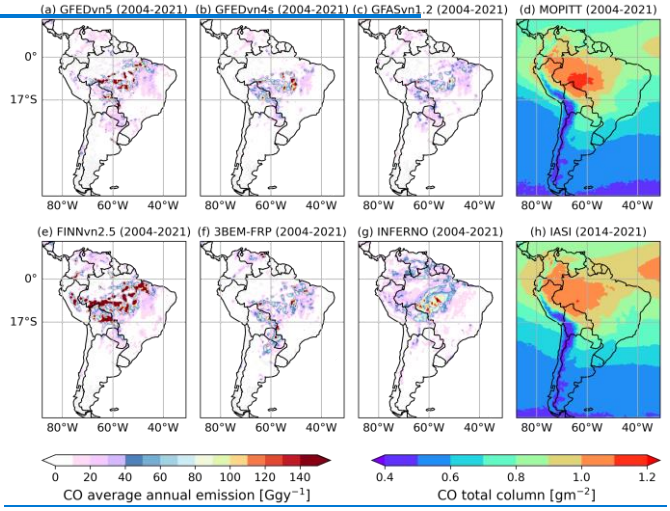

https://doi.org/10.5194/egusphere-2025-3579 Preprint. Discussion started: 19 August 2025

Figure 2. Annual mean fire CO emissions for 2004-2021 estimated by (a) GFEDvn5, (b) GFEDvn4s, (c) GFASvn1.2, (e) FINNvn2.5, (f) 3BEM, and modelled by (g) INFERNO and TCCO retrieved from MOPITT (d) and IASI (h). Note that the average TCCO from IASI ranges from 2014 to 2021.

Tgyr^{-1}). The high CO emissions from 3BEM-FRP were previously linked to the combustion factor used in the inventory based on FEERvn1FEERv1.0 (Pereira et al., 2022).

The ARR magnitudeRange% magnitudes for the Chaco ecoregion, including (and not including) 3BEM-FRP is 132% (66%). are 124% and 55%, respectively. In this ecoregion, INFERNO estimates lower annual CO emissions than the inventories (2.3 *Tgy*$^{-1}$), but still in). The model only falls with the GFED4s annual emission interquartile range of annual emissions estimated by GFEDvn4s, which present significantlyas this inventor is substantially lower emissions than the other inventoriesothers in this ecoregion (see Fig. 2).

These fire active areas assessed in this study (i.e., Arc of Deforestation, Cerrado, Chaco, Llanos, and Amazon northern deforestation front) explain over 70% of CO emissions in SA; however, they account for around 32% of emissions simulated for INFERNO in the region. This is potentially caused by e.g. the model resolution and simplified process representation, andparticular ecoregion is not well represented by TRIFFID either, which simulates higher proportions of C4 Grasses to be the dominant PFT, whereas more satellite-informed datasets describe the dominant PFT as Broadleaf Deciduous Trees (see Fig. S2). Despite not capturing the active fire zone for South-SA, INFERNO annual CO emissions are within the range of CO emissions estimated by the inventories. Here, the CO emissions are balanced by the overestimation of emissions over ecoregions, as within the Amazon forest. The inventories, however, describe a broad split of the estimated CO emissions in the Temperate Broadleaf Evergreen Tree-dominated region in the Andean mountains.

In general, the annual CO emissions estimates from the inventories for Mid-SA and North-SA, with ARRs have a Range% of 138102% and 124196%, respectively. Without including FINNv2.5, the ARRs fall even below half, 62% and 65%, respectively , suggesting higher, indicating lower agreement between the inventories than for South-SA (Range%=76%). Conversely, North-SA has the highest absolute spatiotemporal Bias% (285%), and the inventories differ on whether INFERNO, on average, overestimates or underestimates emissions in South-SA. The Bias% in Mid-SA are lower than 100%, but is the highest in absolute magnitudes (see Table 3). South-SA presents an ARR of 75% (73%) including (no including) FINNvn2.5.2).

In Fig. 2, the TCCO illustrates how these fire emissions are concentrated in Mid-SA on the east side of the Andean mountain, where emitted CO accumulate enhanced by the longer lifetime of CO over the Amazon (Lichtig et al., 2024). The accumulation at the east and north of the Andean mountain range is evidenced in North-SA. Furthermore, the influence of easterly transport of the smoke plume from Africa is clear (Holanda et al., 2020; Lichtig et al., 2024).

3.1.1Intra-annual variability and seasonalSeasonal cycle of CO fire CO emissions in SASouth America

https://doi.org/10.5194/egusphere-2025-3579 Preprint. Discussion started: 19 August 2025

SASouth America has a distinct seasonal cycle in fire activity, illustratedrepresented spatially in Fig. 3 (b),(c),(d),a) with the timing of the emissions peak, and by Fig. 3 (c),(d),(e) with the average monthly CO emissions. The emissions show high fire activity from August to October for in Mid-SA and South-SA, and from January to April forin North-SA. The differences between the inventories in the regions studied are significantly enhanced during the peak CO emissions periods, which drivesAs expected, the more fire-active period is when inventories differ more, leading to the annual differences discussed above. However, the differences between them remain consistent through the study periodover time, allowing the inventories to exhibit a high correlation in their monthly total CO emissions (R > 0.9) for monthly emissions at the regional scale (see Fig. S3). Although INFERNO monthly CO emissions do not capture the desired seasonal cycle acrossS2). In Mid-SA during the peak period, the estimated CO emissions of FINNvn2.5 exceed all other inventories and INFERNO (p-value≤0.05), while GFASvn1.2 has the lowest average CO emissions, yet this is not significantly less than GFEDvn4a and 3BEM-FRP (p-value>0.05). During the peak fire period in North-SA, FINNvn2.5 estimates the largest emissions among inventories, probably due to the larger burned area assumed for forest cover. 3BEM-FRP has the next highest emissions, which are also higher than GFEDvn5, GFASvn1.2 and GFEDvn4s (p-value<0.05). These last two inventories demonstrated a similar monthly regionally accumulated distribution (see Fig. 3) of CO emissions and lower magnitudes than GFEDvn5. For South-SA, the peak CO emissions also showed a significant difference between pairs of inventories. Here, 3BEM-FRP had the highest magnitudes (p-value≤0.05), while GFEDvn4s had the lowest (p-value≤0.05) relative to the other inventories. GFEDvn5 is greater than GFASvn1.2 and FINNvn2.5, while these had a similar distributions.

Figures 3 (b) and (dthe three regions analysed, the monthly total emissions still show a strong correlation with the inventories (R > 0.73). Here, INFERNO is constantly higher than the inventories in non-fire seasons (see Fig. 3), thus over predicting background fire activity.

https://doi.org/10.5194/egusphere-2025-3579 Preprint. Discussion started: 19 August 2025

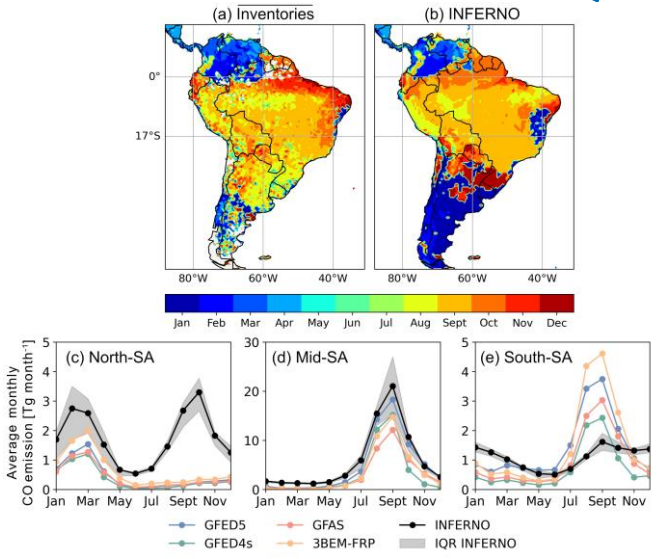

Figure 3. (a) CO emissions peak timing across South America based on the (a) average estimates of CO emissions and (b) INFERNO CO emission simulations, and the average seasonal cycle of the estimates and simulated CO emissions for (c) North-SA, (d) Mid-SA and (e) South-SA. (c), (d) and (e) shadow range describe the inter-quartile range (IQR) of INFERNO monthly emissions.

Figure 3 (d) highlights how INFERNO simulates a seasonal cycle peaking in September, similar to the inventories for Mid-SA. Within the inventory range, the GFED5 average seasonal cycle sits within the INFERNO interquartile range. In fact, between August and October, INFERNO and GFED5 show similar distributions (i.e., not significantly different). However, outside this period, INFERNO total monthly emissions are larger than all of the inventories. Spatially, Fig. 3 shows that INFERNO manages to simulate the timing of the CO emission peaks for the fire-active areas in Mid-SA. In fact, the absolute Bias% in the seasonal cycle amplitude is less than 10% compared to most of the inventories (see Table 2), except for comparison with GFED5. The GFED5 dataset exhibits a large seasonal cycle, particularly across the Arc of Deforestation, which contributes to higher average amplitudes.

Figure 3 (d) and (e) show that INFERNO inaccurately represents the seasonal cycle in both North-SA and South-SA~~,~~

https://doi.org/10.5194/egusphere-2025-3579 Preprint. Discussion started: 19 August 2025

However, its representation in Mid-SA is more consistent with the inventories. For North-SA, the peak period of the fire activity is well represented, but the model generates a second peak slightly higher than the first one, centred on October. This might be related to the relatively high contribution of gross primary productivity (GPP) to fire activity in INFERNO. While the first simulated peak of emissions in the year appears to be driven by high flammability, the second follows GPP variability, with relative average flammability and precipitation conditions (see Fig. S3). Furthermore, the representation of the seasonal cycle of precipitation in this region in particular may be deficient due to ERA5 limited representation of the Intertropical Convergence Zone (ITCZ) (Lavers et al., 2022). In North-SA, INFERNO estimated CO emissions are higher than most inventories (p-value ≤ 0.05), particularly outside the peak fire periods.

In contrast to North-SA, INFERNO's CO emissions in South-SA at the observed peak have lower average values than all inventories; in fact, the peak is barely represented. However, the estimated emissions are higher than those in the inventories from November to February. In this period, both simulated flammability and GPP contribute to high fire activity, despite being the peak of precipitation in the east of the Andean Mountains (Grimm) (see Fig. S3). Although fire activity in this arid ecoregion is highly susceptible to precipitation accumulation which enhanced GPP, it tends to exhibit a delay following the precipitation peak (San Martín et al., 2023).

The TCCO in Fig. 3b-d follows the emission season cycle, showing a rapid increase from August to September in Mid-SA, with a slower decrease corresponding to the long lifetime of CO in the atmosphere. The TCCO in both North-SA and Mid-SA

https://doi.org/10.5194/egusphere-2025-3579 Preprint. Discussion started: 19 August 2025

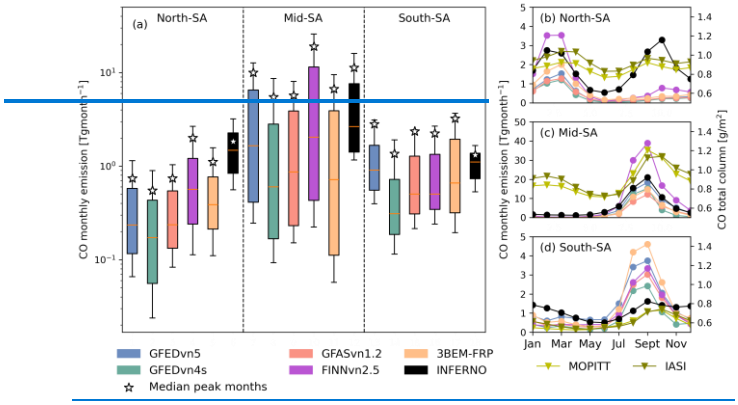

Figure 3. (a) Distribution of monthly regionally accumulated CO fire emissions and seasonal cycle for (b) North-SA, (c) Mid-SA and (d) South-SA and their respective mean TCCO seasonal cycle in the period 2004-2021 (2014-2021 for IASI). The retrieved TCCO is represented only in panels (b), (c) and (d), and their, but with magnitudes are read from the right y-axis; those cycles are marked with an inverted triangle. Panels (b), (c) and (d) have different ranges for the left y-axis, while panel (a) has a logarithmic scale for the y-axis. The stars in (a) describe the mean emissions for the fire activity peak for each region that are: from higher than any of the inventories for January to April for. Additionally North-SA, July to October for Mid-SA and August to October for South-SA.

400 presents a bimodal season, which does not mirror the region's fire CO emissions, but rather evidences transport throughout hemispheres, as well as from Africa to SA.

3.1.2 Trends of CO fire emissions in SA

From 2004 to 2021, Mid-SA experienced an average annual decrease of ~2.8%yr $^{-1}$ in CO emissions according to the inventories, with a significant trend observed for GFASvn1.2 (see Table 3). The INFERNO model aligns with the inventories,

https://doi.org/10.5194/egusphere-2025-3579 Preprint. Discussion started: 19 August 2025

indicating a negative trend of 1.8% yr^{-1}; however, it does not represent a significant decrease in CO emissions in the Arc of Deforestation. In North-SA, both the inventories and INFERNO agree on an increase in CO emissions, with a positive trend ranging from 0.7% yr^{-1} to 9.3% yr^{-1}. This is only significant for 3BEM-FRP, which estimates the highest rise in CO emissions. In South-SA, the calculated trend was not significant for the inventories, and there was some disagreement among them regarding the direction of the trend. Nonetheless, most inventories and INFERNO suggested a negative trend of approximately ~1.0%yr^{-1}.

The observed trends in CO emissions aligned with the observed reduction in BA of around 2%yr^{-1} and 1%yr^{-1} for MidSA/South-SA and North-SA between 2001 and 2020 (Chen et al., 2023). However, as for CO emissions, the BA and the carbon emissions did not decrease significantly across all SA (Chen et al., 2023; Aragão and Shimabukuro, 2010; Chen et al., 2013).

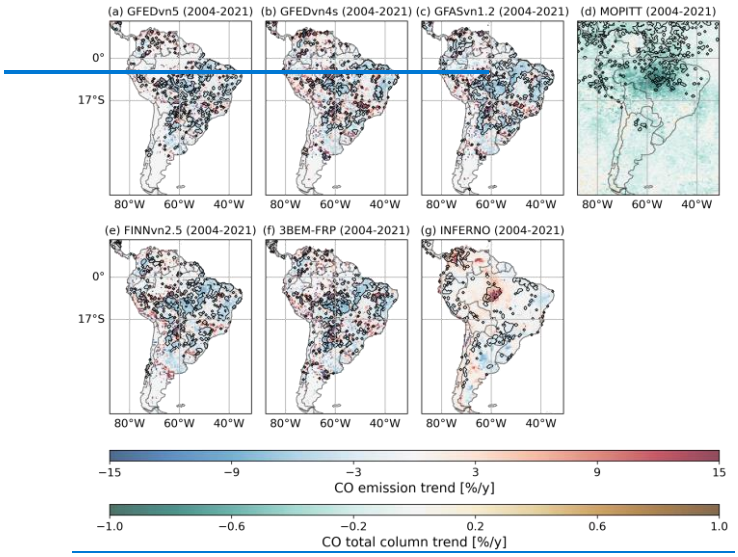

Figure 4. Long-term (2004-2021) fire CO emission trend estimation [%/y] based on (a) GFEDvn5, (b) GFEDvn4s, (c) GFASvn1.2, (e) FINNvn2.5, (f) 3BEM-FRP, and (g) INFERNO and TCCO trend estimated based on retrievals from (d) MOPITT. The areas enclosed by the black contour represent zones with a significant trend in CO emissions (p-value≤ 0.05)

https://doi.org/10.5194/egusphere-2025-3579 Preprint. Discussion started: 19 August 2025

As Figure 4 shows, although a large fraction of SA presents a negative trend, there are also areas of positive trends in CO emissions. The inventories agree with the significant reduction of CO emissions in the Arc of Deforestation, particularly in the states of Pará and Mato Grosso in Brazil, east and south of the Amazon. The emission also decreases significantly in the Caatinga ecoregion in the eastern part of Brazil. In contrast, the northeastern part of the Cerrado, in the large agriculture frontier recognised as MAranhão, TOcantins, PIauí and BAhia (MATOPIBA) presented a positive trend in CO emissions that aligns with an observed increase of BA in part of this frontier (Milare et al., 2024; Pope et al., 2020). Most inventories also agreed with an increase in CO emissions in the northern coastal region of North-SA and South-SA around the Río Negro province of Argentina, in the middle of the latitude range of the country.

Although contrary to the inventories, INFERNO show an increase in CO emissions in the Arc of Deforestation; it captures the decrease in emissions in the Caatinga region and the slight increase in emissions in northern Colombia and Venezuela and the south in Argentina. With this, INFERNO and JULES simulations suggest some underpinning factors driving the observed trend. For Caatinga, INFERNO identified decreased ignitions and carbon availability (See Fig. S5). On the contrary, more wood carbon and increasing ignition were simulated in Argentina (Figs. S4 and S7). For the northern part of North-SA and the Arc of Deforestation, INFERNO describes more flammable conditions.

In support of the general decreasing CO emissions trend among inventories, the MOPITT TCCO identifies a general decreasing trend of 2%yr^{-1}, particularly significant in the Amazon and Cerrado ecoregions (Fig. 4 (d)). This has previously been observed for the period 2003 to 2018, where TCCO evidenced decreasing magnitudes, especially in forested areas (Naus et al., 2022; Deeter et al., 2018), where smouldering ignition dominates, and CO emission factors are high (Deeter et al., 2018). Naus et al. (2022) found a high correlation between the decline in TCCO and a decrease in deforestation enhanced by law enforcement policies in Brazil. In contrast, the increase of CO emissions observed in the north of North-SA and in the northeast of Cerrado was not reproduced by the change in TCCO. Nonetheless, observations suggest an increase in NO_x emissions in the northeast of the Cerrado (2005-2016) (Pope et al., 2020). The increasing emissions from these biomes, with relatively low CO emissions, might be offset by the surrounding decrease in CO, while the relatively high rate of NO_x emissions is substantial.

to the first peak. Although emissions in the Tree PFT domain to the east of the region tend to peak in October (Cummings et al., 2025) (see Fig. S3), these are negligible compared to the regional emissions around March. Furthermore, as this is the second

Table 3. Estimated CO emissions magnitude, seasonal cycle (SC) and trend summary

https://doi.org/10.5194/egusphere-2025-3579 Preprint. Discussion started: 19 August 2025

Table 2. Total annual fire CO emissions average magnitudes, seasonal cycle amplitude and trends for North-SA, Mid-SA and South-SA and INFERNO Bias% in these metrics compared with inventories

Item		GFEDvn5 GFASvn1.2GFED5	GFEDvn4s FINNvn2.5GFED4s	GFAS	3BEM-FRP	INFERNO
		North-SA	CO emission [$Tgyr^{-1}$]			
CO emission [Tgy^{-1}]North-SA	Mean (SD)	5.5 (2.0)	4.4 (1.8) 5.0 (1.3)	5.0 (1.3)	13.1 (4.4) 7.9 (2.9)	21.0 (3.6)
	INFERNO Bias%	279	382	317	164	0
SC amplitude [Tgy^{-1}]Mid-SA	Mean (SD)	1.3 (156.6 (23.1)	37.2 (20.3)	35.2 (17.1 1.1 (1.0) 1.1 (0.7)	3.4 (239.9 (19.5) 1.7 (1.2)	070.2 (2.115.8)
	INFERNO Bias%	24	89	99	76	0
Trend 2004-2021 [% yr^{-1}]South-SA	Mean (SD)	216.8 (4.9] 3.3 1.4	08.7 (4.0) 9.3	011.8 (2.7)	17.4 (6.4)	13.1 (1.2)
	INFERNO Bias%	-22	50	11	-25	0
			SC amplitude [$Tgyr^{-1}$]			
Trend 2014-2021 [% yr^{-1}]North-SA	Amplitude (SD)	0.49 (0.6)	1.1 0.97 (0.5) 5.9	0.58 (0.4)	-1.2.4 (0.7)	0.7 (0.9)
			Mid-SA			
CO emission [Tgy^{-1}]	56.6 (23.1)INFERNO Bias%	37.2 (20.3) 35.2 (17.1)11	108.4 (53.0)45	39.9 (19.5)	70.2 (15.8) 9	0
SC amplitude [Tgy^{-1}]Mid-SA	Amplitude (SD)	13.12.3 (5 7.8)	14.8 (9.8) 9.0 (6.30)	30.7 (18.9 (4.3)	129.8 (5.6 (9.0)	17.0 (6.913.2 (4.5)
	INFERNO Bias%	-31	1	9	-6	0

Deleted Cells
Inserted Cells
Inserted Cells
Deleted Cells
Inserted Cells
Inserted Cells
Deleted Cells
Deleted Cells
Inserted Cells
Inserted Cells
Inserted Cells
Deleted Cells
Inserted Cells
Inserted Cells
Inserted Cells
Inserted Cells
Inserted Cells

https://doi.org/10.5194/egusphere-2025-3579 Preprint. Discussion started: 19 August 2025

Trend 2004–2021 [% yr⁻¹] South-SA	-3.4	-1.8	-3.5	1.6 (1.0)	-1.9 (0.7)	-3.1 -1.8 (1.5)	0.4 (0.2)
	Amplitude (SD)	3.5	2.2 (0.9)				
	INFERNO Bias%	-82		-72	-78	-84	0

	Trend 2014 2004-2021 [% yr⁻¹]				0.5		4 2 3
						1.1	9 4 0
						-0.9	

			South-SA				
CO emission [Tgy⁻¹] North-SA	Trend (confidence)	16.8 (2.7 (-1.4,6.9)	8.7 (4.0) 11.8 (2.7 (-2.2,7.7)	12.5 (1.0 (-1.6,3.96)	17.4 (65.9 (1.5,10.4)	13.0.8 (-1 (1.0,2.6)	
	INFERNO Bias%	21	28	50	23	0	
SC amplitude [Tgy⁻¹] Mid-SA	Trend (confidence)	2.4 (1.3.0 (-5.6, -0.4)	1.9 (1.6) 2.1 (1.0)	-2.5 (6.5, 1.56)	-3.5 (29 (-6.4, -1.5)	-3.2 (-6.3, -0.1 (0.3)	1.6 (-0.8, 4.0)
Trend 2004–2021 [% yr⁻¹]	-2.9	INFERNO Bias%	0.2 1.230		-2.4 20	0.053	-0.827	0
South-SA	Trend 2014–2021 [% yr⁻¹] (confidence)	38.2 0.8 (-3.5,1.8)	3.0 (-2.5,8.5)	1 92 0.9 1 4.4 (-2.9, 1.1)	25. 06	33.51.6 (-2.4, 5.7)	2 0.4 (-1.3, 0.4)
	INFERNO Bias%	-9	-24	-8		-10	0

Note: The SC amplitude was magnitudes of trends are highlighted in bold when the Mann-Kendall test indicates a significant trend at the 95% confidence level (p-value≤0.05). Regionally aggregated annual CO emission time series are used for the temporal trend analysis. In the table, 'SD' and 'confidence' refer to the standard deviation values and the 95% confidence intervals. Notice that all Bias% are calculated by subtracting the maximum monthly based on gridded magnitudes (see Section 2.5.3), while the magnitudes of the metrics are based on total CO emissions for the regions.

rainy period in most of the region, fire activity in the September-October-November trimester is low in North-SA (see Fig. S3). In this trimester, however, JULES simulates particularly dry conditions in eastern North-SA, resulting in relatively low Gross

Inserted Cells
Deleted Cells
Deleted Cells
Deleted Cells
Inserted Cells
Inserted Cells
Inserted Cells
Deleted Cells
Inserted Cells
Inserted Cells
Deleted Cells
Inserted Cells
Inserted Cells

https://doi.org/10.5194/egusphere-2025-3579 Preprint. Discussion started: 19 August 2025

Primary Production (GPP) (see Fig. S5). This means that dry conditions, rather than carbon availability, might be leading to the overestimations in this period. Since fire activity typically peaks during the peak period from the maximum drier seasons, seasonal variability in lightning is not expected to have a significant impact on fire activity during this period. For South-SA, INFERNO's CO emissions during the non fire season. The have lower average peak magnitudes at the observed inventory peaks (average seasonal cycle of Bias% -79%), with no discernible peak period was determined as from shown in Fig. 3 (e). However, the estimated emissions are higher than the inventories from November to February. Spatially, INFERNO captures the September peak in the northern part of South-SA. However, towards the south, the timing of the emission peak changes rapidly, suggesting a simulated CO emission peak in December and January to April for North-SA, July to October for Mid-SA and , when INFERNO shows the largest overestimations of emissions. For the South-SA, both flammability and GPP explain the simulated seasonal cycle in one of the more fire-active zones, the Chaco region (San Martín et al., 2023). Here, although the rainy season coincides with the warmer months (around December to February), the larger dry areas of the Chaco region respond more to wet conditions and vegetation growth than to high temperatures. After this season, late in the colder and drier months (August to October, September), fire activity and emissions peak as the dry, abundant vegetation ignites. The wetter fraction of the Chaco region additionally peaks in February, as this is more sensitive to temperature and precipitation anomalies (San Martín et al., 2023). Peatlands are not represented in the JULES model, which means that INFERNO does not account for South SAthe conditions in the wet Chaco. However, the dry Chaco, which dominates in area, could be more accurately represented. Here, INFERNO's flammability appears to be heavily influenced by temperature and carbon load produced by the increasing GPP (see Fig. S6), so that precipitation does not reduce the likelihood of fires enhanced by the greater carbon availability.

In the short term, from 2014 to

3.1.2 Trends of fire CO emissions in South America

As Fig. 4 shows, the trends in CO emissions between 2004 and 2021, are neither consistent nor significant across South America. Spatially, a slight decrease in CO emissions predominantly cover the regions. The decreasing trend ofin CO emissions changed to positiveis significant across most inventories for some sections of the Arc of Deforestation and the Caatinga ecoregion (eastern part of Brazil), where the trends were around -6% yr^{-1}. GFAS exhibits the strongest trend with a significant decrease of ~2.8% yr^{-1} for the total CO emissions in Mid-SA and South-SA according(see Table 2). Contrary to the inventories. This, INFERNO shows a weak increasing trend for Mid-SA is probably partially explained by the recenttotal emissions (1.6% yr^{-1}), with overall trends overestimating those of the inventories (trend Bias% ~32%). Particularly, the model shows a large increase in emissions in the south of the Amazon forest, which does not agree with the inventories. Similarly, on a finer scale, INFERNO failed to capture the increase

in emissions observed near the Caatinga ecoregion, in the large agricultural frontier across the states of Maranhão, Tocantins, Piauí and Bahia in Brazil (Milare et al., 2024; Pope et al., 2020).

In the Mid-SA, both deforestation and dry conditions significantly influence the trend of fire-related CO emissions (Aragão et al., 2018). The relative influence of these and the lack of deforestation representation in INFERNO induce differences in the model's performance over time, affecting the simulated emissions trend. As deforestation in the Amazon gradually declined over the first 10 years of this study (Aragão et al., 2018), the role of drought in facilitating fires became increasingly prominent. For the period from 2004 to 2010 in Mid-SA, INFERNO showed a spatiotemporal Bias% of ~ 30%, indicating higher simulated CO emissions than the inventories (except for GFED5, for which the difference was only -3%). However, from 2011 to 2018, as deforestation ceased, INFERNO estimates rose to ~ 165% above all inventories (see Fig. S7). ~~in the Brazil portion of the Amazon, which for~~From 2019 ~~rose by ~~to the end of the study period, both deforestation and drought conditions occurred. In 2019, deforestation in Brazil escalated by approximately 80~~% after~~%, following the ~~easing~~relaxation of forest protection regulations~~, which decreased fines and reported infractions against flora by more than 50% despite the increments~~ (Gatti et al., 2023). ~~In Mid-SA, the CO emission trend switched to ~~At the same time, fire occurrence was further ~~1.6%yr $^{-1}$ according to four of five inventories, mainly due to anthropogenic activities~~ exacerbated by the extreme drought period in 2019-2022 (Geirinhas et al., 2023). During this period, INFERNO simulated fire emissions in Mid-SA continued to show an overestimation of around 165%. The shift in performance throughout the study

https://doi.org/10.5194/egusphere-2025-3579 Preprint. Discussion started: 19 August 2025

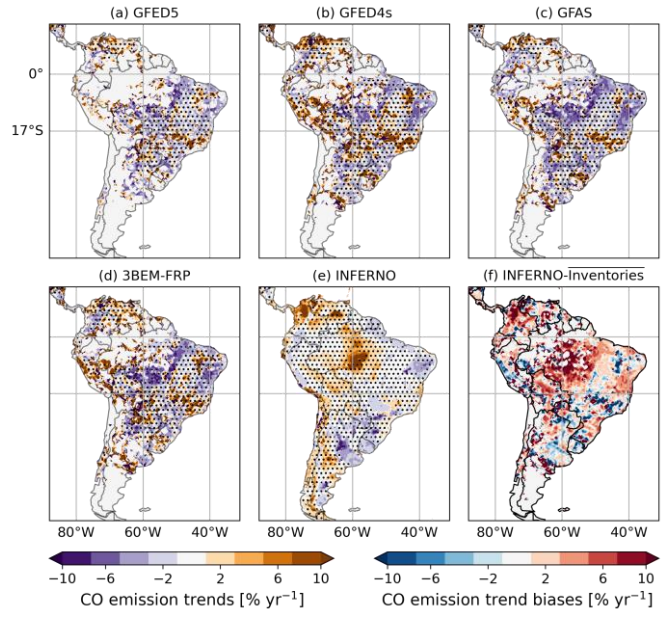

Figure 4. Fire CO emission trend 2004-2021 estimated based on (a) GFED5, (b) GFED4s, (c) GFAS, (d) 3BEM-FRP, and (e) INFERNO. (f) shows the differences between the calculated trend for INFERNO and the average estimates of fire CO emissions. The areas hatched with dots in (a-e) describe when the calculated trend is not significant according to the Mann-Kendall Trend Test.

period suggests a high sensitivity of the simulations to drought conditions, as flammability has increased over time, together with the overestimations. The trends, however (see Fig. S8), are negative across vast areas because they have been offset by diminishing carbon availability. Furthermore, the changing performance exhibits a potentially misleading offset effect over the 405 overestimations due to the lack of deforestation representation in the model.

In ~~2019, according to the inventories, this~~ North-SA, as in Table 2, the inventories and INFERNO agree on a non-significant increase in total annual fire CO emissions, which is only significant for 3BEM-FRP. Despite the weaker annual regional emissions trend, the INFERNO percentage increase in emissions largely covers the northern region. This contrasts with

inventory estimates, which suggest a likely decrease in emissions across Colombia's Andean region. As a result, INFERNO shows higher percentage increases in space, as illustrated in Fig. 4 (f), with a trend Bias% of 30%. The INFERNO total fire CO emissions for the regions show particularly high magnitudes for 2006-2007 and 2015-2016 (see Fig. S7), which corresponded to weak and strong El Niño events, respectively. The CO emissions from the inventories were also significantly higher during these El Niño events, similar to those for 2019 and 2020. While the INFERNO emissions are similar to the estimates for 2019 and 2020, the emissions magnitudes observed in INFERNO relative to 2006-2007 and 2015-2016 are weaker. The higher emissions in North SA in the latter years of the study period were also associated with the drought conditions and deforestation in the region (Gomes et al., 2021; Amador-Jiménez et al., 2020).

For South-SA, none of the inventories showed a significant trend in CO emissions, and there is no consensus on the direction of a possible trend (see Table 2). From 2019 to 2021, South-SA experienced ~~one of the years with the most~~ particularly high fire activity ~~in the recent period. Mid-SA CO emissions were around 116% higher than the average of the previous five years. This increase aligns with a fivefold rise in deforestation compared to the average during the same period across three~~, resulting in ~~Brazilian states surrounding the Amazon (Silveira et al., 2020), which is consistent with the increase in carbon emissions and AOD (Gatti et al., 2023; Yuan et al., 2022). Most of the CO emissions in 2019 came from deforestation fires (Andela et al., 2022).~~

https://doi.org/10.5194/egusphere-2025-3579 Preprint. Discussion started: 19 August 2025

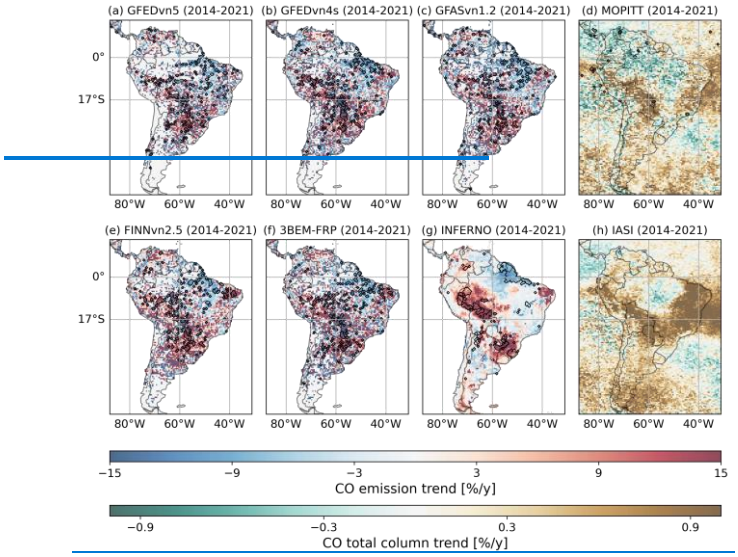

Figure 5. Short term (2014-2021) fire CO emission trend estimated based on (a) GFEDvn5, (b) GFEDvn4s, (c) GFASvn1.2, (e) FINNvn2.5, (f) 3BEM-FRP, and (g) INFERNO and TCCO trend estimated based on retrieved from (d) MOPITT and (h) IASI. The areas enclosed by the black contour represent zones with a significant trend in CO emissions (p values≤ 0.05)

In the short term, South-SA presents the strongest trends in CO emissions, with a dominant increasing trend of ~61.0 %yr $^{-1}$. Significant trends were found for all the inventories studied. Here, the increased CO emissions were concentrated in

the southern parts of Paraguay and Brazil and the northern parts of Argentina according to GFEDvn5, GFEDvn4s and 3BEMFRP, which estimate a trend over 85%yr $^{-1}$ in this area. This region encompasses the ecoregions of Humid Chaco, Pantanal, Alto Paraná, and Araucaria. The region experienced unprecedented fire activity in 2020, resulting in emissions CO emissions that were more than 208126% higher than the average for the previous five years. INFERNO captured the relative increase, estimating that emissions during this period were approximately 121% higher than those of the preceding five years. According to Geirinhas et al. (2023), the 2019-2021 drought period was characterised by an

unprecedented soil drought triggered by large-scale interannual forcing, particularly affected South-SA due to the La Niña phase of the El Niño Southern Oscillation (ENSO), combined with the negative phase of the Pacific Decadal Oscillation. This was additionally The drought conditions were likely enhanced exacerbated by the lack of reduction in warm and, humid air transported from the Amazon, derived from a situation significantly influenced by deforestation (Marengo et al., 2021) and the agricultural expansion in the region (Baumann et al., 2017). Aligned to this, INFERNO describes a significant increase In South-SA, increasing deforestation also directly increases fire occurrence, particularly in flammability the last years of around 10% yr^{-1} the study period (San Martín et al., 2023).

3.2 Sensitivity experiments using INFERNO

The collection of experiments analysing ignition consistently produces lower CO emissions compared to the INFERNO control run (i.e., the model configuration analysed in this previous sections). In fact, as Fig. 5 illustrates, these experiments (IT-CST, IT-NAT, and IT-HDI) are the only ones producing significantly lower CO emissions simulations in the Arc of Deforestation region of the SA low .

In general, the differences within the experiment group are subtle, particularly between IT-CST and IT-NAT, which share a constant anthropogenic ignition but have distinct natural ignitions. While anthropogenic ignition remains constant throughout the year for both IT-NAT and IT-CST, natural ignition has a seasonal cycle for IT-NAT. However, both experiments exhibit a similar seasonal cycle, peaking one month before the real peak for Mid-SA and North-SA (see Fig. 6), while maintaining the same erroneous seasonal cycle shape for North-SA and South-SA. These results show that natural ignition makes a negligible contribution to the spatial, seasonality and trends of simulated fire activity in INFERNO over South America (sef Fig. 7). The results also indicate a limited constraint on human access to different biome locations, as measured by population density, when simulating ignitions. A constant level jet and the low Chaco, where humid air from of anthropogenic ignition, which assumes constant anthropogenic access to the different PFTs, results in lower emissions than in the control scenario, even throughout the Amazon forest is transported to South-SA (see Fig. S5). The . The IT-HDI experiment reduces emissions more strongly than IT-CST and IT-NAT, but it does not change the simulated seasonal cycle shape and trends as IT-CST and IT-NAT did (Fig. S10).

Prescribing different meteorological datasets, ERA5 (control run), 20CRv3 (F-20Cr) and W5E5 (F-W5E5) led to large differences in the CO emissions results, particularly where Tree PFT dominates (see Fig. 5). In particular, the experiment F-20CR, compared with the control run, prescribed lower precipitation for Mid-SA (-13%), reduced soil moisture by 12%, increased fire burnt area by 45%, and CO emissions along by 118%, based on the eastern part of Bias%. Meanwhile, for the same region, F-W5E5

https://doi.org/10.5194/egusphere-2025-3579 Preprint. Discussion started: 19 August 2025

the Andean Mountains in Mid-SA also seem to be caused by the same phenomenon. Some inventories also show a propagated pattern in the east of Brazil, reaching the Caatinga. INFERNO does not represent this pattern, although the model represents prescribed (-7%) less precipitation, which consistently reduced soil moisture by 7%, increased CO emissions in Caatinga, derived from higher ignitionsburnt area by 17%, and available biomass.

For North-SA, three out of five inventories suggest an increasing CO emission of around 1%/yr^{-1} in the short-term. This region was also marked by high fire activity in 2020, which caused CO emissions to increase increased emissions by ~120% for this yearr11%, compared with the average of the previous five years. For Colombia, this, in addition to the particular dry conditions from September 2019 to March 2020 (Gomes et al., 2021), is also associated with the post-conflict transition. After the peace agreement, when the land occupied by FARC (the Revolutionary Armed Forces of Colombia) was suddenly released, unruled, provoking "uncontrolled" exploitation of natural resources and causing deforestation and fire ignition (Amador-Jiménez et al., 2020).

These 2020 CO emissions were around 86% of the CO emissions in 2016, when the fire season was prolonged due to the influence of the El Niño phase of ENSO. Here, as in other studies, INFERNO evidenced the increase in fire activity for this year (Fonseca et al., 2017; Burton et al., 2020). However, INFERNO disagrees with most inventories for North-SA, indicating a negative but insignificant trend in CO emissions. This discrepancy may be due to a model bias in the simulated CO emissions for 2016, which was estimated to be significantly larger than in the subsequent years. However, the inventories that describe the same emissions rate in 2020 do not support this estimate (see Fig. S4). In the short term, INFERNO underestimated the observed increase in CO emissions in northern Venezuela.

For the short term, satellite retrievals support the finding with a positive trend of TCCO through the SA low-level jet along the eastern and central Andes (~1%yr^{-1}). This is particularly clear in the TCCO retrieved from IASI, which has more data available and is more sensitive to changes in the upper troposphere. An increase in CO emissions is also observed in the eastern part of SA within the same latitudinal range, which can be attributed to emissions in the Caatinga region. As the inventories with CO emissions, the retrieval products disagree on the direction of the trend of TCCO for North-SA; still, none of the estimates showed a significant trend.

3.2 Sensitivity experiments using INFERNO

https://doi.org/10.5194/egusphere-2025-3579 Preprint. Discussion started: 19 August 2025

Due to the likely overestimation of CO emissions from FINNvn2.5 in Mid-SA and North-SA compared to other inventories, and the to the control run. The resulting increase in disagreement, we only used GFEDvn4s, GFEDvn5, GFASvn1.2, and 3BEM FRP to compare theCO emissions is reduced by the lower carbon

485 experiments and calculate the MB% in this section. Here, the INFERNO run assessed in the previous sections is referred to as the control experiment.

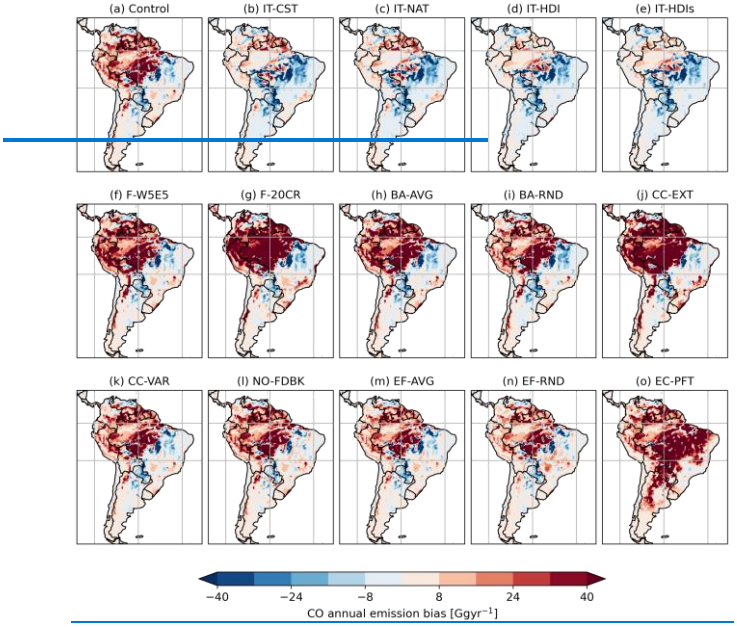

https://doi.org/10.5194/egusphere-2025-3579 Preprint. Discussion started: 19 August 2025

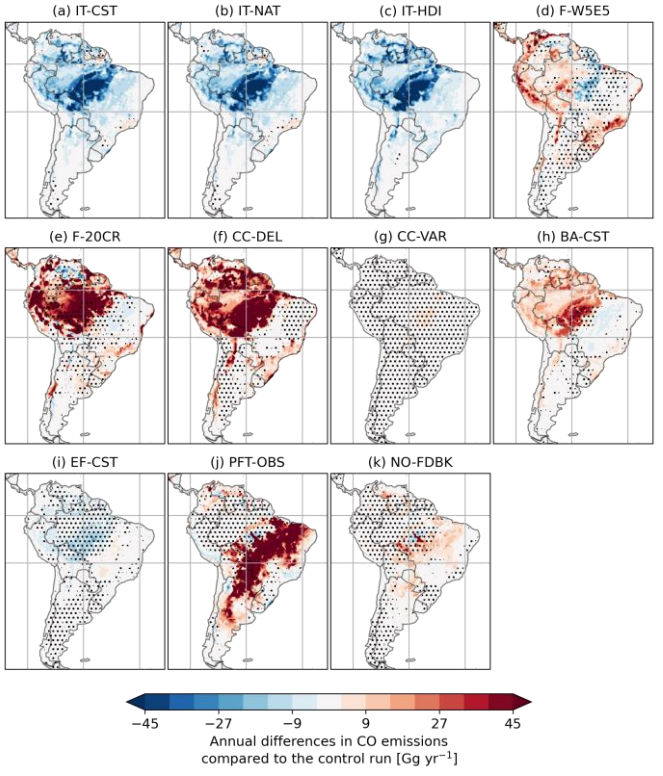

Figure ~~6. INFERNO's experiments~~5. Average annual CO emissions ~~biases (i.e. difference~~differences between ~~CO emissions from INFERNO~~(a-k) each sensitive experiment and the ~~mean~~control run model of ~~GFEDvn4s, GFEDvn5, GFASvn1.2 and 3BEM-FRP).~~ INFERNO. The control run is the same configuration assessed in Section 3.1. ~~The experiment description can be found in Table 2~~The experiment descriptions are summarised in Table 1. The areas hatched with dots indicate when the simulated and estimated emissions are statistically similar, as determined by the Mann-Whitney test.

available in both experiments (-7%). From this, and given that soil moisture and carbon load are the main factors describing the seasonal cycle in INFERNO, we found a dominant effect of meteorological conditions. Remarkably, in North-SA, the distinct meteorological conditions in F-20Cr resulted in higher magnitudes of CO emissions at the wrong annual peak of emissions, as Tree PFTs are particularly influenced by drier conditions.

Removing the CC factor and giving complete control to soil moisture to simulate burnt carbon leads to increased CO emissions in the south of the Amazon forest and towards the north. In Tree PFT dominant areas, a key carbon pool, extending

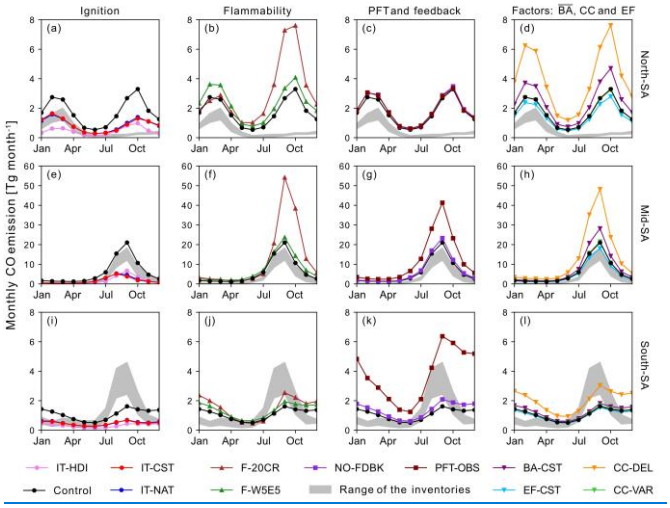

Figure 6. CO emissions seasonal cycle modelled by the different INFERNO experiments and control run in (a-d) North-SA, (e-h) Mid-SA and (i-l) South-SA.

constraints ($CC_{max,wood}$) increases emissions because the model can burn all wood carbon during the driest seasons, while in the control run, a maximum of 40% of the wood carbon was allowed to be burned. This is despite the fact that burning non-leaf carbon was also permitted in this experiment. This experiment results in an insignificant change in CO emissions for east MidSA and South-SA, where much less Tree PFT is modelled. The results support the consistent finding that Tree PFTs are more sensitive to dry conditions than other PFTs. Additionally, the study highlights the importance of soil moisture in representing

https://doi.org/10.5194/egusphere-2025-3579 Preprint. Discussion started: 19 August 2025

these dry conditions. However, it is important to note that this experiment did not account for the effects of meteorological conditions in the burnt area, which may be less sensitive. It should be noted that the change of CC factors over wood and leaf do not directly change the carbon loss output to JULES. This is because other combustion completeness parameters are used for outputting the carbon lost in JULES, and we did not change them (Burton et al., 2019). As a consequence, the calculated trends differ little from those in the control run.

Although experiment CC-DEL clearly shows the constraining power of $CC_{max,wood}$, CC-VAR demonstrates that discrete changes and adding PFT dependence in the factors lead to negligible changes (see Fig. 7). The control run shows positive (negative) biases against the average values of the selected inventories over BDT and BET-Tr (C4G) dominated lands based on the PFTs modelled by TRIFFID (see Figs 1 and 6-a). The overestimation of emissions is offset only by the ignition experiments (Fig. 6-b-e), which reduce CO emissions through the territory in about 60%, increasing the underestimation of emissions in the northern part of South-SA and eastern Mid-SA, where most C4G-dominated lands are located (see Fig. S6). The low emissions rate of these experiments, particularly the one related to the addition of the HDI (i.e. IT-HID and IT-HDIs), produces the underestimation of the seasonal cycle amplitude on the three subregions, as Fig. 7 illustrates. The seasonal cycles estimated by the experiments were lower than any estimation from the included inventories and yet produced a lower absolute MB% in Mid-SA (53.4%) than for the control run (96.5%), whose emissions peak is significantly higher than the estimations of GFEDvn4s, GFEDvn5, GFASvn1.2 and 3BEM-FRP. In North-SA, the CO emissions estimated by the ignition experiments, particularly for IT-HDI and IT-HDIs reduced spatiotemporal MB% since the control run presented overestimations.

Both HDI experiments (i.e. IT-HID and IT-HDIs) show the highest level of spatiotemporal agreement with GFEDvn4s in SA (See Fig. S7). Accounting for socioeconomic factors by including the HDI has demonstrated better performance in SA and various other regions compared to GFEDvn4s (Teixeira et al., 2021). However, the spatiotemporal comparison against GFEDvn5 suggests an increment in the absolute MB% for Mid-SA and South-SA. The spatiotemporal MB% for both HDI experiments in North-SA is lower than the control experiment against all the inventories (Figure S6). The trend described by IT-HDI and IT-HDIs in North-SA also shows a lower MB% than the control experiment, as shown in Fig. 8. The better performance is evidenced by the long-term negative trend of CO emission over the centre of Colombia and the increase of emission in the north of Colombia. The results here might be due to

$CC_{max,wood}$ not being adjusted for the tree PFTs, which use the same values as the control run.

Based on the literature, we set lower $CC_{min,leaf}$ for tree PFT and higher $CC_{max,wood}$ for grasses and pastures. Nonetheless, as Fig. 5 shows, the CO emissions simulated from CC-VAR are not significantly different to those simulated by the control run, which uses constant CC values regardless of PFT. This suggests that the $CC_{max,wood}$ used for tree PFTs tends to be the main factor controlling soil moisture in the simulation of burnt carbon (see Equation 6).

As noted earlier, Broadleaf Deciduous Trees and ~~part of Venezuela (see Figs. S7 and S8).~~Tropical Broadleaf Evergreen Trees can control how changes in model factors (e.g., CC, BA) affect simulations over South America. Using an average constant BA and EF_{CO} (specifically in experiments BA-CST and EF-CST), produced respectively increasing and decreasing emissions compared to the control run (see Fig. 7). ~~subnational scale HDI (IT-HDIs), rather than national HDI (IT-HDI),~~This as a consequence of the relatively low BA and high EF_{CO} that Tree PFTs have. The effect of BA-CST was particularly significant and high in the southern Amazon and towards the north of South America. In general, BA-CST differs more from the control run than EF-CST, not only spatially but also in seasonal cycle amplitude and trend.

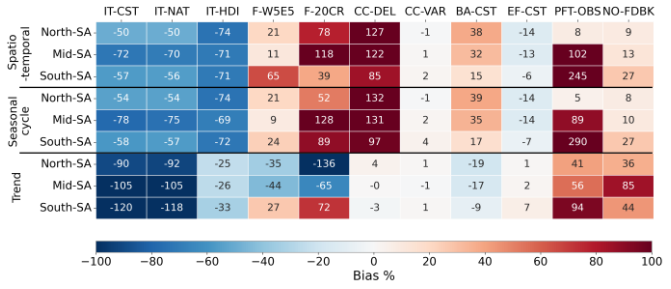

Figure 7. CO emissions spatiotemporal, seasonal cycle and trend percentage mean bias (Bias%) for the sensitive experiments based on the control run of INFERNO. The Bias% are shown independently for the study regions in South America. The trends of fire CO emissions calculated for the sensitivity experiments are shown in Fig. S10

Changing the PFT (i.e., PFT-OBS) results in a few changes in the southern Amazon forest, even when the Tropical Broadleaf Evergreen Trees greatly dominate over the simulated Broadleaf Deciduous Trees (see Fig. S2). As Fig. 5 shows, the main

difference between this experiment and the control run is seen in the east of Mid-SA and in South-SA, where higher emissions are observed in regions with dominant grasses and pastures. In this region, the PFT-OBS tends to exhibit a higher tree fraction, greater wood carbon availability, and consequently higher CO emissions. Using observations of vegetation to represent PFTs did not improve the simulated emissions nor the seasonal cycle representation in Mid-SA or South-SA (see Fig. S9). ~~performance of INFERNO. On the contrary,~~Still, they did increase CO emissions in South-SA to the estimated range from the inventories during the peak of emissions, while in Mid-SA the emissions were further overestimated (see Fig. 6).

Although all experiments lack feedback from the atmosphere, as this is a land-only model, the results from the NO-FDBK experiment illustrates the proportional error that the omission of feedback to land can introduce into the fire model. According to the experiment, this omission results in significant increases in the spatiotemporal magnitudes and seasonal cycle amplitudes of the simulated CO emissions (Bias% ~ 15%). However, as expected, it does have a more substantial influence on the simulated trends, where differences against the control run have a Bias% of 85% in Mid-SA. The No-FDBK experiment results in spatiotemporal CO emissions that are approximately 94% higher than the inventory estimates for Mid-SA, which is 22% higher than the Bias% observed in the control run (~72%) compared to the inventories (see Table 2).

3.3 Explaining INFERNO CO Emission Biases Using Machine Learning

Across the five-fold cross-validation iterations, the XGBoost model achieved an average R^2 of 0.67. The mean Root Mean Square Error (RMSE) was 6.6 Gg yr^{-1}, corresponding to approximately the 75th percentile of the absolute magnitude of the target variable (CO emission biases). The Mean Absolute Error (MAE) averaged 2.5 Gg yr^{-1}, close to the median absolute bias. Overall, the XGBoost model explains 67% of the variability in the target variable; however, the prediction errors remain comparable to or greater than the median of INFERNO CO emission absolute biases. Notably, the machine learning model struggles to capture negative biases (see Fig. S12). However, the model is particular suitable for explaining the overestimation of CO emissions in Mid-SA, where most fire activity and the INFERNO absolute biases concentrate.

https://doi.org/10.5194/egusphere-2025-3579 Preprint. Discussion started: 19 August 2025

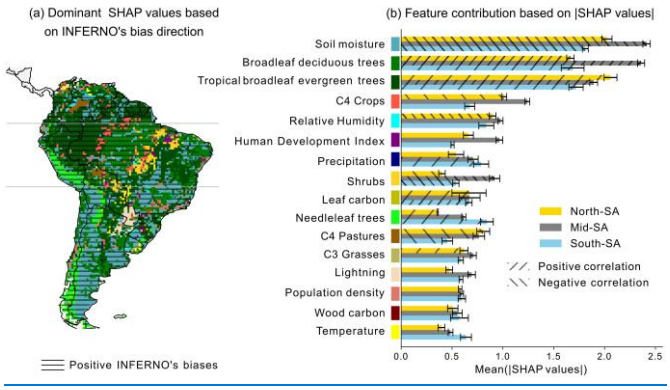

Figure 8. (a) Gridded dominant feature contribution of the XGBoost model according to the bias direction and (b) feature contribution to the XGBoost predicted biases using absolute SHAP values. The horizontal line hatched area in (a) describes where INFERNO CO emissions biases are, on average, positive. The diagonal and back diagonal hatched bars in (b) indicate when the magnitude of the variable correlates positively ($R > 0.5$) or negatively ($R < -0.5$) with their contribution to the modelled CO emission biases. For both diagonal lines, hatch is more frequent when the correlation is stronger ($|R| > 0.7$). Notice that this figure does not include all XGBoost features, as the three with the lowest SHAP values were omitted.

Figure 8 illustrates the feature contributions at two levels: gridded (a) and regional (b). Since SHAP values can be both positive and negative, we used the absolute SHAP values for the subregional assessment. We focused on the larger positive or negative SHAP values to characterise the dominant contributions associated with the bias direction in the gridded map. According to the SHAP values, soil moisture and the tree PFT Broadleaf Deciduous Trees and Tropical Broadleaf Evergreen Trees particularly stand out in driving INFERNO biases. This aligns with the particular sensitivity that INFERNO showed regarding these variable changes in Section 2.4. Despite the low correlation between soil moisture and the biases ($R = 0.18$, see Fig. S11), soil moisture is the top variable to explain and then address the spatiotemporal biases of INFERNO in South America. As Fig. 8 shows, the SHAP values of soil moisture negatively correlate with soil moisture magnitudes in the three regions ($R \sim -0.8$), showing that low values of soil moisture tend to explain high positive biases of CO emissions, while negative or low biases are present when there are wetter conditions.

The fractions of Broadleaf Deciduous Trees and Tropical Broadleaf Evergreen Trees show a strong positive correlation of

their contribution to predicting CO emission biases. Higher proportions of these PFTs are associated with positive biases, particularly in North-SA, the performance on trend MB% of IT-HDIs (81%) was significantly poorer than that of IT-HDI (27%).

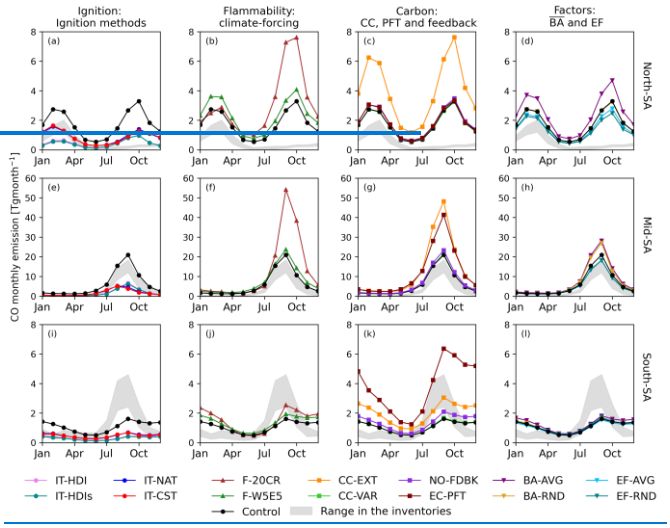

Figure 7. CO emissions seasonal cycle modelled by the different INFERNO experiments in North-SA (a-d), Mid-SA (e-h) and South-SA (i-l). The experiments are grouped by type. The inventories range presented in the shaded region omit FINNvn2.5.

Although the Ignition experiment with constant anthropogenic ignition, IT-NAT and IT-CST, performed close to the HDI experiments (i.e. IT-HDI and IT-HDIs) (see Figs. 7 and 8), they particularly differentiated in the trend estimation in Mid-

SA and South-SA. The two experiments described a more negative trend than IT-HDI, IT-HDIS and the control experiment, which reduced biases. However, the strong tendency identified by IT-CST and IT-NAT misses some of the details identified by the control experiments and described in Section 3.1.2. For instance, the trends calculated for Argentina and Caatinga in

the long-term and short-term, respectively (see Fig. S8 and Fig. and Mid-SA. The results S9), This exhibits the importance of anthropogenic ignition in this region, which INFERNO can partially describe. Furthermore, IT-NAT and IT-CST have similar CO emissions, even when

IT-NAT have varying natural ignition, which is evidence that the estimated CO emissions have a low sensitivity to the natural ignition variation by the lightning annual cycle, as was described previously for burned area simulation (Burton et al., 2022).

In contrast to the ignition experiments, the experiments using other climatic datasets for simulating flammability (i.e. F-20CR and F-W5E5) do not reduce MB% against the inventories compared to the control experiment run in any of the subregions when evaluated spatiotemporally (see Figs. 6 f-g and 8). Both datasets 20CRvn3 and W5E5 produced higher CO emissions than the control experiment (i.e., using ERA5), particularly in the BDT and BET-Tr dominant land cover types. The higher monthly estimates of INFERNO based on these two climatologies provide a better representation of emission amplitude in South-SA (see Fig. 7.i), reaching the emissions range of the inventories at their peak, although still high during the non-fire season. In North-SA, the incorrect representation of the seasonal emissions cycle was extenuated, with an incorrect increase in emissions in the non-fire season, as illustrated in Fig. 7.b. This experiment led to the most noticeable changes in the shape of the seasonal cycle (see Fig. 7b,f,j); however, this is still misrepresented for South-SA and North-SA. This result indicates a systematic bias affecting the simulation of the seasonal cycle, likely because a variable outside the experiments conducted (e.g. GPP), since the simulations only alter the magnitudes of the marked season (see Fig. 7).

The F-W5E5 experiment (i.e., using the W5E5 dataset) represents better trends in the three regions in its shorter run period (i.e. 2004 - 2019) as Fig. 8 shows. In fact, F-W5E5 long-term data show a more accurate decrease in CO emissions in Bolivia and an increase in CO emissions in Río Negro, Argentina (See Fig. S8).

Changing the PFT (i.e. EC-PFT) was the only experiment that consistently switched the negative spatiotemporal MB% over the TRIFFID C4G-dominated land into positive (see Fig. 6o). This is since the prescribed PFT exhibits rather dominant BET-Tr and BDT, as Fig. 1 illustrates. In Mid-SA and South-SA, because of the land cover change, the EC-PFT calculates significant changes in the seasonal cycle amplitude, which were consistently higher on the emissions peak exceeding the inventory range (see Fig. 7). In North-SA, however, the changed PFT did not significantly affect the calculated MB% (see Fig. 8 a). For South-SA, the EC-PFT closely describes the trend observed by the inventories (trend bias ~ 12%, see Fig. 8 c).

Since the PFTs were prescribed, the EC-PFT did not include feedbacks, like the NO-FDBK experiment. The NO-FDBK experiment indicated that, on average, not including fire feedback in the land model produces 8% higher CO emissions than including it. This can cause a spatiotemporal overestimation of around 50%. Hence, the exclusion of feedbacks could lead to an increase in biases of EC-PFT emissions.

https://doi.org/10.5194/egusphere-2025-3579 Preprint. Discussion started: 19 August 2025

As expected, due to the contribution of emissions in BDT and BET-Tr, which exhibit a relatively low BA and high EF_{CO}, the selection of a random or average scheme (i.e., BA-RND, BA-AVG, EF-RND, EF-AVG) consistently increases (reduces) emissions led by higher (lower) BA (EF_{CO}). Similarly, by extending both wood carbon CC and leaf CC in CC-EXT, the model increases emissions, weighting the now higher potential combustion of wood over the lower combustion of leaf. These experiments also described the influence of the PFT in BA, EF, and CC by comparing the control experiments with BA-AVG, EF-AVG, and CC-VAR. The influence of the PFT is distributed as BA>EF>CC, according to the absolute spatiotemporal MB% of 30%, 10% and 1% against the control run. Notice that CC-EXT managed a large change (111%) in CO emissions,

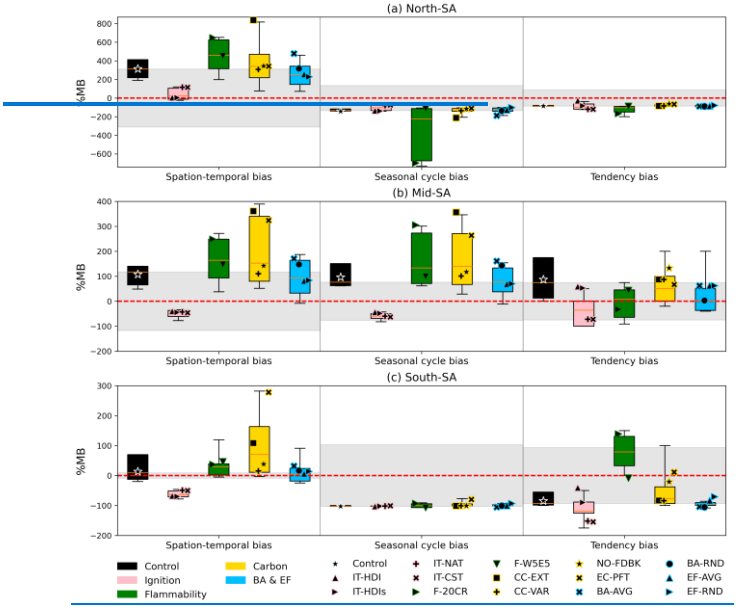

Figure 8. Percentage mean bias (MB%) of spatiotemporal, seasonal cycle and trend of CO emissions modelled in the different INFERNO experiments against the studied inventories. The boxes include the comparison of each experiment against the five inventories, with the marker describing the median value of the comparison without including FINNvn2.5. The shaded region in the background represents the absolute median MB% of the control run in each subplot, the reason why it goes from zero to the

± control's median magnitude. A red line highlights the zero MB%. Note that every subplot has a different y axis to facilitate visualisation.

but an extreme and hypothetical range was used for this experiment. Contrary to the flammability and ignition experiment, this experiment did not drastically change the INFERNO MB% direction. CC-EXT, however, drastically increases emissions at the same level or higher than any other experiment conducted here. It represented the sensitivity experiment with perturbed input values to the INFERNO model which were far outside the typical range used for these factors. In contrast, the intent to use more accurate CC (CC-VAR), which depends on PFT, did not show a significant change in any assessment.

In general, including only experiments with realistic values/ranges (i.e. excluding CC-EXT), the Ignition, flammability and PFT sensitivity experiments resulted in the largest changes compared to the control experiment. This is represented in the average absolute MB% of 115%, 65% and 47% for PFT, ignition and flammability in the spatiotemporal assessment. Flammability presented the largest changes to the seasonal cycles (MB% = 116%), followed by PFTs (MB% = 88%) and then ignition (MB% = 46%). The changes on the trend were led by PFTs (MB% = 167%), followed by flammability (MB% = 158%) and ignition (MB% = 142%).

3.3 Understanding of INFERNO CO emission biases through application of ML

As in the previous section, only the inventories GFEDvn4s, GFEDvn5, GFASvn1.2, and 3BEM-FRP were utilised for the machine learning approach. The XGBoost model's target was the bias of the CO emissions estimated from INFERNO when compared to the average emissions from the selected inventories. After evaluating the features, 14 inputs from INFERNO were included in the final model: 10 PFTs (BDT, BER-Te, NT, C3G, C3Cr, C3Pa, C4G, C4Cr, C4Pa, Sh), soil moisture, lightning, population, and HDI. None of the selected features exhibited a correlation greater than 0.6 with any other feature (see Fig. S10), and the VIFs for these features were below 10. In particular, soil moisture covaries with multiple variables with which its correlation is high, such as relative humidity (R = 0.79), leaf carbon (R = 0.73), wood carbon (R = 0.70), BET-Tr (R = 0.70), and precipitation (R = 0.suggest that7). Therefore, these other features were not included directly, but were represented by soil moisture, since soil moisture highly depends on precipitation and is a key variable for GPP, which in turn affects leaf and wood carbon that favour PFTs as BET-Tr.

With the best parameters identified through hyperparameter tuning, the ML model trained using 5-fold cross-validation yielded an R^2 value between 0.62 and 0.68 (average 0.64), an RMSE ranging from 18.8 $Ggyr^{-1}$ to 21.3

Ggyr.$^{-1}$ (mean of 20.4 Ggyr.$^{-1}$), and a MAE ranging from 7.8 Ggyr.$^{-1}$ to 8.2 Ggyr.$^{-1}$ (mean of 8.0 Ggyr.$^{-1}$). Therefore, the ML model is able to explain around 64% of the biases with the available data and data accuracy level. Capturing finer temporal and spatial resolution interactions within the input data can also contribute to reducing the error, since we are using annual datasets. The ML model has particular difficulties addressing negative biases (see Figure S11). This suggests that there are structural and/or parametric deficiencies within INFERNO that particularly limit its ability to represent different fire process patterns through SA. This finding is consistent with Section 2.5, where none of the experiments manage to represent a consistent low MB% compared to the control model for all studied subregions.

Figure 9 presents the feature contributions on two levels: subregional (a) and pixel-by-pixel (b). Since SHAP values can be both positive and negative, we utilised the absolute SHAP values for subregional assessment and the larger positive (or negative) SHAP values to identify areas with an average positive (or negative) bias. According to the SHAP values and consistent with Section 2.5, the BDT fraction (which correlates with BET-Te R=0.6) is the feature of most importance in the three subregions, as Fig. 9.a shows. The higher the BDT fraction, the higher the SHAP values (R = 0.80), and vice-versa. This suggests that low values of BDT modelled by TRIFFID also values of the Tree PFTs contribute to modelling the lower and/or negative bias of INFERNO CO emissions. BDT is emissions. Spatially, it is clear that Broadleaf Deciduous Trees and Tropical Broadleaf Evergreen Trees are the dominant feature of importance where INFERNO overestimates CO emissions in the Amazon rainforest (see Fig. 9.b). While Teixeira et al. (2021) suggested that an overestimation of tree cover might be a potential driver for the overestimation of emissions in this area, our study shows that even with a lower fraction of tree cover compared to the ESA land-cover based PFTs, we still observe an overestimation of emissions. This indicates that, in addition to the fraction of tree cover, there is also a lack of representation of the fire dynamics affecting these PFTs. From this and based on the observed overestimation of emissions extended in the Amazon forest, we consider that a more accurate representation of fire dynamics 8.b). However, the more frequent contribution of the variable toward negative biases in South-SA is probably

https://doi.org/10.5194/egusphere-2025-3579 Preprint. Discussion started: 19 August 2025

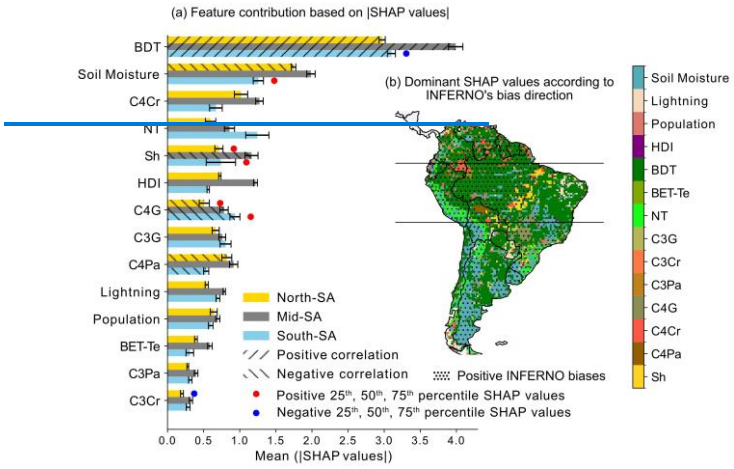

Figure 9. (a) Feature contribution of the XGBoost model using absolute SHAP values and (b) map of dominant features based on the largest positive (negative) SHAP values for pixels where INFERNO's average CO emission biases are positive (negative). In (a), the hatch marks describe the correlation between the SHAP values and the annual average magnitude of each feature; only |R| > 0.7 is displayed. The red (blue) filled circles in front of the bars describe when the complete interquartile range (IQR) of the SHAP values in a specific subregion is positive (negative). In (b), the dotted areas indicate when INFERNO's bias is on average positive, while the remaining area shows when the bias is on average negative.

can be achieved by considering landscape fragmentation, representing both forest vulnerability (see Silva-Junior et al. (2022)) and land management (see Andela et al. (2017)), can lead to improved calculation of burned area and fire suppression effect.

In contrast to the Amazon forest, the BDT contribution in the east of Mid-SA and South-SA is negative when CO emissions biases are negative (see Fig. 9. b without dotted marks), which is additionally linked to the low modelled BDT fraction in these areas. In the Chaco region, the negative contribution of BDT highlights a possible underestimation of tree cover, which is evident when compared to TRIFFID and the ESA land-cover based PFT (see Fig. 15) related to the fact that tree fractions are underestimated in this region. Particularly, in the Chaco ecoregion, the underestimation is evident when comparing TRIFFID and the

ESA land-cover-based PFTs (see Fig. S2). In 2019, the tree cover fraction in Chaco was over 30%; however, Scrublands dominated in the Dry Chaco (38.2%) (San Martín et al., 2023). On average, for the study period, theHowever, TRIFFID modelled C4G, C4PaC4 Grasses, C4 Pastures, and bare soil asare dominant PFTs with 88% cover in the Chaco region; none of the treeTree PFTs had an average fraction over 2%. Furthermore, since this region has emerged as a hotspot of deforestationThis aligns well with the results of the experiment prescribing PFT, PFT-OBS. PFT-OBS, which had higher CO emissions than the control run in areas of previous underestimation.

and agricultural expansion (Baumann et al., 2017), in addition to more accurate PFTs, incorporating landscape fragmentation would also be potentially beneficial.

Despite the low correlation between soil moisture feature and the bias (R = 0.18), soil moisture is the second most significant feature in explaining these spatiotemporal biases in SA, particularly for North-SA and Mid-SA. For North-SA, the soil moisture also presents a high but negative correlation with SHAP values (R = -0.70), indicating that the overestimations (underestima-

tions) of CO emissions by INFERNO are related to drier (wetter) conditions. This suggests that fire emissions in North-SA are highly sensitive to soil moisture, leading to an inflated response. This aligns with the overestimations observed during the El Niño event in 2016, discussed in Section 3.1.2. In Mid-SA and South-SA, the correlation between SHAP values and soil moisture is low. This indicates that both dry and wet conditions contribute to negative and positive biases, suggesting a complex interaction with other variables included in the analysis. In South-SA, both low and high soil moisture particularly contribute

to explaining positive biases (see Fig. 9. a, positive SHAP values quantiles). This complexity might be related to the role of precipitation/soil moisture in flammability and GPP, which have been observed to have different responses from different PFTs in the region (San Martín et al., 2023). Evidence of deficient representation of the complex interaction between soil moisture and fire in this region is the misrepresentation of the seasonal cycle (see Section 3.1.1 and Fig. S3), where flammability and GPP follow the precipitation peak.

The crop fraction, C4CrC4 Crops, ranks third in contributing to the explanation of the CO emission bias from INFERNO in North-SA and South-SA; however, the fourth in its contribution and the variable magnitudes were not significantly correlated, either positively or to explaining CO emission biases. C4 Crops SHAP values negatively. A few patches where C4Cr contributes the most are visible in Fig. 9.b, similarly for Sh in the south of the Arc of Deforestation. Since anthropogenic interactions are not associated with the simulated C4Cr, reducing bias through this variable would mean correlate with the PFT fractions in North-SA (R=-0.52), particularly describing crop activities as harvesting (Li et al., 2013); and socioeconomic factors (Li et al., 2013). Furthermore, agricultural expansion and landscape fragmentation.

Although the INFERNO run did not include HDI, this feature appears to be around fourth place in terms of contribution for North-SA and Mid-SA, where this has demonstrated MB% reduction (see Section 2.5). HDI is then a prospective feature to address INFERNO biases.

4 Conclusions

We evaluated the fire CO emissions and sensitivity of the global fire model INFERNO estimations in South America (SA). The study quantified and assessed the spatiotemporal, seasonal cycle, and trend accuracy of the model's estimated CO emissions against five biomass burning inventories. For this, SA was divided into three subregions: North-SA, Mid-SA, and South-SA to compare differences in fire activity and biomes. With the least forest cover, South-SA exhibited the lowest disagreement in CO emissions between inventories, including FINNvn2.5 (Relative percentage range = 65%). The agreement was similar for North-SA and Mid-SA, if excluding FINNvn2.5. INFERNO was able to reproduce emissions in key active fire zones, such as deforestation fronts (e.g. Arc of Deforestation) and ecoregions like the Cerrado and Llanos, but likely underestimates CO emissions in the Chaco region, although still within GFEDvn4s range. Overestimation outside these regions, such as within the Amazon forest, led to enhanced CO emission overestimations, particularly in Mid-SA and North-SA. In Mid-SA,

INFERNO demonstrated good performance reproducing the seasonal cycle of emissions, although with general overestimation of the magnitudes. In contrast, over North-SA, INFERNO exhibited a large spatiotemporal bias due to an erroneous bimodal representation of the seasonal cycle, while biases on South-SA were low despite the incorrect seasonal cycle. In both places,

the simulated CO emission closely follows both the flammability and GPP cycles; however, it waspositive biases when GPP was high that the emissions incorrectly peaked.

INFERNO was able to reproduce the overall trend direction of CO emissions, although it erroneously reproduced an increasing trend near the Arc of Deforestation from 2004 to 2021. During the period from 2014 to 2021, INFERNO correctly estimated an increase in CO emissions along the SA low-level jet region. This region, which crosses Mid-SA and South-SA, has been particularly dry and vulnerable in recent years due to multiple meteorological factors, including the La Niña phase of the ENSO, as well as policy and socioeconomic factors. Due to the complexity of the fire regime in this region, INFERNO underestimates the magnitude of the trend in CO emissions but accurately identifies the direction of the trend. Over the short-

https://doi.org/10.5194/egusphere-2025-3579 Preprint. Discussion started: 19 August 2025

term period, the inventories and satellite retrievals of TCOO disagree on the CO trend in North SA; however, neither presents a significant result.

Multiple sensitivity experiments were conducted by modifying factors related to ignition, flammability, PFT, and also the individual factors: combustion completeness, average Burned Area, and emission factor. We evaluated the proposed use of the

Human Development Index (HDI) in INFERNO, which improved performance in the Mid SA and North SA by reducing CO

emissions; however, further reductions in CO emissions over South SA resulted in poorer model performance. Additionally, the reduction in absolute bias observed when using constant anthropogenic and natural ignition was similar for all regions, although they described significantly different trends from the results with HDI in Mid SA. Furthermore, the climatic datasets used for the control run, ERA5, demonstrate strong spatiotemporal performance. In contrast, using the W5E5 dataset to calculate flammability shows a lower bias in CO trends for Mid SA and South SA. The seasonal cycle across the three subregions

was consistent for all climate input datasets, with ERA5 resulting in fewer monthly emissions. Changes in flammability were the most important factor driving changes in the simulated fire CO emissions seasonal cycle (MB%=116) compared with the experimental run. The experiment, which examines the effects of constant and varying factors on PFT, highlights the importance of forest cover (Broadleaf deciduous trees and Broadleaf - BDT evergreen tropical trees - BET Tr) in determining the simulated fire CO emission magnitudes in SA. Using a prescribed PFT based on the satellite based ESA Land Cover

product, results in the highest spatiotemporal (MB%=115) and trend (MB%=167) changes against the control run, which are related to the relatively higher the fraction of BET Tr in Mid SA and BDT in South SA.

In line with the findings from the sensitive experiments, the feature importance analysis of the ML model indicated that BDT was the most significant feature contributing to the bias in INFERNO's CO emissions. A large (short) this PFT is low. Surprisingly, the fraction of BDT contributes to overestimations (underestimations) of the emissions in SA. Both improving PFTs accuracy and incorporating

the representation of human land use management of the vegetation through variables, such as land fragmentation, might help reduce biases. Soil moisture was the second most significant contributor. In North SA, the positive bias of CO emissions dominates inside the Amazon forest near the Amazon River. The C4 Crops contribution is also dominant around the Arc of Deforestation, along with Shrub fractions, which correlates with dry conditions, suggesting hypersensitivity to soil moisture. In South SA, INFERNO biases exhibited a more complex relationship with soil moisture, which is likely associated with varying contributions of soil moisture/precipitation to

GPP and flammability. C4 Crop negatively with its contribution to the ML model emphasised the potential of including crop fire dynamics intobiases (R=-0.70). There, the high fraction seems to be related to negative biases.

Finally, although the INFERNO configuration in this study did not include HDI, this feature shows potential to address INFERNO CO emission biases. However, its contribution to address them is not linear as it weakly correlates with HDI magnitudes. In North-SA, the correlation is 0.48, indicating that higher HDI is associated with positive biases. This aligns with the results from Teixeira et al. (2021), which suggested that countries with high living standards may more easily suppress fires, resulting in lower CO emissions than simulations that do not include the HDI.

4 Discussion

4.1 INFERNO performance and main factors explaining biases

The results of this study were consistent in showing that soil moisture, particularly low magnitudes, and Tree PFTs in South America are the top drivers of biases in INFERNO. The few inputs used by INFERNO to represent anthropogenic influence on fire ranked after these meteorological and vegetation conditions; however, including more socioeconomic factors could help explain the remaining 33% of the bias in the XGBoost model.

The XGBoost model identified soil moisture as the primary variable explaining the biases observed in INFERNO, while relative humidity also emerged as a significant factor related to meteorological conditions. The lack of global, long-term soil moisture datasets has prevented the assessment of the direct effect of soil moisture on the performance of fire models (Hantson et al., 2020). Nonetheless, other variables that describe drought conditions have been assessed. According to Forkel et al. (2019)'s evaluation, for INFERNO, maximum temperature contributes the most to the simulated burnt area, even more than for other models. However, wet conditions, represented by the number of days with significant precipitation, had little influence on burnt area (Forkel et al., 2019). Although reported with different variables, the role of dry conditions in INFERNO, identified by Forkel et al. (2019), supports the observed sensitivity to soil moisture, as this was also particularly evident in INFERNO simulations under dry conditions. Still, both studies differ in evaluation targets, the independent variables selected, and the variations in temporal and spatial resolution. Furthermore, burnt areas may be less sensitive to soil moisture than CO emissions, as evidenced by experiments that varied meteorological conditions. This observation is consistent with the results reported by Mathison et al. (2023), where INFERNO produced stable results for the burnt area across various meteorological datasets.

Our evaluation consistently supports that INFERNO-simulated CO emissions were too sensitive to drier conditions, particularly in Broadleaf Deciduous Trees (see Fig. S13). In fact, Teckentrup et al. (2019) shows that increasing probability of fires driven by soil moisture begins to manifest in wetter conditions for INFERNO than for other models. In general, most overestimations relative to the inventories were in areas where modelled Broadleaf Deciduous Trees and Tropical Broadleaf Evergreen Trees dominate. The control of the Tree PFTs is particularly clear around the Arc of Deforestation in Mid-SA, where the relative fraction of these two tree PFTs appears to shape this main source of CO emissions in South America. In North-SA, with lower absolute emissions, the sensitivity of Tree-PFT to drought conditions underpinned the incorrect representation of the seasonal cycle. There, fire emissions from the Tree PFTs were incorrectly simulated with similar magnitudes to the fire-prone Llanos ecoregion emissions, where pasture is the dominant modelled PFT. Furthermore, the role of drought conditions in Tree PFTs was evident in the increasing biases over time, consistent with the growing influence of drought events. Finally, the large differences in simulated CO emissions resulting from different meteorological datasets used as inputs to JULES indicate that the response to drought conditions in Tree PFTs-dominated areas outweighs the influence of carbon availability, particularly in shaping the seasonal cycle of emissions. Compared with other models, the INFERNO fuel load index reaches its maximum much more rapidly in response to fuel density (Teckentrup et al., 2019), which is why, with high carbon availability, changes in fuel density may lead to muted differences.

Tree PFTs as top factors to describe CO emissions biases were associated with both overestimations and underestimations, according to the XGBoost model. INFERNO simulations underestimate CO emissions in key South America ecoregions: Cerrado, Llanos and Chaco. In JULES, these ecoregions tend to be dominated by modelled C4 Pastures and Grasses (see Fig. S13). According to the machine learning results, the Broadleaf Deciduous Trees fraction is the main factor explaining the underestimation of emissions in these ecoregions, given its low abundance. Indeed, for the Chaco region, we observed likely underestimation of the Tree PFTs fraction compared to observation-based PFTs and the literature (Harper et al., 2023; San Martín et al., 2023). In our experiments, using observation-based PFTs increases emissions estimates in the three ecoregions, but less so in the Llanos. Consistently, it has been suggested that INFERNO biases might be enhanced by disproportionately reducing the Tree fraction in savannas (Mathison et al., 2023), to which the model simulations seems highly sensitive (Teixeira et al., 2021; Mathison et al., 2023).

In South-SA, a significant portion of the trees in the dominated pasture and grass areas may be consumed due to the incorrectly simulated two-peak fire activity. In general, the seasonal cycle of emissions in the southern extratropics varies significantly, and fire models often struggle to accurately reflect this variability (Hantson et al., 2020). As in INFERNO, simulations frequently emphasise the global peak in December-January (Hantson et al., 2020). Our findings indicate that the simulated seasonal

cycle of CO emissions by INFERNO closely follows the rise in GPP and flammability during December-January, a period marked by high temperatures and rainfall. As shown by Teckentrup et al. (2019), the INFERNO fuel load index, which is used in the flammability calculation, is highly sensitive to minor changes in fuel density when the overall fuel amount is small. Therefore, even during the rainy season, there may be hot days without rain, during which the relative humidity is sufficiently low to enable flammability to peak according to the fuel load index.

Ranked fourth in contributing to bias prediction in the XGBoost model, the low fraction of C4 crops explains the positive CO emissions bias. As this feature particularly dominates in explaining biases in the Amazon, the feature is likely representing the lack of anthropogenic activities. In INFERNO, the anthropogenic ignition representation does not seem well-bounded by population density, as even constant ignitions result in lower CO emissions in the centre of the Amazon forest, where almost no fires occur. The representation of anthropogenic activities and threats, including crop and deforestation, is a factor largely missing in the global fire modelling community (Hantson et al., 2020). In general, there is substantial disagreement over the response of modelled fire activity to socioeconomic factors (Forkel et al., 2019). In the XGBoost model, HDI also ranked high, which helps explain the underestimation of CO emissions. In the machine learning model, the low values of the index push the bias toward negative biases. The finding aligns with the idea that countries with, in this case, low living standards may face more difficulties in suppressing fires, resulting in higher burnt area and CO emissions Teixeira et al. (2021).

4.2 Implications for future development

Soil moisture is the top factor limiting fire activity in tropical forests (Kelley et al., 2019). This variable is widely used in fire models, as in INFERNO, to describe fuel moisture (Rabin et al., 2017). However, using soil moisture to represent fuel moisture without a PFT-dependent factor might lead to incorrect representation, as fuel moisture, particularly in live plants, depends on soil conditions and plant physiology (Forkel et al., 2023). ~~670 the model to reduce biases. Similarly, the contribution of HDI suggests potential bias mitigation in North-SA and Mid-SA, as was observed in the sensitivity experiments.~~

~~This study highlights the capabilities and limitations of INFERNO in supporting the UKESM's new developments in a challenging region. Here, we conducted sensitivity experiments for various parameters and recommend a perturbed parameter ensemble method for a more in-depth evaluation of INFERNO's performance and uncertainty. Future research should also~~

~~675 focus on accurately representing the seasonal cycle of fire activity in SA, addressing issues related to the role of precipitation on both GPP and flammability through soil moisture.~~

This incorrect representation is pronounced for forest land covers, where the correlation between soil moisture and live fuel moisture content is low, with a long lag time for the best correlation (Vinodkumar et al., 2021). For INFERNO, the combustion completeness factor, particularly $CC_{max,wood}$, varying across PFTs, could be utilised to diminish the effect of soil moisture on CO emissions. As it was shown in the study, this particularly constrains the soil moisture effect in the simulated burnt carbon. Similarly, although the burnt area's over response to soil moisture might be weaker, targeting fuel moisture representation in flammability can help capture better the seasonal cycle variability of fire activity. Multiple variables to describe the fuel moisture content on fire danger can be used instead of or in synergy with soil moisture, such as fire danger indexes (e.g. the Nesterov index) (Drüke et al., 2019; Rabin et al., 2017). For South America, Drüke et al. (2019) shows improved representation of the burnt area using a vapour-pressure-deficit-based fire danger index in flammability calculation. The Fire Weather Index and Nesterov Fire Index are readily testable, as they are already calculated along with burnt area and emissions by INFERNO (Mangeon et al., 2016).

Socioeconomic factors have, overall, demonstrated diverse influences on fire activity across different parts of the world, making it very difficult to capture in a fire model (Forkel et al., 2019). Including deforestation representation and crop influence has shown little improvement (Hantson et al., 2020; Gallup et al., 2024), particularly in the accuracy of fine-scale representation, which remains unattainable at this stage (Gallup et al., 2024). However, it has been observed that including or excluding crops in fire models can yield different trends in burnt area and emissions (Li et al., 2019). In the study, Crops were particularly highlighted as a possible variable to bound the extent of biases due to anthropogenic factors. However, the XGBoost model's still-missing 33% of bias representation indicates that a fairly large portion of the bias is not explained by the current INFERNO inputs. Therefore, bias in Crop representation could be reduced by incorporating additional information beyond its fraction. In a fire model, crop representation needs to include the agriculture management cycle (Li et al., 2013), the influence of socioeconomic factors on management practices (Li et al., 2013), agricultural expansion, and landscape fragmentation (SilvaJunior et al., 2022), among others. Crop representation would also need to include the agricultural role in fire suppression (Haas et al., 2022). To include a representation of deforestation in fire models, in addition to parameters such as the deforestation rate, human accessibility represented by distance to roads and rivers, could be explored (Haas et al., 2022; dos Reis et al., 2021).

In regions such as South America, individually representing deforestation in INFERNO can increase simulated fire emissions and, in turn, exacerbate biases that hinder their potential improvement. At the same time, having a more accurate response to soil moisture would reduce emissions, possibly below estimates, making the lack of deforestation representation more visible.

Both developments individually would yield no obvious benefit compared to emissions inventories, but would improve the

model's ability to represent fire-relevant processes. We recommend evaluating the benefits of this development, weighing the interannual variability of the simulated factors and derived consequences on the model. Additionally, pursuing synergistic development could provide added advantages.

4.3 Future work

This study presents several important limitations that can be addressed in future research. For the sensitivity analysis, we employed a one-at-a-time approach, reason why only a few experiments were run across the full range of input variability. Therefore, we see significant benefits in utilising methods such as the perturbed ensemble member approach. We recommend paying special attention to the interactions between soil moisture and PFT. Furthermore, in this study, we used similar weightedaverage estimates to calculate the biases modelled by the XGBoost model. For this, employing a weighted average based on inventory performance would allow for a more accurate benchmark. Alternatively, to better account for the uncertainty introduced by multiple inventories, an approach could involve running multiple machine learning models to target the different biases present across them. Lastly, while we aim to identify pathways for improvement using the current inputs to INFERNO, incorporating additional variables into the machine learning model could help address further, and even fine-scale, biases.

Code and data availability. The ~~*Code and data availability.* The cut~~ JULES-ES control configuration (based on JULES version 7.5) is stored at ~~https://code.metoffice.gov. uk/trac/roses-u/browser/d/l/3/2/3/trunk (~~[https://code.metoffice.gov. uk/trac/roses-u/browser/d/l/3/2/3/trunk, last access:11 March 2025~~). The fire CO emission are download from~~]. JULES and associated configurations are freely available for non-commercial research use, as set out in the JULES user terms and conditions [http://jules-lsm.github.io/access_req/JULES_Licence.pdf, last access: 10 November 2025]. For a comprehensive guide to accessing, installing, and running the configurations, we direct the reader to Appendix A in Wiltshire et al. (2020). Note that to view and use the JULES-ES source code, access will be required via the Met Office Science Repository Service [https://code.metoffice.gov.uk/trac/home, last access: 10 November 2025], and is available to those who have signed the JULES user agreement. The easiest way to access the repository is to complete the online form to register at [http: 645 //jules-lsm.github.io/access_req/JULES_access.html, last access: 10 November 2025].

The fire CO emission are downloaded from the inventories GFEDvn5 at [https://surfdrive.surf.nl/files/index.php/s/VPMEYinPeHtWVxn, last access: 18 November 2025], GFEDvn4s [https://daac.ornl.gov/VEGETATION/guides/fire_emissions_v4_R1.html, last access: 20 October 2025] (van der Werf et al., 2017), GFASvn1.2 [https://ads.atmosphere.copernicus.eu/datasets/cams-global-fire-emissions-gfas?tab=overview, last access: 18 November 2025] (Kaiser et al., 2012). The 3BEM-FRP dataset was provided directly by (Pereira et al., 2022). ~~https://surfdrive.surf.nl/files/index.php/s/VPMEYinPeHtWVxn, GFEDvn4s https://daac.ornl.gov/VEGETATION/guides/fire_emissions_v4 The~~

R1.html (van der Werf et al., 2017), GFASv1.2 https://rda.ucar.edu/datasets/d312009/dataaccess/ (Kaiser et al., 2012), FINNv2.5 https://ads.atmosphere.copernicus.eu/datasets/cams-global-fire-emissions-gfas?tab=overview (Wiedinmyer and Emmons, 2022). The 3BEM FRP dataset was provided directly by the authors. The TCCO were downloaded from MOPPIT at https://asdc.larc.nasa.gov/project/MOPITT/ MOP02J_9. The data from the IASI retrieval product is now available at https://dx.doi.org/10.5285/4b31d47716604b9f84714fab39ce973c (Moore and Remedios, 2025). The HDI datasets were downloaded on a national scale https://datadryad.org/dataset/doi:10.5061/dryad.dk1j0 [https://datadryad.org/dataset/doi:10.5061/dryad.dk1j0, last access: 18 November 2025] and on a subnational scale from https://globaldatalab.org/shdi/ [https://globaldatalab.org/shdi/, last access: 18 November 2025]. Some assessments were done using the deforestation front for 2020 provided at and the ecoregion [https://globil.panda.org/datasets/panda::deforestation-fronts-2020-1/about, last access: 18 November 2025] and the ecoregion for 2017 provided at https://globil.panda.org/datasets/panda::deforestation-fronts-2020-1/about. [https://ecoregions.appspot.com/, last access: 18 November 2025]. The model inputs are provided by ISIMIP3a at https://protocol.isimip.org/#/ISIMIP3a/fire [https://protocol.isimip.org/#/ISIMIP3a/fire, last access: 18 November 2025]

Author contributions. All the authors participated in reviewing and editing this manuscript. MPV: conceptualisation; data curation; formal analysis; investigation; methodology; software; visualisation; writing (original draft). RJP: conceptualisation; investigation; methodology; supervision; project administration. STT: conceptualisation; investigation; methodology; supervision; project administration. CD: methodology. DPM: resources. GM: resources. MPC: project administration

Competing interests. The contact author has declared that none of the authors has any competing interests

Acknowledgements. We thank the NCAS Computational Modelling Services Helpdesk for the software support regarding JULES-INFERNO.

The authors also thank Camilla Mathison, Eleanor Burke, and Rich Ellis for their help in setting up the suite. This work was funded by the UK Natural Environment Research Council (NERC), which provided funding for the National Centre for Earth Observation (NCEO; grant no. NE/R016518/1, NE/X019071/1 and NE/R016518/1) and the NERC Panorama Doctoral Training Partnership (DTP; grant no. NE/S007458/1). The contributions of Steven Turnock were funded by the Met Office Climate Science for Service Partnership (CSSP) China project under the International Science Partnerships Fund (ISPF). São Paulo Research Foundation (FAPESP; grants 2019/25701-8, 2023/03206-0) funded the contributions from Guilherme Mataveli.

EUMETSAT provided spectral (L1C) and retrieved meteorological data (L2) for MetOp-B IASI. The IASI retrievals and JULES-INFERNO runs were produced using JASMIN, the UK collaborative data analysis environment (https://www.jasmin.ac.uk), with the University of Leicester IASI retrieval Scheme (ULIRS). Pre-processing of IASI data into a structure suitable for ULIRS was performed using the ALICE High Performance Computing facility at the University of Leicester.

References

Akagi, S. K., Yokelson, R. J., Wiedinmyer, C., Alvarado, M. J., Reid, J. S., Karl, T., Crounse, J. D., and Wennberg, P. O.: Emission factors for open and domestic biomass burning for use in atmospheric models, Atmospheric Chemistry and Physics, 11, 4039–4072, https://doi.org/10.5194/acp-11-4039-2011, 2011.

Amador-Jiménez, M., Millner, N., Palmer, C., Pennington, R. T., and Sileci, L.: The Unintended Impact of Colombia's Covid-19 Lockdown on Forest Fires, Environmental and Resource Economics, 76, 1081–1105, https://doi.org/10.1007/s10640-020-00501-5, 2020.

Andela, N., Morton, D. C., Giglio, L., Chen, Y., van der Werf, G. R., Kasibhatla, P. S., DeFries, R. S., Collatz, G. J., Hantson, S., Kloster, S., Bachelet, D., Forrest, M., Lasslop, G., Li, F., Mangeon, S., Melton, J. R., Yue, C., and Randerson, J. T.: A human-driven decline in global burned area, Science, 356, 1356–1362, https://doi.org/10.1126/science.aal4108, 2017.

Andela, N., Morton, D. C., Schroeder, W., Chen, Y., Brando, P. M., and Randerson, J. T.: Tracking and classifying Amazon fire events in near-real time, Science Advances, 8, eabd2713, https://doi.org/10.1126/sciadv.abd2713, 2022.

Andreae, M. O. and Merlet, P.: Emission of trace gases and aerosols from biomass burning, Global Biogeochemical Cycles, 15, 955–966, https://doi.org/https://doi.org/10.1029/2000GB001382, 2001.

Aragão, L. E. O. C., Anderson, L. O., Fonseca, M. G., Rosan, T. M., Vedovato, L. B., Wagner, F. H., Silva, C. V. J., Junior, C. H. L. S., Arai, E., Aguiar, A. P., Barlow, J., Berenguer, E., Deeter, M. N., Domingues, L. G., Gatti, L., Gloor, M., Malhi, Y., Marengo, J. A., Miller, J. B., Phillips, O. L., and Shimabukuro, Y. E.: The IncidenceSaatchi, S.: 21st Century drought-related fires counteract the decline of Fire in Amazonian Forests with Implications for REDD, Science, 328, 1275–1278Amazon deforestation carbon emissions, Nature Communications, 9, 536, https://doi.org/10.1126/science.1186925, 2010/10.1038/s41467-017-02771-y, 2018.

Arrizaga, R., Clarke, D., Cubillos, P. P., Ruiz-Tagle V, C., et al.: Wildfires and Human Health: Evidence from 15 Wildfire Seasons in Chile, 720 Tech. rep., Inter-American Development Bank, 2023.

Baumann, M., Gasparri, I., Piquer-Rodríguez, M., Gavier Pizarro, G., Griffiths, P., Hostert, P., and Kuemmerle, T.: Carbon emissions from agricultural expansion and intensification in the Chaco, Global Change Biology, 23, 1902–1916, https://doi.org/https://doi.org/10.1111/gcb.13521, 2017.

Bauters, M., Drake, T. W., Verbeeck, H., Bodé, S., Hervé-Fernández, P., Zito, P., Podgorski, D. C., Boyemba, F., Makelele, I., Ntaboba, L. C.,

Spencer, R. G. M., and Boeckx, P.: High fire-derived nitrogen deposition on central African forests, Proceedings of the National Academy of Sciences, 115, 549–554, https://doi.org/10.1073/pnas.1714597115, 2018.

Beckett, H., Staver, A. C., Blackford, K. R., Charles-Dominique, T., and Bond, W. J.: Pathways of savannization in a mesic African savanna–forest mosaic following an extreme fire, Journal of Ecology, 110, 902–915, https://doi.org/10.1111/1365-2745.13851, 2022.

Kaseaar, M., Burton, C., Burke, E., Prentice, I. C., and Voulgarakis, A.: INFERNO-peat v1.0.0: a representation of northern high-latitude peat fires in the JULES-INFERNO global fire model, Geoscientific Model Development, 17, 3063–3079, https://doi.org/10.5194/gmd-17-3063-2024, 2024.

Burton, C., Betts, R., Cardoso, M., Feldpausch, T. R., Harper, A., Jones, C. D., Kelley, D. I., Robertson, E., and Wiltshire, A.: Representation of fire, land-use change and vegetation dynamics in the Joint UK Land Environment Simulator vn4.9 (JULES), Geoscientific Model Development, 12, 179–193, https://doi.org/10.5194/gmd-12-179-2019, 2019.

Burton, C., Betts, R. A., Jones, C. D., Feldpausch, T. R., Cardoso, M., and Anderson, L. O.: El Niño driven changes in global fire 2015/16, Frontiers in Earth Science, 8, 199, https://doi.org/10.3389/feart.2020.00199, 2020.

Burton, C., Kelley, D. I., Jones, C. D., Betts, R. A., Cardoso, M., and Anderson, L.: South American fires and their impacts on ecosystems increase with continued emissions, Climate Resilience and Sustainability, 1, e8, https://doi.org/https://doi.org/10.1002/cli2.8, 2022.

Burton, C., Lampe, S., Kelley, D. I., Thiery, W., Hantson, S., Christidis, N., Gudmundsson, L., Forrest, M., Burke, E., Chang, J., Huang, H., Ito, A., Kou-Giesbrecht, S., Lasslop, G., Li, W., Nieradzik, L., Li, F., Chen, Y., Randerson, J., Reyer, C. P., Canadell, J. G., Monteiro, P. M., Costa, M. O., and Mengel, M.: Global burned area increasingly explained by climate change, Nature Climate Change, 14, 1186–1192, https://doi.org/10.1038/s41558024-02140-w, 2024.

H., Da Cunha, L. C., Cox, P. M., Eliseev, A. V., Henson, S., Ishii, M., Jaccard, S., Koven, C., et al.: Global carbon and other biogeochemical cycles and feedbacks, IPCC AR6 WGI, final government distribution, 2021.

Candido da Silva, A. M., Moi, G. P., Mattos, I. E., and Hacon, S. d. S.: Low birth weight at term and the presence of fine particulate matter and carbon monoxide in the Brazilian Amazon: a population-based retrospective cohort study, BMC pregnancy and childbirth, 14, 1-8, https://doi.org/https://doi.org/10.1186/1471-2393-14-309, 2014.

Chen, T., He, T., Benesty, M., Khotilovich, V., Tang, Y., Cho, H., Chen, K., Mitchell, R., Cano, I., Zhou, T., Li, M., Xie, J., Lin, M., Geng, Y., Li, Y., Yuan, J., and Cortes, D.: XGBoost Parameters, https://xgboost.readthedocs.io/en/latest/parameter.html, https://xgboost.readthedocs.io/en/latest/parameter.html, 2025.

Chen, Y., Morton, D. C., Jin, Y., Collatz, G. J., Kasibhatla, P. S., van der Werf, G. R., DeFries, R. S., and Randerson, J. T.: Long-term trends and interannual variability of forest, savanna and agricultural fires in South America, Carbon Management, 4, 617–638, https://doi.org/10.4155/cmt.13.61, 2013.

Chen, Y., Hall, J., van Wees, D., Andela, N., Hantson, S., Giglio, L., van der Werf, G. R., Morton, D. C., and Randerson, J. T.: Multi-decadal trends and variability in burned area from the fifth version of the Global Fire Emissions Database (GFED5), Earth System Science Data, 15, 5227–5259, https://doi.org/10.5194/essd-15-5227-2023, 2023.

Cunningham, C. X., Williamson, G. J., Bowman, D. M. J. S., Cummings, A. R., Kennady, B. J., and Bowman, D. M.: Increasing frequency and intensity of the most extreme wildfires on Earth, Nature Ecology Evolution, 8, 1420–1425, https://doi.org/10.1038/s41559-024-02452-2, 2024.

Adeuga, A. M.: Fire Regions of a Northern Amazonian Landscape Relative to Indigenous Peoples' Lands, Remote Sensing, 17,

de Oliveira Alves, N., Vessoni, A. T., Quinet, A., Fortunato, R. S., Kajitani, G. S., Peixoto, M/10.3390/rs17193386, 2025. S., Hacon, S. d. S., Artaxo, P., Saldiva, P., Menck, C. F. M., et al.: Biomass burning in the Amazon region causes DNA damage and cell death in human lung cells, Scientific reports, 7, 10 937, 2017.

755 Deeter, M., Francis, G., Gille, J., Mao, D., Martínez-Alonso, S., Worden, H., Ziskin, D., Drummond, J., Commane, R., Diskin, G., and McKain, K.: The MOPITT Version 9 CO product: sampling enhancements and validation, Atmospheric Measurement Techniques, 15, 2325–2344, https://doi.org/10.5194/amt-15-2325-2022, 2022.

Deeter, M. N., Edwards, D. P., Francis, G. L., Gille, J., G., Martínez Alonso, S., Worden, H. M., and Sweeney, C.: A climatescale satellite record for carbon monoxide: the MOPITT Version 7 product, Atmospheric Measurement Techniques, 10, 2533–2555, 760 https://doi.org/10.5194/amt-10-2533-2017, 2017.

Deeter, M. N., Martínez Alonso, S., Andreae, M. O., and Schlager, H.: Satellite-Based Analysis of CO Seasonal and Interannual Variability Over the Amazon Basin, Journal of Geophysical Research: Atmospheres, 123, 5641–5656, https://doi.org/https://doi.org/10.1029/2018JD028425, 2018.

Dinerstein, E., Olson, D., Joshi, A., Vynne, C., Burgess, N. D., Wikramanayake, E., Hahn, N., Palminteri, S., Hedao, P., Noss, R., Hansen,

765705 M., Locke, H., Ellis, E. C., Jones, B., Barber, C. V., Hayes, R., Kormos, C., Martin, V., Crist, E., Sechrest, W., Price, L., Baillie, J. E. M., Weeden, D., Suckling, K., Davis, C., Sizer, N., Moore, R., Thau, D., Birch, T., Potapov, P., Turubanova, S., Tyukavina, A., de Souza, N., Pintea, L., Brito, J. C., Llewellyn, O. A., Miller, A. G., Patzelt, A., Ghazanfar, S. A., Timberlake, J., Klöser, H., Shennan-Farpón, Y., Kindt, R., Lillesø, J.-P. B., van Breugel, P., Graudal, L., Voge, M., Al-Shammari, K. F., and Saleem, M.: An Ecoregion-Based Approach to Protecting Half the Terrestrial Realm, BioScience, 67, 534–545, https://doi.org/10.1093/biosci/bix014, 2017.

710 dos Reis, M., de Alencastro Graça, P. M. L., Yanai, A. M., Ramos, C. J. P., and Fearnside, P. M.: Forest fires and deforestation in the central Amazon: Effects of landscape and climate on spatial and temporal dynamics, Journal of Environmental Management, 288, 112 310, https://doi.org/10.1016/j.jenvman.2021.112310, 2021.

Drüke, M., Forkel, M., von Bloh, W., Sakschewski, B., Cardoso, M., Bustamante, M., Kurths, J., and Thonicke, K.: Improving the LPJmL4-SPITFIRE vegetation–fire model for South America using satellite data, Geoscientific Model Development, 12, 5029–5054, 715 https://doi.org/10.5194/gmd-12-5029-2019, 2019.

Forkel, M., Andela, N., Harrison, S. P., Lasslop, G., van Marle, M., Chuvieco, E., Dorigo, W., Forrest, M., Hantson, S., Heil, A., Li, F., Melton, J., Sitch, S., 770 Fonseca, M. GYue, C., and Arneth, A.: Emergent relationships with respect to burned area in global satellite observations and fire-enabled vegetation models, Biogeosciences, 16, 57–76, https://doi.org/10.5194/bg-16-57-2019, 2019.

Forkel, M., Schmidt, L., Zotta, R.-M., Dorigo, W., and Yebra, M.: Estimating leaf moisture content at global scale from passive microwave 720 satellite observations of vegetation optical depth, Hydrology and Earth System Sciences, 27, 39–68, https://doi.org/10.5194/hess-27-392023, 2023.

, Andersen, L. O., Arai, E., Shimabukuro, Y. E., Xaud, H. A. M., Xaud, M. R., Madani, N., Wagner, F. H., and Aragão, L. E. O. C.: Climatic and anthropogenic drivers of northern Amazon fires during the 2015–2016 El Niño event, Ecological Applications, 27, 2514–2527, https://doi.org/https://doi.org/10.1002/eap.1628, 2017.

Frieler, K., Volkholz, J., Lange, S., Schewe, J., Mengel, M., del Rocío Rivas López, M., Otto, C., Reyer, C. P. O., Karger, D. N., Malle, J. T., Treu, S., Menz, C., Blanchard, J. L., Harrison, C. S., Petrik, C. M., Eddy, T. D., Ortega-Cisneros, K., Novaglio, C., Rousseau, Y.,

775 Watson, R. A., Stock, C., Liu, X., Heneghan, R., Tittensor, D., Maury, O., Büchner, M., Vogt, T., Wang, T., Sun, F., Sauer, I. J., Koch, J.,

725 Vanderkelen, I., Jägermeyr, J., Müller, C., Rabin, S., Klar, J., Vega del Valle, I. D., Lasslop, G., Chadburn, S., Burke, E., Gallego-Sala, A., Smith, N., Chang, J., Hantson, S., Burton, C., Gädeke, A., Li, F., Gosling, S. N., Müller Schmied, H., Hattermann, F., Wang, J., Yao, F., Hickler, T., Marcé, R., Pierson, D., Thiery, W., Mercado-Bettín, D., Ladwig, R., Ayala-Zamora, A. I., Forrest, M., and Bechtold, M.: Scenario setup and forcing data for impact model evaluation and impact attribution within the third round of the Inter-Sectoral Impact 780 Model Intercomparison Project (ISIMIP3a), Geoscientific Model Development, 17, 1–51, https://doi.org/10.5194/gmd-17-1-2024, 2024.

730 Gallup, S. M., Ford, B., Naus, S., Gallup, J. L., and Pierce, J. R.: Equations to Predict Carbon Monoxide Emissions from Amazon Rainforest Fires, Fire, 7, https://doi.org/10.3390/fire7120477, 2024.

Gatti, L. V., Basso, L. S., Miller, J. B., Gloor, M., Domingues, L. G., Cassol, H. L. G., Tejada, G., Aragão, L. E. O. C., Nobre, C., Peters, W., Marani, L., Arai, E., Sanches, A. H., Corrêa, S. M., Anderson, L., Randow, C. V., Correia, C. S. C., Crispim, S. P., and Neves, R. A. L.: Amazonia as a carbon source linked to deforestation and climate change, Nature, 595, 388–393, https://doi.org/10.1038/s41586021-03629-6, 10.1038/s41586735 021-03629-6, 2021.

785 Gatti, L. V., Cunha, C. L., Marani, L., Cassol, H. L., Messias, C. G., Arai, E., Denning, A. S., Soler, L. S., Almeida, C., Setzer, A., et al.: Increased Amazon carbon emissions mainly from decline in law enforcement, Nature, 621, 318–323, https://doi.org/10.1038/s41586-02306390-0, 10.1038/s41586-02306390-0, 2023.

Geirinhas, J. L., Russo, A. C., Libonati, R., Miralles, D. G., Ramos, A. M., Gimeno, L., and Trigo, R. M.: Combined large-scale tropical trop-

740 ical and subtropical forcing on the severe 2019–2022 drought in South America, npj Climate and Atmospheric Science, 6, 185, 790 https://doi.org/10.1038/s41612-023-00510-3, 2023. https://doi.org/10.1038/s41612-023-00510-3, 2023.

Gomes, M. S., de Albuquerque Cavalcanti, I. F., and Müller, G. V.: 2019/2020 drought impacts on South America and atmospheric and oceanic influences, Weather and Climate Extremes, 34, 100 404, https://doi.org/https://doi.org/10.1016/j.wace.2021.100404, 10.1016/j.wace.2021.100404, 2021.

Grimm, A. M.: Interannual climate variability in South America: impacts on seasonal precipitation, extreme events, Haas, O., Prentice, I. C., and possible effects of climate change, StochasticHarrison, S. P.: Global environmental controls on wildfire burnt area, size, and intensity, Environmental Research and Risk Assessment, pp. 537–554745 Letters, 17, 065 004, https://doi.org/10.1007/s00477-010-0420-1/10.1088/1748-9326/ac6a69, 2022.

795 Hamilton, D. S., Perron, M. M., Bond, T. C., Bowie, A. R., Buchholz, R. R., Guieu, C., Ito, A., Maenhaut, W., Myriokefalitakis, S., Olgun, N., Rathod, S. D., Schepanski, K., Tagliabue, A., Wagner, R., and Mahowald, N. M.: Earth, Wind, Fire, and Pollution: Aerosol Nutrient Sources and Impacts on Ocean Biogeochemistry, Annual Review of Marine Science, 14, 303–330, https://doi.org/10.1146/annurevmarine-031921-013612, 10.1146/annurevmarine-031921-013612, 2022.

Hanan, E. J., Kennedy, M. C., Ren, J., Johnson, M. C., and Smith, A. M. S.: Missing Climate Feedbacks in Fire Models: Limitations and Uncertainties in Fuel Loadings and the Role of Decomposition in Fine Fuel Accumulation, Journal of Advances in Modeling Earth Systems, 14, e2021MS002 818, https://doi.org/https://doi.org/10.1029/2021MS002818, e2021MS002818 2021MS002818,/10.1029/2021MS002818, 2022.

Hantson, S., Arneth, A., Harrison, S. P., Kelley, D. I., Prentice, I. C., Rabin, S. S., Archibald, S., Mouillot, F., Arnold, S. R., Artaxo, P., Bachelet, D., Ciais, P., Forrest, M., Friedlingstein, P., Hickler, T., Kaplan, J. O., Kloster, S., Knorr, W., Lasslop, G., Li, F., Mangeon, S., Melton, J. R., Meyn, A., Sitch, S., Spessa, A., van der Werf, G. R., Voulgarakis, A., and Yue, C.: The status and challenge of global fire modelling, Biogeosciences, 13, 3359–3375, https://doi.org/10.5194/bg-13-3359-2016, 2016.

Hantson, S., Kelley, D. I., Arneth, A., Harrison, S. P., Archibald, S., Bachelet, D., Forrest, M., Hickler, T., Lasslop, G., Li, F., Mangeon, S., Melton, J. R., Nieradzik, L., Rabin, S. S., Prentice, I. C., Sheehan, T., Sitch, S., Teckentrup, L., Voulgarakis, A., and Yue, C.: Quantitative assessment of fire and vegetation properties in simulations with fire-enabled vegetation models from the Fire Model Intercomparison Project, Geoscientific Model Development, 13, 3299–3318, https://doi.org/10.5194/gmd-13-3299-2020,/10.5194/gmd-13-3299-2020, 2020.

Harper, K. L., Lamarche, C., Hartley, A., Peylin, P., Ottlé, C., Bastrikov, V., San Martín, R., Bohnenstengel, S. I., Kirches, G., Boettcher, M., Shevchuk, R., Brockmann, C., and Defourny, P.: A 29-year time series of annual 300 m resolution plant-functional-type maps for climate models, Earth System Science Data, 15, 1465–1499, https://doi.org/10.5194/essd-15-1465-2023,/10.5194/essd-15-1465-2023, 2023.

Heilman, W. E., Liu, Y., Urbanski, S., Kovalev, V., and Mickler, R.: Wildland fire emissions, carbon, and climate: Plume rise, atmospheric transport, and chemistry processes, Forest Ecology and Management, 317, 70–79, https://doi.org/https://doi.org/10.1016/j.foreco.2013.02.001, wildland fire emissions, carbon, and climate: Science overview and knowledge needs, 2014.

Hess, P., Lange, S., Schötz, C., and Boers, N.: Deep Learning for Bias-Correcting CMIP6-Class Earth System Models, Earth's Future, 11, e2023EF004 002, https://doi.org/https://doi.org/10.1029/2023EF004002, e2023EF004002 2023EF004002,/10.1029/2023EF004002, 2023.

Holanda, B. A., Pöhlker, M. L., Walter, D., Saturno, J., Sörgel, M., Ditas, J., Ditas, F., Schulz, C., Franco, M. A., Wang, Q., Donth, T., Artaxo, P., Barbosa, H. M. J., Borrmann, S., Braga, R., Brito, J., Cheng, Y., Dollner, M., Kaiser, J. W., Klimach, T., Knote, C., Krüger, O. O., Fütterer, D., Lavric, J. V., Ma, N., Machado, L. A. T., Ming, J., Morais, F. G., Paulsen, H., Sauer, D., Schlager, H., Schneider, J., Su, H., Weinzierl, B., Walser, A., Wendisch, M., Ziereis, H., Zöger, M., Pöschl, U., Andreae, M. O., and Pöhlker, C.: Influx of African biomass burning aerosol during the Amazonian dry season through layered transatlantic transport of black carbon-rich smoke, Atmospheric Chemistry and Physics, 20, 4757–4785, https://doi.org/10.5194/acp-20-4757-2020, 2020.

Hua, W., Lou, S., Huang, X., Xue, L., Ding, K., Wang, Z., and Ding, A.: Diagnosing uncertainties in global biomass burning emission inventories and their impact on modeled air pollutants, Atmospheric Chemistry and Physics, 24, 6787–6807, https://doi.org/10.5194/acp24-6787-2024,/10.5194/acp24-6787-2024, 2024.

Illingworth, S. M., Remedios, J. J., Boesch, H., Moore, D. P., Sembhi, H., Dudhia, A., and Walker, J. C.: ULIRS, an optimal estimation retrieval scheme for carbon monoxide using IASI spectral radiances: sensitivity analysis, error budget and simulations, Atmospheric 830 Measurement Techniques, 4, 269–288, https://doi.org/10.5194/amt-4-269-2011, 2011.

Jury, M. R. and Pabón, A. R. G.: Dispersion of Smoke Plumes over South America, Earth Interactions, 25, 1 – 14, https://doi.org/10.1175/EID-20-0004.1, 2021.

Júnior, A. C. P., Oliveira, S. L. J., Pereira, J. M. Hussain, M. and Mahmud, I.: pyMannKendall: a python package for non parametric Mann Kendall family of trend tests., Journal of Open 770 Source Software, 4, 1556, https://doi.org/10.21105/joss.01556, 2019.

Intergovernmental Panel on Climate Change (IPCC): Global Carbon and Other Biogeochemical Cycles and Feedbacks, Cambridge University Press, https://doi.org/10.1017/9781009157896.007, 2023.

G., and Turkman, M. A. A.: Modelling Fire Frequency in a Cerrado Savanna Protected Area, PLoS ONE, 9, e102 380, https://doi.org/10.1371/journal.pone.0102380, 2014.

835 Kaiser, J. W., Heil, A., Andreae, M. O., Benedetti, A., Chubarova, N., Jones, L., Morcrette, J.-J., Razinger, M., Schultz, M. G., Suttie, M., and van der Werf, G. R.: Biomass burning emissions estimated with a global fire assimilation system based on observed fire radiative 775 power, Biogeosciences, 9, 527–554, https://doi.org/10.5194/bg-9-527-2012, /10.5194/bg-9-527-2012, 2012.

Kelley, D. I., Bistinas, I., Whitley, R., Burton, C., Marthews, T. R., and Dong, N.: How contemporary bioclimatic and human controls change global fire regimes, Nature Climate Change, 9, 690–696, https://doi.org/10.1038/s41558-019-0540-7, 2019.

Kim, H.-J., Kim, J.-S., Ham, Y.-G., Park, J.-H., Milodowski, D., Aragão, L. E. O. C., and Williams, M.: Anomalous temperature in North Tropical Atlantic linked to Brazilian Cerrado fires, npj Climate and Atmospheric Science, 8, 63, https://doi.org/10.1038/s41612-025-780 00945-w, 2025.

Kloster, S. and Lasslop, G.: Historical and future fire occurrence (1850 to 2100) simulated in CMIP5 Earth System Models, Global and Planetary Change, 150, 58–69, https://doi.org/https://doi.org/10.1016/j.gloplacha.2016.12.017, /10.1016/j.gloplacha.2016.12.017, 2017.

Kummu, M., Taka, M., and Guillaume, J. H. 840A.: Gridded global datasets for Gross Domestic Product and Human Development Index over 1990–2015, Scientific Data, 5, 180 004, https://doi.org/10.1038/sdata.2018.4, 2018.

785 Lasslop, G., Coppola, A. I., Voulgarakis, A., Yue, C., and Veraverbeke, S.: Influence of Fire on the Carbon Cycle and Climate, Current Climate Change Reports, 5, 112–123, https://doi.org/10.1007/s40641-019-00128-9, /10.1007/s40641-019-00128-9, 2019.

Lavers, D. A., Simmons, A., Vamborg, F., and Rodwell, M. J.: An evaluation of ERA5 precipitation for climate monitoring, Quarterly Journal of the Royal Meteorological Society, 148, 3152–3165, https://doi.org/https://doi.org/10.1002/qj.4351, 2022.

Li, F., Levis, S., and Ward, D. S.: Quantifying the role of fire in the Earth system ndash; Part 1: Improved global fire modeling in the 845 Community Earth System Model (CESM1), Biogeosciences, 10, 2293–2314, https://doi.org/10.5194/bg-10-2293-2013, 2013.

Li, F., Val Martin, M., Andreae, M. O., Arneth, A., Hantson, S., Kaiser, J. W., Lasslop, G., Yue, C., Bachelet, D., Forrest, M., Kluzek, E., Liu, 790 X., Mangeon, S., Melton, J. R., Ward, D. S., Darmenov, A., Hickler, T., Ichoku, C., Magi, B. I., Sitch, S., van der Werf, G. R., Wiedinmyer,

C., and Rabin, S. S.: Historical (1700–2012) global multi-model estimates of the fire emissions from the Fire Modeling Intercomparison Project (FireMIP), Atmospheric Chemistry and Physics, 19, 12 545–12 567, https://doi.org/10.5194/acp-19-12545-2019, 2019.

Li, F., Song, X., Harrison, S. P., Marlon, J. R., Lin, Z., Leung, L. R., Schwinger, J., Marécal, V., Wang, S., Ward, D. S., Dong, X., Lee, H., Nieradzik, L., Rabin, S. S., and Séférian, R.: Evaluation of global fire simulations in CMIP6 Earth system models, Geoscientific Model Development, 17, 8751–8771, https://doi.org/10.5194/gmd-17-8751-2024, 2024.

Lichtig, P., Gaubert, B., Emmons, L. K., Jo, D. S., Callaghan, P., Ibarra-Espinosa, S., Dawidowski, L., Brasseur, G. P., and Pfister, G.: Multiscale CO Budget Estimates Across South America: Quantifying Local Sources and Long Range Transport, Journal of Geophysical Research: Atmospheres, 129, e2023JD040434, https://doi.org/https://doi.org/10.1029/2023JD040434, e2023JD040434 2023JD040434, 2024.

Liu, T., Mickley, L. J., Marlier, M. E., DeFries, R. S., Khan, M. F., Latif, M. T., and Karambelas, A.: Diagnosing spatial biases and uncertainties in global fire emissions inventories: Indonesia as regional case study, Remote Sensing of Environment, 237, 111 557, https://doi.org/https://doi.org/10.1016/j.rse.2019.111557, /10.1016/j.rse.2019.111557, 2020.

Liu, Y., Fu, R., and Dickinson, R.: The Impacts of Smoke Aerosols on South American Monsoon, Bull. Amer. Meteor. Soc, 86, 1062–1063, 2005.

Liu, Z., Doherty, R. M., Wild, O., O'Connor, F. M., and Turnock, S. T.: Correcting ozone biases in a global chemistry–climate model: implications for future ozone, Atmospheric Chemistry and Physics, 22, 12 543–12 557, https://doi.org/10.5194/acp-22-12543-2022, 2022/10.5194/acp-22-12543-2022, 2022a.

Lundberg, S. M. and Lee, S. I.: A unified approach to interpreting model predictions, vol. 30 of *NIPS'17*, Curran Associates Inc., ISBN 9781510860964, https://dl.acm.org/doi/10.5555/3295222.3295230, 2017.

Liu, Z., Eden, J. M., Dieppois, B., and Blackett, M.: A global view of observed changes in fire weather extremes: uncertainties and attribution to climate change, Climatic Change, 173, 14, https://doi.org/10.1007/s10584-022-03409-9, 2022b.

Liu, Z., Zhou, K., Yao, Q., and Reszka, P.: An interpretable machine learning model for predicting forest fire danger based on Bayesian optimization, Emergency Management Science and Technology, 4, https://doi.org/10.48130/emst-0024-0026, 2024.

Lundberg, S. M., Erion, G., Chen, H., DeGrave, A., Prutkin, J. M., Nair, B., Katz, R., Himmelfarb, J., Bansal, N., and Lee, S.I.: From local explanations to global understanding with explainable AI for trees, Nature Machine Intelligence, 2, 2522–5839, https://doi.org/10.1038/s42256-019-0138-9, 2020.

Magahey, S. and Kooperman, G. J.: Isolating the effect of biomass burning aerosol emissions on 20th century hydroclimate in South America and Southeast Asia, Environmental Research Letters, 18, 104 029, https://doi.org/10.1088/1748-9326/acf7d4, 2023.

Mangeon, S., Voulgarakis, A., Gilham, R., Harper, A., Sitch, S., and Folberth, G.: INFERNO: a fire and emissions scheme for the UK Met Office's Unified Model, Geoscientific Model Development, 9, 2685–2700, https://doi.org/10.5194/gmd-9-2685-2016, /10.5194/gmd-9-2685-2016, 2016.

Marengo, J. A., Cunha, A. P., Cuartas, L. A., Leal, K. R. D., Broedel, E., Seluchi, M. E., Michelin, C. M., Baião, C. F. D. P., Angulo,

E. C., Almeida, E. K., Kazmierczak, M. L., Mateus, N. P. A., Silva, R. C., and Bender, F.: Extreme Drought in the Brazilian Pantanal in 870 2019–2020: Characterization, Causes, and Impacts, Frontiers in Water, 3, https://doi.org/10.3389/frwa.2021.639204, 2021.

Marques, E. Q., Marimon-Junior, B. H., Marimon, B. S., Matricardi, E. A., Mews, H. A., and Colli, G. R.: Redefining the Cerrado–Amazonia transition: implications for conservation, Biodiversity and conservation, 29, 1501–1517, https://doi.org/https://doi.org/10.1007/s10531019 01720 z, /10.1007/s10531-019-01720-z, 2020.

Mataveli, G., Pereira, G., Sanchez, A., de Oliveira, G., Jones, M. W., Freitas, S. R., and Aragão, L. E. O. C.: Updated Land Use and Land 875 Cover Information Improves Biomass Burning Emission Estimates, Fire, 6, https://doi.org/10.3390/fire6110426, /10.3390/fire6110426, 2023.

Mathison, C., Burke, E., Hartley, A. J., Kelley, D. I., Burton, C., Robertson, E., Gedney, N., Williams, K., Wiltshire, A., Ellis, R. J., Sellar, A. A., and Jones, C. D.: Description and evaluation of the JULES-ES set-up for ISIMIP2b, Geoscientific Model Development, 16, 4249– 4264, https://doi.org/10.5194/gmd-16-4249-2023, /10.5194/gmd-16-4249-2023, 2023.

Menezes, L. S., de Oliveira, A. M., Santos, F. L., Russo, A., de Souza, R. A., Roque, F825 , O., and Libonati, R.: Lightning pat-

880 terns in the Pantanal: Untangling natural and anthropogenic-induced wildfires, Science of The Total Environment, 820, 153 021, https://doi.org/https://doi.org/10.1016/j.scitotenv.2022.153021, 2022.

Milare, G., Giarolla, A., and Escada, M. I. S.: Burned area occurrence in agrarian reform settlement projects in the Matopiba region, Brazil, Applied Geography, 166, 103 243, https://doi.org/https://doi.org/10.1016/j.apgeog.2024.103243, /10.1016/j.apgeog.2024.103243, 2024.

Moore, D. and Remedios, J.: EOCIS: Total Column CO Product, V1.0, https://doi.org/https://dx.doi.org/10.5285/4b31d47716604b9f84714fab39ce973c,

885 2025.

NASA/LARC/SD/ASDC: MOPITT Derived CO (Near and Thermal Infrared Radiances) V009, https://doi.org/10.5067/TERRA/MOPITT/ MOP02J.009, 2022.

Naus, S., Domingues, L. G., Krol, M., Luijkx, I. T., Gatti, L. V., Miller, J. B., Gloor, E., Basu, S., Correia, C., Koren, G., Worden, H. M., Flemming, J., Pétron, G., and Peters, W.: Sixteen years of MOPITT satellite data strongly constrain Amazon CO fire emissions, Atmospheric 890 Chemistry and Physics, 22, 14 735–14 750, https://doi.org/10.5194/acp-22-14735-2022, /10.5194/acp-22-14735-2022, 2022.

830 Pacheco, P., Mo, K., Dudley, N., Shapiro, A., Aguilar-Amuchastegui, N., Ling, P., Anderson, C., and Marx, A.: Deforestation fronts: Drivers and responses in a changing world, Tech. rep., WWF, Gland, Switzerland, 2021.

and responses in a changing world, Tech. rep., WWF, Gland, Switzerland, Pacifico, F., Folberth, G. Ahttps://www.worldwildlife.org/documents/508/ocuoxmdil_

Deforestation_fronts__drivers_and_responses_in_a_changing_world__f_3DJ6oVP.pdf, 2021.

Pedregosa, F., Varoquaux, G., Gramfort, A., Michel, V., Thirion, B., Grisel, O., Blondel, M., Prettenhofer, P., Weiss, R., Dubourg, V., Vanderplas, J., Passos, A., Cournapeau, D., Brucher, M., Perrot, M., and Duchesnay, E.: Scikit-learn: Machine Learning in Python, Journal

835 of Machine Learning Research, 12, 2825–2830, https://doi.org/10.48550/arXiv.1201.0490, 2011.

, Sitch, S., Haywood, J. M., Rizzo, L. V., Malavelle, F. F., and Artaxo, P.: Biomass burning related ozone damage on vegetation over the Amazon forest: a model sensitivity study, Atmospheric Chemistry and Physics, 15, 2791–2804, 895 https://doi.org/10.5194/acp-15-2791-2015, 2015.

Pereira, G., Longo, K. M., Freitas, S. R., Mataveli, G., Oliveira, V. J., Santos, P. R., Rodrigues, L. F., and Cardozo, F. S.: Improving the south America wildfires smoke estimates: Integration of polar-orbiting and geostationary satellite fire products in the Brazilian biomass burning emission model (3BEM), Atmospheric Environment, 273, 118 954, https://doi.org/https://doi.org/10.1016/j.atmosenv.2022.118954,/10.1016/j.atmosenv.2022.118954, 2022.

Perktold, J., Seabold, S., Sheppard, K., ChadFulton, Shedden, K., jbrockmendel, j grana6, Quackenbush, P., Arel-Bundock, V., McKinney, W., Langmore, I., Baker, B., Gommers, R., yogabonito, s scherrer, Zhurko, Y., Brett, M., Giampieri, E., yl565, Millman, J., Hobson, P., Vincent, Roy, P., Augspurger, T., tvanzyl, alexbrc, Hartley, T., Perez, F., Tamiya, Y., and Halchenko, Y.: statsmodels/statsmodels: Release 0.14.2, https://doi.org/10.5281/zenodo.10984387, 2024.

Pope, R. J., Arnold, S. R., Chipperfield, M. P., Reddington, C. L. S., Butt, E. W., Keslake, T. D., Feng, W., Latter, 900 B. G., Kerridge, B. J.,

Siddans, R., Rizzo, L., Artaxo, P., Sadiq, M., and Tai, A. P. K.: Substantial Increases in Eastern Amazon and Cerrado Biomass Burning-Burning845 Sourced Tropospheric Ozone, Geophysical Research Letters, 47, e2019GL084 143, https://doi.org/https://doi.org/10.1029/2019GL084143, e2019GL084143 2019GL084143,/10.1029/2019GL084143, 2020.

Power, J., Côté, M.-P., and Duchesne, T.: A Flexible Hierarchical Insurance Claims Model with Gradient Boosting and Copulas, North American Actuarial Journal, 28, 772–800, https://doi.org/10.1080/10920277.2023.2279782, 2024.

Rabin, S. S., Melton, J. R., Lasslop, G., Bachelet, D., Forrest, M., Hantson, S., Kaplan, J. O., Li, F., Mangeon, S., Ward, D. S., Yue, C., Arora, V. K., Hickler, T., Kloster, S., Knorr, W., Nieradzik, L., Spessa, A., Folberth, G. A., Sheehan, T., Voulgarakis, A., Kelley, D. I., 850 Prentice, I. C., Sitch, S., Harrison, S., and Arneth, A.: The Fire Modeling Intercomparison Project (FireMIP), phase 1: experimental and analytical protocols with detailed model descriptions, Geoscientific Model Development, 10, 1175–1197, https://doi.org/10.5194/gmd10-1175-2017, 2017.

Reddington, C. L., Morgan, W. T., Darbyshire, E., Brito, J., Coe, H., Artaxo, P., Scott, C. E., Marsham, J., and Spracklen, D. V.: Biomass burning aerosol over the Amazon: analysis of aircraft, surface and satellite observations using a global aerosol model, Atmospheric 855 Chemistry and Physics, 19, 9125–9152, https://doi.org/10.5194/acp-19-9125-2019, 2019.

Rovithakis, A., Burke, E., Burton, C., Kasoar, M., Grillakis, M. G., Seiradakis, K. D., and Voulgarakis, A.: Qi, B., Zhang, Z., Long, T., He, G., Wang, G., Peng, Y., and Xu, Z.: High Resolution (30 m) Burned Area Product Improves the Ability for Carbon Emission Estimation in Africa, Earth's Future, 12, e2024EF005 051, https://doi.org/https://doi.org/10.1029/2024EF005051, 905 e2024EF005051 2024EF005051, 2024.

Estimating future wildfire burnt area over Greece using the JULES-INFERNO model, Natural Hazards and Earth System Sciences, 25, 3185–3200, https://doi.org/10.5194/nhess-25-3185-2025, 2025.

San Martín, R., Ottlé, C., and Sörensson, A.: Fires in the South American Chaco, from dry forests to wetlands: response to climate depends 860 on land cover, Fire Ecology, 19, 57, https://doi.org/10.1186/s42408-023-00212-4,/10.1186/s42408-023-00212-4, 2023.

Sellar, A. A., Jones, C. G., Mulcahy, J. P., Tang, Y., Yool, A., Wiltshire, A., O'Connor, F. M., Stringer, M., Hill, R., Palmieri, J., Woodward,

S., de Mora, Senf, F., Heinold, B., Kubin, A., Müller, J., Schrödner, R., and Tegen, I.: How the extreme 2019–2020 Australian wildfires affected global circulation and adjustments, Atmospheric Chemistry and Physics, 23, 8939–8958, https://doi.org/10.5194/acp-23-8939-2023, 2023.

Ly, Kuhlbrodt, T., Rumbold, S. T., Kelley, D. I., Ellis, R., Johnson, C. E., Walton, J., Abraham, N. L., Andrews, M. B., Andrews, T., Archibald, A. T., Berthou, S., Burke, E., Blockley, E., Carslaw, K., Dalvi, M., Edwards, J., Folberth, G. A., Gedney, N., Griffiths, P. T., Harper, A. B., Hendry, M. A., Hewitt, A. J., Johnson, B., Jones, A., Jones, C. D., Keeble, J., Liddicoat, S., Morgenstern, O., Parker, R. J., Predoi, V., Robertson, E., Siahaan, A., Smith, R. S., Swaminathan, R., Woodhouse, M. T., Zeng, G., and Zerroukat, M.: UKESM1: Description and Evaluation of the U.K. Earth System Model, Journal of Advances in Modeling Earth Systems, 11, 4513–4558, https://doi.org/https://doi.org/10.1029/2019MS001739, 2019.

Silva-Junior, C. H. L., Buna, A. T. M., Bezerra, D. S., Costa, O. S., Santos, A. L., Basson, L. O. D., Santos, A. L. S., Alvarado, S. T., Almeida, C. T., Freire, A. T. G., Rousseau, G. X., Celentano, D., Silva, F. B., Pinheiro, M. S. S., Amaral, S., Kampel, M., Vedovato, L. B., Anderson, L. O., and Aragão, L. E. O. C.: Forest Fragmentation and Fires in the Eastern Brazilian Amazon–Maranhão State, Brazil, Fire, 5, https://doi.org/10.3390/fire5030077, /10.3390/fire5030077, 2022.

Silveira, M. V. F., Petri, C. A., Broggio, I. S., Chagas, G. O., Macul, M. S., Leite, C. C. S. S., Ferrari, E. M. M., Amim, C. G. V., Freitas, A.

L. R., Motta, A. Z. V., Carvalho, L. M. E., Silva Junior, C. H. L., Anderson, L. O., and Aragão, L. E. O. C.: Drivers of Fire Anomalies in the Brazilian Amazon: Lessons Learned from the 2019 Fire Crisis, Land, 9, https://doi.org/10.3390/land9120516, 2020.

Snyder, P. K.: The Influence of Tropical Deforestation on the Northern Hemisphere Climate by Atmospheric Teleconnections, Earth Interactions, 14, 1 – 34, https://doi.org/10.1175/2010EI280.1, /10.1175/2010EI280.1, 2010.

Teckentrup, L., Harrison, S. P., Hantson, S., Heil, A., Melton, J. R., Forrest, M., Li, F., Yue, C., Arneth, A., Hickler, T., Sitch, S., and Lasslop, G.: Response of simulated burned area to historical changes in environmental and anthropogenic factors: a comparison of seven fire models, Biogeosciences, 16, 3883–3910, https://doi.org/10.5194/bg-16-3883-2019, 2019.

Teixeira, J. C., Folberth, G. A., O'Connor, F. M., Unger, N., and Voulgarakis, A.: Coupling interactive fire with atmospheric composition and climate in the UK Earth System Model, Geoscientific Model Development, 14, 6515–6539, https://doi.org/10.5194/gmd-14-6515-2021, /10.5194/gmd-14-6515-2021, 2021.

Teixeira, J. C. M., Burton, C., Kelly, D. I., Folberth, G. A., O'Connor, F. M., Betts, R. A., and Voulgarakis, A.: Representing socioeconomic factors in the INFERNO global fire model using the Human Development Index, Biogeosciences Discussions, 2023, 1–27, https://doi.org/10.5194/bg-2023-136, 2023.

Thornhill, G. D., Ryder, C. L., Highwood, E. J., Shaffrey, L. C., and Johnson, B. T.: The effect of South American biomass burning aerosol emissions on the regional climate, Atmospheric Chemistry and Physics, 18, 5321–5342, https://doi.org/10.5194/acp-18-5321-2018, 2018.

emissions on the regional climate, Atmospheric Chemistry and Physics, 18, 5321–5342, https://doi.org/10.5194/acp-18-5321-2018, 2018. van der Werf, G. R., Randerson, J. T., Giglio, L., Collatz, G. J., Mu, M., Kasibhatla, P. S., Morton, D. C., DeFries, R. S., Jin, Y., and van Leeuwen, T. T.: Global fire emissions and the contribution of deforestation, savanna, forest, agricultural, and peat fires (1997–2009), Atmospheric Chemistry and Physics, 10, 11 707–11 735, https://doi.org/10.5194/acp-10-11707-2010, /10.5194/acp-10-11707-2010, 2010.

van der Werf, G. R., Randerson, J. T., Giglio, L., van Leeuwen, T. T., Chen, Y., Rogers, B. M., Mu, M., van Marle, M. J. E., Morton, D. C., Collatz, G. J., Yokelson, R. J., and Kasibhatla, P. S.: Global fire emissions estimates during 1997–2016, Earth System Science Data, 9, 697–720, https://doi.org/10.5194/essd-9-697-2017, 2017.

van Leeuwen, T. T., van der Werf, G. R., Hoffmann, A. A., Detmers, R. G., Rücker, G., French, N. H. F., Archibald, S., Carvalho Jr., J. A., Cook, G. D., de Groot, W. J., Hély, C., Kasischke, E. S., Kloster, S., McCarty, J. L., Pettinari, M. L., Savadogo, P., Alvarado, E. C., Boschetti, L., Manuri, S., Meyer, C. P., Siegert, F., Trollope, L. A., and Trollope, W. S. W.: Biomass burning fuel consumption rates: a field measurement database, Biogeosciences, 11, 7305–7329, https://doi.org/10.5194/bg-11-7305-2014, 2014.

van Marle, M. J. E., Kloster, S., Magi, B. I., Marlon, J. R., Daniau, A.-L., Field, R. D., Arneth, A., Forrest, M., Hantson, S., Kehrwald, N. M., Knorr, W., Lasslop, G., Li, F., Mangeon, S., Yue, C., Kaiser, J. W., and van der Werf, G. R.: Historic global biomass burning emissions for CMIP6 (BB4CMIP) based on merging satellite observations with proxies and fire models (1750–2015), Geoscientific Model Development, 10, 3329–3357, https://doi.org/10.5194/gmd-10-3329-2017, 2017.

Vinodkumar, V., Dharssi, I., Yebra, M., and Fox-Hughes, P.: Continental-scale prediction of live fuel moisture content using soil moisture information, Agricultural and Forest Meteorology, 307, 108 503, https://doi.org/10.1016/j.agrformet.2021.108503, 2021.

Volkholz, J. and Ostberg, S.: ISIMIP3a landuse input data, https://doi.org/10.48364/ISIMIP.571261.1, 2022.

Wang, S., Foster, A., Lenz, E. A., Kessler, J. D., Stroeve, J. C., Anderson, L. O., Turetsky, M., Betts, R., Zou, S., Liu, W., Boos, W. R., and Hausfather, Z.: Mechanisms and Impacts of Earth System Tipping Elements, Reviews of Geophysics, 61, e2021RG000 757, https://doi.org/https://doi.org/10.1029/2021RG000757, e2021RG000757 2021RG000757, 2023.

https://doi.org/10.1029/2021RG000757, 2023a.

Wang, S. S.-C., Qian, Y., Leung, L. R., and Zhang, Y.: Interpreting machine learning prediction of fire emissions and comparison with FireMIP process-based models, Atmospheric Chemistry and Physics, 22, 3445–3468, https://doi.org/10.5194/acp-22-3445-2022, 2022.

Wang, S. S.-C., Leung, L. R., and Qian, Y.: Projection of Future Fire Emissions Over the Contiguous US Using Explainable Artificial Intelligence and CMIP6 Models, Journal of Geophysical Research: Atmospheres, 128, e2023JD039 154, https://doi.org/10.1029/2023JD039154, 2023b.

Wiltshire, A. J., Duran Rojas, M. C., Edwards, J. M., Gedney, N., Harper, A. B., Wiedinmyer, C. and Emmons, L.: Fire Inventory from NCAR version 2 Fire Emission, https://doi.org/10.5065/XNPA-AF09, 2022.

Wiedinmyer, C., Kimura, Y., McDonald-Buller, E. C., Emmons, L. K., Buchholz, R. R., Tang, W., Seto, K., Joseph, M. B., Barsanti, K. C.,

Carlton, A. G., and Yokelson, R.: The Fire Inventory from NCAR version 2.5: an updated global fire emissions model for climate and chemistry applications, Geoscientific Model Development, 16, 3873–3891, https://doi.org/10.5194/gmd-16-3873-2023, 2023.

Hartley, A. J., Hendry, M. A., Robertson, E., and Smout-Day, K.: JULES-GL7: the Global Land configuration of the Joint UK Land Environment Simulator version 7.0 and 7.2, Geoscientific Model Development, 13, 483–505, https://doi.org/10.5194/gmd-13-483-2020, 2020.

Wu, L., Su, H., and Jiang, J. H.: Regional simulations of deep convection and biomass burning over South America: 2. Biomass burning

aerosol effects on clouds and precipitation, Journal of Geophysical Research: Atmospheres, 116, https://doi.org/https://doi.org/10.1029/2011JD016106, /10.1029/2011JD016106, 2011.

Yuan, S., Bao, F., Zhang, X., and Li, Y.: Severe Biomass-Burning Aerosol Pollution during the 2019 Amazon Wildfire and Its Direct Radiative Forcing Impact: A Space Perspective from MODIS Retrievals, Remote Sensing, 14, https://doi.org/10.3390/rs14092080, 2022.

Yue, C., Ciais, P., Zhu, D., Wang, T., Peng, S. S., and Piao, S. L.: How have past fire disturbances contributed to the current carbon balance of boreal ecosystems?, Biogeosciences, 13, 675–690, https://doi.org/10.5194/bg-13-675-2016, 2016.

Zheng, B., Ciais, P., Chevallier, F., Chuvieco, E., Chen, Y., and Yang, H.: Increasing forest fire emissions despite the decline in global burned area, Science Advances, 7, eabh2646, https://doi.org/10.1126/sciadv.abh2646, 2021.

Zheng, B., Ciais, P., Chevallier, F., Yang, H., Canadell, J. G., Chen, Y., van der Velde, I. R., Aben, I., Chuvieco, E., Davis, S. J., Deeter, M., Hong, C., Kong, Y., Li, H., Li, H., Lin, X., He, K., and Zhang, Q.: Record-high CO₂ emissions from boreal fires in 2021, Science, 379, 912–917, https://doi.org/10.1126/science.ade0805, 2023.

Zhou, Y., Yan, H., and Luo, J.-J.: Impacts of Amazon fire aerosols on the subseasonal circulations of the mid-high latitudes, Frontiers in Earth Science, 8, 609 554, 2021.https://doi.org/10.3389/feart.2020.609554, 2020.